Methods for Solving Nonequilibrium Green's Functions with Application to Driven Quantum Transport

Thomas Honeychurch

Thesis submitted
to the
College of Science and Engineering
at

James Cook University

in partial fulfillment of the requirements
for the degree of

Doctor of Philosophy (Physical Sciences)

June 2024

$\hbar$ electronics

Daniel Kosov's research group

James Cook University

Primary advisor:

A/Prof. Daniel Kosov

Secondary advisor:

Prof. Ronald White

Declaration of originality

I declare that this thesis is my own work and has not been submitted in any form for another degree or diploma at any university or other institute of tertiary education. Every reasonable effort has been made to gain permission and acknowledge the owners of copyright material. I would be pleased to hear from any copyright owner who has been omitted or incorrectly acknowledged.

Acknowledgments

I want to thank my supervisor, Daniel Kosov, for his support over the last six years. His guidance and patience have helped me complete this thesis, and I'm grateful to him. Atop of this, I'd like to thank Daniel for entertaining my tangents and sharing his knowledge with me, however far afield. While this usually took the form of simple conservations, it was an education and something I'll treasure.

I'd also like to thank Prof. Ronald White, my secondary advisor and the Chair of my Candidature Committee, A/Prof. Shaun Belward. Thank you to the college and university community that keeps JCU running.

I'd also like to thank DK's minions, past and present, for their help with everything from paperwork to programming to physics and everything in between, as well as the additional fat chats. I'd also like to thank Tiria, Adam, Dale, and the Mythics gang for the lunchtime conservations and the friendships they have developed.

Finally, I'd like to thank my mother for her support, patience, and understanding, without which this thesis wouldn't have been possible.

For those I've missed, your collective assistance is evident, and I'm also grateful to you.

Statement of contribution of others

Beyond the personal contributions listed above, there are several sources of support that I gratefully acknowledge.

Financial support

Intellectual support

Abstract

Molecular electronics is the multidisciplinary field seeking to employ molecules, often single molecules, as functional components in electronics. These explorations into molecular electronics for the solutions to fundamental research questions and potential applications are driven by the miniaturization and fabrication of electronic components. However, while progressing from being once a science fiction to a fully-fledged scientific discipline today, the widescale adoption of molecular electronics has yet to manifest, owing to various difficulties. Among these difficulties is the appropriate tailoring of molecular junctions to operate under the time-dependent driving of the surrounding environment. We utilize nonequilibrium Green's functions and self-consistent perturbation theory to model the transport paradigm of two electrodes connected by a quantum central region in the presence of time-dependent driving. In the case of slow driving of electrode voltages relative to the transfer scales across the system, timescale separation methods are utilized to calculate non-adiabatic corrections to the system observables. This method was applied to explore the corrections to the dynamics of a single-level electronic system coupled to leads with driven voltages in both the noninteracting and Hartree single-level cases for electron-phonon interactions. Assuming the periodicity of the dynamics of the systems in question allows one to take a Floquet approach to the calculation of nonequilibrium Green's functions. This method was coupled with full counting statistics to investigate time-averaged cumulants of the current and applied to noninteracting single-level and Fano resonance systems in the presence of driving. The Floquet approach was also used to calculate electron-phonon interaction for the Holstein model in the presence of driven leads. In particular, this was completed with the self-consistent Born approximation. It was shown that periodic driving in resonance with the vibrational frequency resulted in large phonon occupations. Finally, the Floquet approach was applied to the study of two capacitively coupled quantum dots, each coupled to its own lead. The calculation was completed utilizing the fluctuation-exchange approximation to approximate electron-electron interactions between the quantum dots. It was found that the driving of the one lead resulted in an energy current through the system, one dependent on the driving frequency.

Research output

Publications

[1] *Timescale separation solution of the Kadanoff-Baym equations for quantum transport in time-dependent fields*,
T. D. Honeychurch and D. S. Kosov, Phys. Rev. B **100**, 245423 (2019)

[2] *Full counting statistics for electron transport in periodically driven quantum dots*,
T. D. Honeychurch and D. S. Kosov, Phys. Rev. B **102**, 195409 (2020)

[3] *Quantum transport in driven systems with vibrations: Floquet nonequilibrium Green's functions and the self-consistent Born approximation*,
T. D. Honeychurch and D. S. Kosov, Phys. Rev. B **107**, 035410 (2023)

[4] *Floquet Nonequilibrium Green's functions with Fluctuation-Exchange Approximation: Application to Periodically Driven Capacitively Coupled Quantum Dots*,
T. D. Honeychurch and D. S. Kosov, arXiv preprint, arXiv:2307.09774

[5] *Cooling molecular electronic junctions by AC current* ,
R.J. Preston, T.D. Honeychurch, D.S. Kosov, J. Chem. Phys., 153, 121102 (2020)

[6] *Emergence of negative viscosities and colored noise under current-driven Ehrenfest molecular dynamics*,
R.J. Preston, T.D. Honeychurch, D.S. Kosov, Phys. Rev. B **106**, 195406 (2022)

Conference Posters

[1] Poster title: *Electron-Vibration Interactions Within a Periodically Driven Molecular Junction*
Frontiers of Quantum and Mesoscopic Thermodynamics
Prague, Czech Republic, 2022

Contents

List of Figures

Introduction

1.1 General Motivations

Electronics have come to touch every aspect of our lives. Of the electronic technologies that have developed in the modern age, computers have arguably had the most considerable effect on their users. Their great success as tools has led to unprecedented connectivity and productivity, with the emergence of digital and data economies and artificial intelligence, to name a few consequences.

The continued miniaturization of electronics has resulted in cheaper and more powerful devices, a successful cycle under which large sections of the world economy have prospered. This was foreseen by Gordon Moore, who predicted that the number of transistors on an integrated circuit would grow exponentially [1, 2], which, in turn, has led to the size of the transistor to decline exponentially, from micrometers to nanometres in 40 years [1, 3].

Yet recently, the costs and complications confronting research and manufacturing have challenged Moore's law and the scaling of transistor technology [4], spurring new transistor designs to keep Moore's prediction on track [5, 6]. As the technology enters into the realm of quantum physics, it seems inevitable, due to economic [4] and physical limitations [7], that the microelectronics industry would seek to support and one day replace current technologies with radically different avenues.

1.2 Molecular Electronics

One possible avenue is molecular electronics, a diverse, multi-discipline field that seeks to create electrical components with molecules, mimicking conventional components and generating new functionalities. While molecular electronics is still growing as a field, the approach has many tentative advantages [8]. The variety of possible molecules as candidates for use in molecular electronics is great and, given the sheer variety of possible characteristics, suggests

the possibility of a diversity of functionalities.

Molecular electronics was born of a desire to manipulate matter for functionality on the smallest scales. Researchers like von Hippel[9] promoted the benefits of engineering with a top-down approach, leveraging the fundamental science of molecules to design materials and devices. At the same time, Feynman[10] highlighted the vast potential for miniaturization and new functionalities when design occurs at the atomic level. While such inquiries were confined to vivid speculation, the sentiments espoused inspired further research.

Experimentally, the first results to resemble molecular electronics were done by Mann and Kuhn in 1971 [11]. The duo managed to deposit monolayers of organic material onto solids to a high degree of accuracy before sandwiching these monolayers of material between electrodes. Completing this for Cd salts of fatty acids $CH_3(CH_2)_{n-2}COOH$, the researchers confirmed that conductance decayed exponentially with chain length.

In 1974, Aviram and Ratner published a work that postulated a molecular rectifier based on charge transfer salts [12]. This was the first work that made predictions that considered a single molecule as the functional component in an electronic device. This research invigorated the debate surrounding molecular electronics and molecular rectification within the scientific community [13].

Within fifty years after their first imagining, molecular electronics has graduated from science fiction to a fully-fledged scientific field, with growing prospects for commercial viability [14]. Aided by advances in experimental technique, researchers succeeded in accomplishing feats like synthesizing a monolayer photodiode in 1985 [15] and experimentally verifying the current rectification of a monolayer in 1997 [16]. Since these early works, the research into molecular electronics has grown steadily [14, 17, 18].

1.3   General Background

Most molecular junction designs follow the simple structure of a molecule connected to two leads. These leads are usually metallic, the most popular being gold [8, 21]. The central molecules often have additional anchoring groups chosen to bond to the metal in question, like a thiol group for bonding to gold [8, 22]. The molecule's structure beyond an anchor group's possible restrictions can vary significantly to achieve a specific outcome. Of the many methods for realizing such systems, we will look at the two prominent solutions: scanning probe techniques and mechanically controllable break junctions.

Scanning probe techniques work by moving a probe, usually a scanning tunneling microscope,
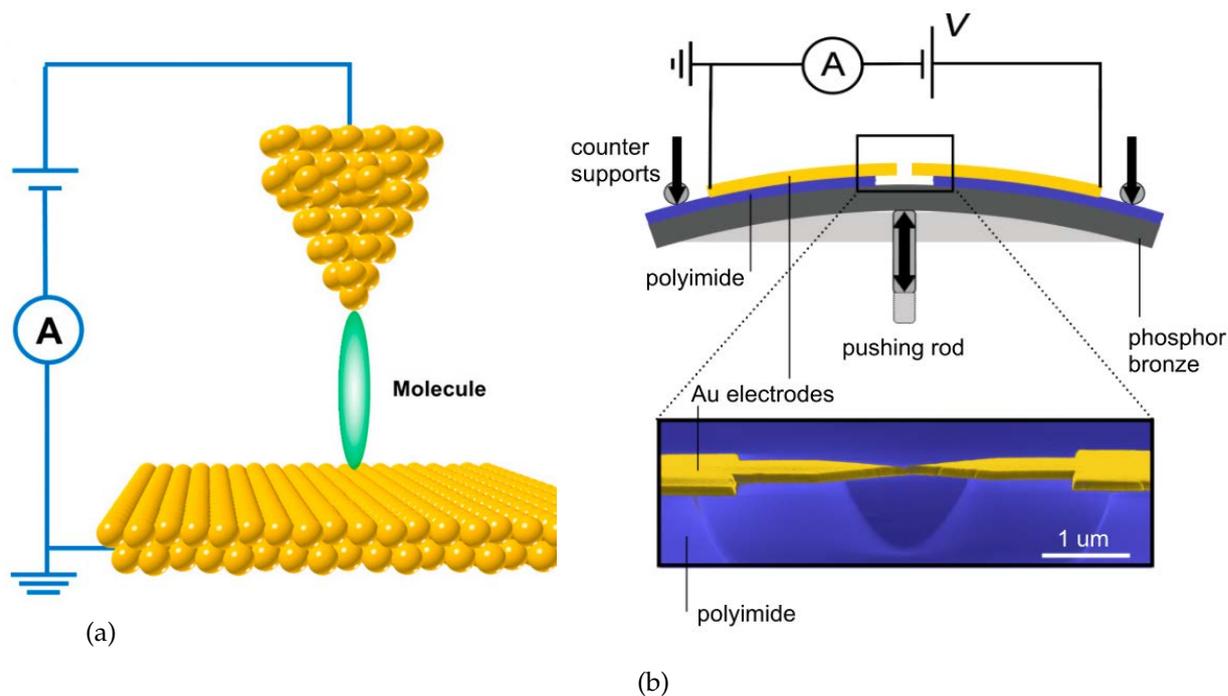
Figure 1.1: (a) A diagram of a scanning tunneling microscope break-junction (STMBJ). Reproduced with permission from reference [19]. (b) A mechanically controllable break-junction (MCBJ) and inset of scanning electron micrograph of an MCBJ's suspended bridge. Reproduced with permission from reference [20].

close to a surface such that, given a molecule bonded to either the surface or tip of the probe, a junction is formed (see figure 1.1a). This is often signified by a jump and plateau in the conductance [8]. This process often results in the molecule having a larger coupling to the electrode it is bonded to before the movement of the probe. These junctions, especially for STMs, are also often short-lived due to factors like temperature and vibrations. However, the flexibility of the approach and the ability to make many observations in a relatively short time means that scanning probe techniques lend themselves to statistical analysis, with the averaging of many results made in relatively quick succession [13].

Mechanically controlled break junctions consist of electrodes upon a flexible insulating layer, which can be bent mechanically to form a nanogap with high precision, usually with a piezo-electric device or stepping motor [14] (see figure 1.1b). The electrodes are constructed by first fashioning a suspended bridge of material before bending. The device pulls the material apart to form a constriction and eventually breaks it in two, generating a gap of $\sim 0.6nm$ [13]. For various experimental designs, the ratio of actuator movement electrode separation are on the order of 10^{-2} to 10^{-6}[8]. The deposition of molecules often happens after the breaking of the junction, with molecules being absorbed into the nanogap left by the breakage [13].

1.4 Vibrationally Assisted Transport

For a molecular junction, the deformation of the molecule can significantly affect the device's functionality, with electrons transferring energy to the molecule transferring energy to it and vice versa. The molecular backbone of a junction can have vibrational modes of varying rigidity and coupling to the electronic component, resulting in a wide range of phenomena. This propensity for deformation has been a significant challenge in molecular electronics, with runaway vibrations causing disassociation of the central molecules. Molecular deformation can also be leveraged as a tool in junction design, as seen with conformal switches and pressure-sensitive junctions. Moreover, vibrational signatures within observables, like current and noise, can often be utilized for discern the goings-on of the junction, including the particular molecule within the junction, its orientation, and its sensitivity to the spin flipping and light emission [8, 23, 24].

There are many different realizations of vibrations in molecular junctions. In the case where vibrations can be modeled with quantized harmonic modes, i.e., localized phonons, while the molecular backbones of many junctions are rather large molecules consisting of various vibrational modes, to understand the interactions between vibrational modes and transiting electrons, it helps to consider a simplistic model of a single level coupled to a single vibration. There are two important timescales for this simplistic model and the discussion below. First is the lifetime of the occupation of an energy level by an electron. This timescale is informed by the coupling strength of the level to the leads, Γ, and the distance between the voltage window and the closest molecular energy level, ΔE. These parameters allow us to estimate the traversal time as

$$\tau_t = \hbar \left(\sqrt{\Gamma^2 + (\Delta E)^2} \right)^{-1}. \tag{1.1}$$

The second timescale is the time the electrons and phonons take to interact, which can be approximated simply as $\tau_{ep} = \hbar/\lambda$, where λ is the coupling strength between the electronic and phononic components of the molecule. Comparing these two timescales gives us two parameter regimes: when electron-vibration interactions are low because $\lambda \ll \sqrt{\Gamma^2 + \Delta E^2}$ and when electron-vibration interactions are high because $\lambda \gg \sqrt{\Gamma^2 + \Delta E^2}$.

Within the strong electron-vibration interaction regime, the case where $\lambda \gg \sqrt{\Gamma^2 + \Delta E^2}$, investigated in resonant inelastic tunneling spectroscopy (RIETS), electron-phonon interactions can lead to significant changes in the current profile. In the case of RIETS, where the voltage profile is investigated in the context of resonant driving and low molecule-electrode coupling, current steps are present in the voltage profile. Due to resonance, these new peaks were found to be $n\hbar\omega/e$ volts away from the current step. One of the first experiments within this regime is that of Park et al., who, by varying the gate voltage of a junction, investigated the center-of-mass vibrations of C_{60} molecule (see figure 1.2) [25]. Physically, these additional steps within

the current-voltage profile arise due to electrons absorbing or emitting energy $n\hbar\omega$ to the vibrational mode in the form of phonons, resulting in fracturing for pathways through the junction.
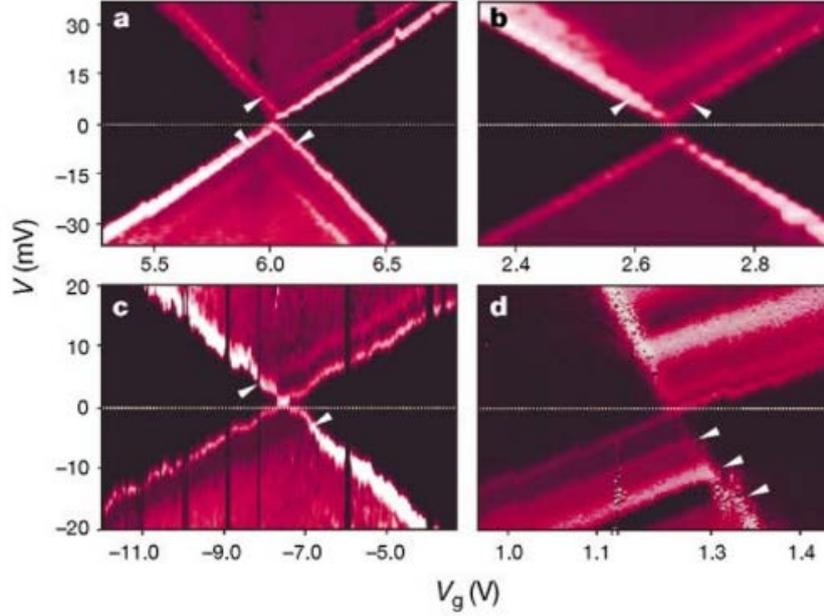
Figure 1.2: The differential conductance plotted against the gate voltage (horizontal axis) and bias voltage (vertical axis) for four realisations of a single- C_{60} transistor. The conductance gap (the dark regions) give away to the initial increases in current followed by those induced by the interaction with vibrations (marked by white arrows). Reproduced with permission from reference [25].

A new current-voltage profile emerges when the interaction rate between the vibrational and electronic components is low, i.e., $\lambda \ll \sqrt{\Gamma^2 + \Delta E^2}$. In this setting, when the voltage window increases to be equal to the energy of a phonon, i.e. $|V| = \hbar\omega/e$, the differential conductance jumps, either lower or higher, depending on the device's parameters. Within the second derivative of the current, d^2I/dV^2, this manifests as peaks or dips. This process of identifying vibrations, in this particular regime, by identifying shapes within the second-order differential conductance is called inelastic electron transport spectroscopy and is one of the oldest and most thoroughly investigated forms of electron-vibration interactions [24, 26]. An example of this is given in figure 1.3, which shows the dips in conductance within $Pt - D_2 - Pt$ and $Pt - H_2 - Pt$ junctions.

The appearance of either a dip or a peak in the second-order differential conductance varies with the conductance of the device, with some experiments having conductances low enough to generate peaks [28, 29]. In contrast, others have a high conductance, resulting in dips [30]. This quantitative change in the behavior conductance can be seen in works like Tal et al.[31], in which the different configurations of Pt/H_2O junctions resulted in varying measured con-
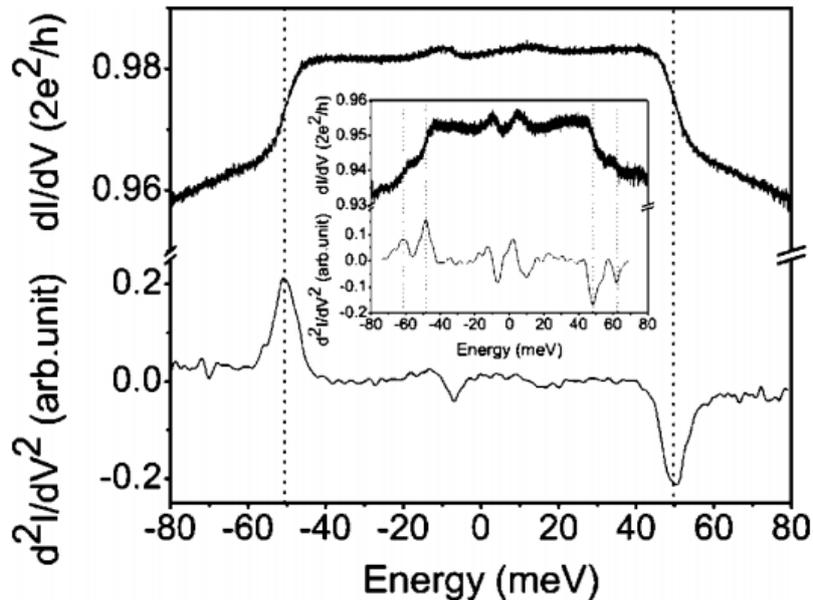
Figure 1.3: Conductance of a $Pt - D_2 - Pt$ junction. The inset shows the case for a $Pt - H_2 - Pt$ junction. The subsequent derivative were obtained numerically. Reproduced with permission from [27].

ductances, and subsequently, both jumps up and down in conductance due to interaction with the vibrations (see figure 1.4).
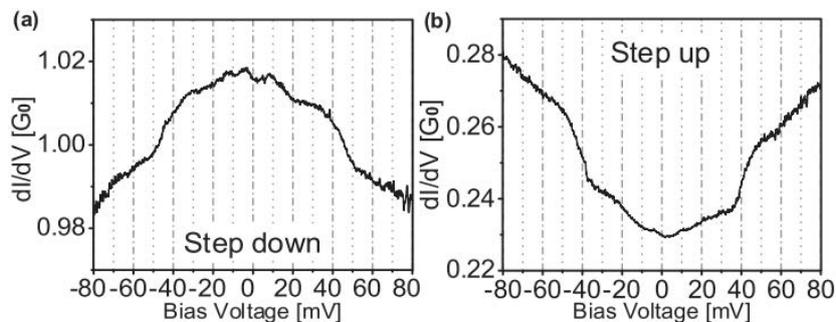
Figure 1.4: The differential conductance of two different configurations of a $Pt - H_2O - Pt$ junction, with linear conductance measures of $1.02 \pm 0.01 G_0$ (a) and $0.23 \pm 0.01 G_0$. Reproduced with permission from [31].

Whether a peak or a dip is observed in the second-order differential conductance is due to the competing effects of the inelastic channel, introduced by the possible emission and absorption of a phonon of energy, and the correction to the elastic channel, which is due to the interference between the zero-order elastic channel and the generated by the emission and absorption of a phonon. In the case of low conductance, the positive contributions of the inelastic channels dominate, resulting in peaks. In the case of high conductance, close to G_0, the negative contribution from the correction to the elastic channel dominates, resulting in

dips [8]. Beyond the conductance of the junction, other factors may affect these contributing channels and, therefore, the features found in IETS, like asymmetry in coupling between leads [32, 33].

1.5 Driven Phenomena

The ability to react to changes in their environment is essential to the functionality of many molecular junctions. Memory and logic components, transistors, rectifiers, charge pumps, and sensors are all devices that do or may need to function with changes to voltage, temperature, and surrounding electric fields, to name a few of the system's properties that may change. The speed at which these properties vary can be at timescales fast enough to be comparable to those governing the mechanisms of a junction's functionality. In such cases, one cannot assume adiabaticity and rely on theoretical tools for modeling static environments. This difficulty means that tools for modeling such scenarios are necessary.

Among these external stimuli, variations in the voltage profile of devices due to alternating driving or exposure to electromagnetic radiation are of particular interest. Historically, the first attempts to explain the effects of modulated driving come with the work of Tien and Gordon [34]. This work was in response to the experimental investigations of Dayem and Martin [35], who investigated the tunneling of electrons in superconductor-insulator-superconductor junctions where one of the superconductors was irradiated. The work showed that, with the addition of a time-dependent potential for the irradiated superconductor, i.e., $V(t) = V_{DC} + V_{AC} \cos(\Omega t)$, the time-averaged current can be seen to fracture into various contributions from the case without driving [36]:

$$\frac{1}{P} \int_{-P/2}^{P/2} dt I(t) = \sum_{n=-\infty}^{\infty} J_n^2 \left(\frac{eV_{AC}}{\hbar\Omega} \right) I_{DC} \left(V_{DC} + \frac{\hbar\Omega n}{e} \right), \qquad (1.2)$$

where $P = 2\pi/\Omega$ is the period of the driving, $J_n(x)$ is the Bessel function of the first kind and I_{DC} is the current without any irradiation. Equation (1.2) suggests the physical interpretation that the periodic variation of the electrodes' energies results in the absorption or emission of n photons with probability $J_n^2 \left(\frac{eV_{AC}}{\hbar\Omega} \right)$, which then travel through the junction. Since these early investigations, this phenomenon, called photon-assisted transport (PAT), has been observed in many disparate settings, in both theory and experiments [36–40].

For particular regimes, PAT can help explain junctions operating under illumination. In this situation, the illumination results in surface plasmons, collective oscillations of the conductive electrons, in the skin layer of the leads of the junction, resulting in a strong electromagnetic field across the junction. These effects can significantly affect the charge transport across the

junction, resulting in many new mechanisms for transport [41]. However, when the frequency of the light is sufficiently low, the excitation of electron-hole pairs within the lead and molecule can be disregarded, and the plasmonic field can be treated as an AC voltage bias oscillating at the plasmon frequency [41–44]. While this approximation holds in the low-frequency limit, in reality, PAT can be one of many mechanisms at play within an illuminated junction, with particular difficulties distinguishing between PAT and hot electron transport [43, 45]. Hot electrons occur when plasmons decay through generating highly energetic electrons via Landau damping [41], with those close enough participating in transport across the junction. To avoid contributions to transport from hot electrons, one can have a junction where charge transfer times are larger than the lifetime of hot electrons or investigate illumination with frequencies not absorbable by the electrodes, the latter motivating the study of the terahertz regime for gold electrodes [45, 46].

Many researchers have utilized PAT to explain the features of experiments. Optical rectification has been observed in nanogaps for gold electrodes induced by illumination [47]. Alternating voltages over atomic-sized contacts have also been realized for both conventional means of voltage driving and in the context of light-induced plasmonics [48–50]. For gold contacts with conductances of $G_0 = 2e^2/h$, increases in conductance were observed upon illumination of the junction. Specifically, for laser frequencies not absorbed by the gold electrodes, PAT was found to explain the changes in conductance. However, for wavelengths that are absorbed by the gold contacts, the PAT mechanism failed to explain experiments, with hot electron transport appearing to be the dominant contributor [49].

In the context of molecular junctions, several experiments have been undertaken in various regimes [40, 42, 43, 45, 46, 51]. Optical rectification of thiolated alkyl chains in a suspended wire molecular junction under 658nm laser light has been investigated [42]. With the PAT mechanism, the assumption that AC driving voltage is smaller than the incident photon energy, $eV_{AC} \ll \hbar\omega$, and the assumption that the conductance varies slowly on the scales of $\hbar\omega$, the additional current due to optical rectification can be related to the current in the case without illumination [41, 42]:

$$\Delta I_{DC} = \frac{1}{4} V_{AC}^2 \frac{d^2 I_{dc}}{dV_{dc}^2}. \tag{1.3}$$

Given experimental measures for the terms in equation (1.3), V_{AC}^2 could be calculated and found to be a linear function of the laser power. Moreover, owing to the known lengths of the thiolated alkyl chains utilised in the investigation, the effective average electric field and the field enhancement in the junction could be estimated, with the latter increasing as the molecular length decreased. This field enhancement was attributed to the surface plasmons of the metal electrodes, which generate strong electromagnetic fields within the restricted region of the junction [42, 43].
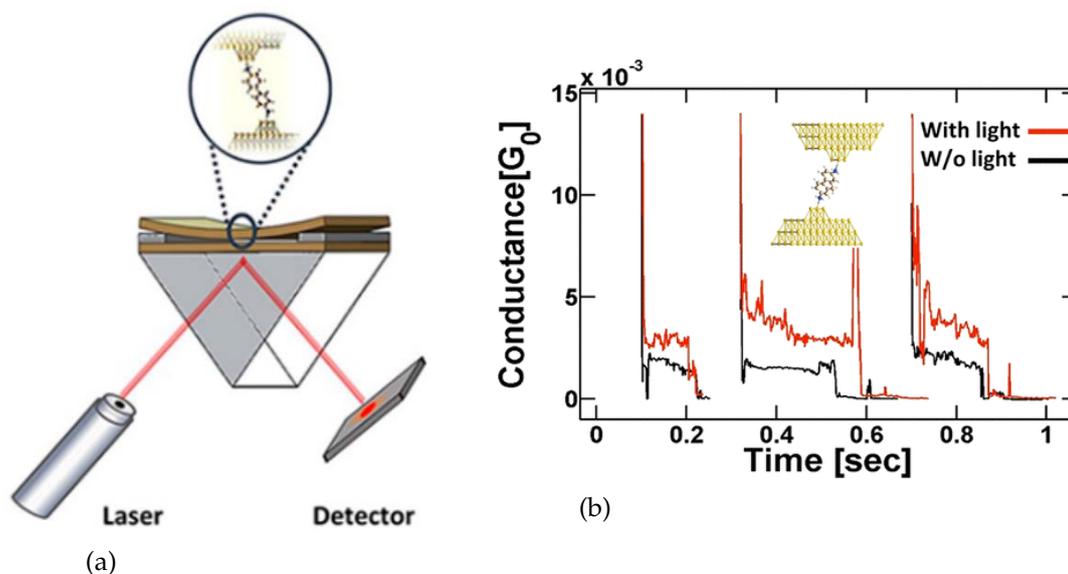
Figure 1.5: (a) The squeezable break junction setup for single-molecule conductance measures. (b) Representative conductance-time traces showing without (black) and with (red) illumination, showing the increase in conductance for a 2,7-diaminofluorene single-molecule junction. From reference [43].Adapted with permission from reference [43]. Copyright 2024 American Chemical Society.

Enhanced conductance was also induced by surface plasmons for 2,7-diaminofluorene single-molecule squeezable break junctions, illuminated with a 781nm laser [43], see figure 1.5. Ruling out the possibility of enhanced conductance by photon absorption by the molecule, PAT was suggested to explain the increase in conductance, with the zero-bias transmission for the molecule in gold electrodes suggesting that the PAT mechanism's single-photon emission tunneling process was to blame. However, this conductance enhancement could have also been due to hot electrons, with researchers showing analytically that the theory for both mechanisms was identical for the regime investigated.

This problem of the indistinguishability of PAT and hot electron transport contributions was further probed by experimentalists who used polarisation-dependent illumination of a 4,4'-bipyridine molecular junction [45] to investigate increases in conductance under illumination. The researchers calculate that the effects of hot electrons should be dominated when the laser wavelength can be absorbed by the electrodes and generate hot electrons, whose lifetimes are larger than the traversal time of the molecule. This claim was further investigated experimentally by changing the polarisation axis of the incident light from parallel to orthogonal with respect to the junction axis, which, due to the need for a parallel electric field for PAT, should see a reduction in conductance enhancement. For the orthogonal polarization, conductance enhancement was still observed, suggesting the presence of hot electrons.

In addition to molecular junctions, other methods for investigating nanoscale transport with driving voltages have been explored. A notable method is utilizing lateral quantum dots,

which are generated by taking a 2D electron gas, usually generated at the interface of two semiconductor sheets like GaAs/AlGaAs, and, by using gates deposited atop the semiconductors, applying a voltage to create regions of spatial confinement with the 2D electron gas, trapping holes or electrons, forming the quantum dots [52].
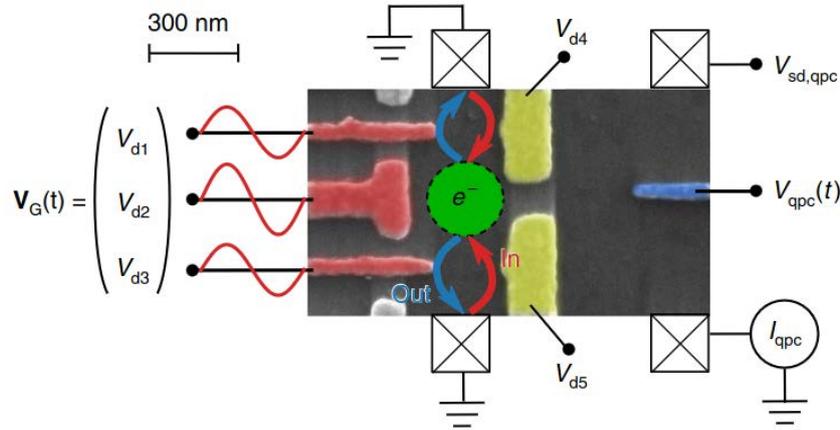
Figure 1.6: An STM image of the device utilized in references [53] and [54]. The quantum dot (green island) is capacitively coupled to the quantum point contact, generated by V_{d4}, V_{d5} and $V_{qpc}(t)$, which acts as a time-resolved charge detector. The gates of $V_G(t)$ are modulated periodically to drive the tunneling in and out of the quantum dot. Reproduced with permission from reference [53].

When researchers modulate the voltages confining the quantum dots, they can change various parameters defining them, like energy levels and coupling between dots and surrounding baths [55]. Such investigations have seen much interest given the promise of precise manipulation of electrons for metrological purposes [56, 57]. Stochastic resonance has been investigated in the context of a quantum dot with periodically driven gate voltages, where statistics collected about the number of tunneling events per period between dot and baths revealed a decrease in the Fano factor with a specific driving frequency [53] (see figure 1.6 for experimental setup). Researchers also investigated the emission statistics of a quantum dot with periodically driven gate voltages controlling tunneling between the dot and baths and have observed the crossover of adiabatic to non-adiabatic driving due to increases in frequency [54]. The effects of driven gates on a double quantum dot, where the dots were coupled to each other and to respective baths, has also been investigated, with current being able to be induced across the system without a source-drain voltage due to the application of microwave driving to vary the energies and coupling of the dots [58].

1.6 Outline

The thesis is organised as follows. In Chapter 2, we introduce nonequilibrium Green's functions as the tool of choice for modelling the dynamics of driven molecular junctions. The chapter covers the derivations of nonequilibrium Green's functions and their application to molecular junctions. The inclusion of electron-electron and electron-phonon interactions are handled with self-consistent perturbation theory, with the use of Feynman diagrams set out. The observables of electronic current and occupation, as well as phonon occupation, are set out, whilst full counting statistics for nonequilibrium Green's functions is also derived.

In Chapter 3, we investigate the driving of lead voltages within the regime of fast electron tunnelling and slow driving timescales. This allows for a perturbative solution the equations of motion for the Green's functions in terms of the ratio of characteristic electron tunneling time with the speed of driving. The method is applied to both a driven noninteracting resonant level and a Holstein model under the Hartree approximation.

In Chapter 4, the statistics of current transfer for a periodically driven molecular junction are investigated. This was achieved by utilising full counting statistics to compute the cumulants of the electronic current and the equations of motion are solved with a Floquet approach. The method is applied to single resonant level and Fano resonance scenarios. It is shown that the driving generates noisier current in both cases.

In Chapter 5, the effects of periodic driving of voltage on a molecular junction with a localised phonon mode with a junction are investigated. A Floquet approach to nonequilibrium Green's functions is married with self-consistent perturbation theory, specificially the self-consistent Born approximation for the electron-phonon interaction. A model of a single electronic level coupled to a phononic mode was investigated, with driving at multiples of the phonon's frequency resulting in pronounced increases in phonon occupation.

In Chapter 6, the transfer of energy between two driven, capacitively coupled quantum dots was investigated. Specifically, the driving of one of the lead's in an energy current between the opposing dot and lead. The electron-electron interaction was handled with the fluctuation-exchange approximation whilst a Floquet approach was used for solving the equations of motion. Four stages were identified in the process, with the energy current being found to be sensitive to the driving frequency.

Finally, in Chapter 7, we summarize the findings of the thesis and present several possible extensions.

Natural units for quantum transport are used throughout the thesis, with $\hbar$, e, and k_B set to

unity.

Nonequilibrium Green's Functions

This chapter introduces the machinery of nonequilibrium Green's functions and its application to time-periodic systems. The Hamiltonian of the model investigated is explained, and its realization in nonequilibrium Green's functions with self-consistent perturbation theory is derived and discussed [59–65].

2.1 Hamiltonian

We use a second quantization description of the Hamiltonian to model our junction system. Our system can be separated into its isolated components and their interacting terms:

$$H(t) = H_0(t) + H_{int}(t), \tag{2.1}$$

$$H_0(t) = H_C(t) + H_L(t) + H_V, \tag{2.2}$$

$$H_C(t) = \sum_{ij} \epsilon_{ij}(t) \hat{d}_i^\dagger \hat{d}_j, \tag{2.3}$$

$$H_L(t) = \sum_\alpha H_\alpha(t) = \sum_{k,\alpha} \epsilon_{k\alpha}(t) \hat{c}_{k\alpha}^\dagger \hat{c}_{k\alpha}, \tag{2.4}$$

$$H_V = \sum_\nu \omega_\nu \hat{a}_\nu^\dagger \hat{a}_\nu = \sum_\nu \frac{\omega_\nu}{2} \left(\hat{P}_\nu + \hat{Q}_\nu \right), \tag{2.5}$$

$$H_{int}(t) = H_T(t) + H_{el-el} + H_{el-ph}, \tag{2.6}$$

$$H_T(t) = \sum_\alpha H_{\alpha C}(t) = \sum_{k,\alpha,i} t_{k\alpha i}(t) \hat{c}_{k\alpha}^\dagger \hat{d}_i + t_{k\alpha i}^*(t) \hat{d}_i^\dagger \hat{c}_{k\alpha}, \tag{2.7}$$

$$H_{el-el} = \frac{1}{2} \sum_{mkjn} w_{mkjn} \hat{d}_m^\dagger \hat{d}_k^\dagger \hat{d}_j \hat{d}_n, \tag{2.8}$$

$$H_{el-ph} = \sum_{\nu,ij} \lambda_{ij}^\nu \hat{d}_i^\dagger \hat{d}_j \hat{Q}_\nu \tag{2.9}$$

Here, the total system Hamiltonian is divided into the noninteracting leads, given by $H_L(t)$, an interacting central region, given by $H_C(t)$, and the tunneling between them, contained in $H_{\alpha C}(t)$. The central region includes both electron-electron and electron-phonon interaction terms. Here, the energies of a particular lead α are given by $\epsilon_{k\alpha}(t)$, while the tunneling from the site k of the lead α to the site ith site of the central region is informed by the coupling coefficients $t_{k\alpha i}$. The central region is composed of noninteracting components, informed by the kinetic and potential energy single-particle terms, $\epsilon_{ij}(t)$ and the interacting terms, given by the electron-electron interaction strength w_{mkjn} and electron-phonon coupling strength λ_{ij}^{ν}. The second quantization operator $\hat{c}_{k\alpha}^{\dagger}$ ($\hat{c}_{k\alpha}$) creates (destroys) electrons within site k of lead α. The operator $\hat{d}_i^{\dagger}$ ($\hat{d}_i$) creates (destroys) an electron in the central region and $\hat{a}_{\nu}^{\dagger}$ ($\hat{a}_{\nu}$) creates (destroys) a phonon within the phonon modes ν. For the phonons, we have the normalized position and momentum operators $\hat{Q}_{\nu} = \frac{1}{\sqrt{2}}\left(\hat{a}_{\nu} + \hat{a}_{\nu}^{\dagger}\right)$ and $\hat{P}_{\nu} = \frac{1}{i\sqrt{2}}\left(\hat{a}_{\nu} - \hat{a}_{\nu}^{\dagger}\right)$. All of electronic operators follow the standard canonical anti-commutation relations , $\left[\hat{c}_i, \hat{c}_j\right]_{+} = \left[\hat{c}_i^{\dagger}, \hat{c}_j^{\dagger}\right]_{+} = 0$ and $\left[\hat{c}_i, \hat{c}_j^{\dagger}\right]_{+} = \delta_{ij}$, whereas the phononic operators follow the commutation relations $\left[\hat{a}_{\nu}, \hat{a}_{\mu}\right]_{-} = \left[\hat{a}_{\nu}^{\dagger}, \hat{a}_{\mu}^{\dagger}\right]_{-} = 0$, $\left[\hat{a}_{\nu}, \hat{a}_{\mu}^{\dagger}\right]_{-} = \delta_{\nu\mu}$, $\left[\hat{Q}_{\nu}, \hat{Q}_{\mu}\right]_{-} = \left[\hat{P}_{\nu}, \hat{P}_{\mu}\right]_{-} = 0$ and $\left[\hat{Q}_{\nu}, \hat{P}_{\mu}\right]_{-} = i\delta_{\nu\mu}$.

For convenience, we consider a compact notation for the phononic part of the Hamiltonian introduced in references [61, 62, 66]:

$$\hat{\phi}_{n,\nu} = \begin{cases} \hat{Q}_{\nu}, & n = 1 \\ \hat{P}_{\nu}, & n = 2 \end{cases}, \tag{2.10}$$

for which the commutation relations read

$$\left[\hat{\phi}_{n,\nu}, \hat{\phi}_{n',\nu'}\right] = \alpha_{\{n\nu\}\{n'\nu'\}} = \alpha_{\bar{\nu}\bar{\nu}'} = i\delta_{\nu\nu'}\begin{pmatrix} 0 & 1 \\ -1 & 0 \end{pmatrix}_{nn'}. \tag{2.11}$$

This notations can be further summarised with the introduction of collective notation of $\bar{\nu} = \{n, \nu\}$ and have the handy identity $\sum_{\bar{\eta}} \alpha_{\bar{\nu}\bar{\eta}} \alpha_{\bar{\eta}\bar{\nu}'} = \delta_{\bar{\nu}\bar{\nu}'} = \delta_{\nu\nu'}\delta_{nn'}$. The terms of the Hamiltonian can be rewritten in terms of this new notation:

$$H_V = \sum_{\bar{\nu}\bar{\mu}} \frac{\Omega_{\bar{\nu}\bar{\mu}}}{2}\, \hat{\phi}_{\bar{\mu}}\hat{\phi}_{\bar{\nu}} \tag{2.12}$$

and

$$H_{el-ph} = \sum_{\bar{\nu},ij} M_{ij}^{\bar{\nu}} \hat{d}_i^{\dagger}\hat{d}_j\hat{\phi}_{\bar{\nu}}, \tag{2.13}$$

where $\Omega_{\bar{\nu}\bar{\mu}} = \omega_{\nu}\delta_{\bar{\nu}\bar{\mu}}$ and $M_{ij}^{\bar{\nu}} = M_{ij}^{n,\nu} = \delta_{1,n}\lambda_{ij}^{\nu}$ relate the new parameters to those of equations (2.5) and (2.9). This collective notation will be used for most derivations within the text so that the bar will be omitted for comprehension purposes, i.e., $\bar{\nu} \to \nu$, and will be shown when explicitly needed.

2.2 Time-Dependent Observables and the Contour

To calculate observables out of equilibrium, we begin with our system in equilibrium, at some time t_0, with its components unconnected:

$$\hat{\rho}_0 = \frac{e^{-\beta\left(\hat{H}_0 - \mu\hat{N}_{el}\right)}}{\text{Tr}\left[e^{-\beta\left(\hat{H}_0 - \mu\hat{N}_{el}\right)}\right]}. \tag{2.14}$$

Here, density matrix ρ_0 describes the system at $t \leq t_0$, with an initial uncoupled and non-interacting state, where β is the inverse temperature, μ is the chemical potential and $\hat{N}_{el}$ is the electron occupation operator. The system is also time-independent up to this point, with $\hat{H}_0\left(t \leq t_0\right) = \hat{H}_0$ and $\hat{N}_{el}\left(t \leq t_0\right) = \hat{N}_{el}$.

After time t_0, we push the system out of equilibrium by turning on the interactions and couplings within and between the various composite sections of the total system, evolving the system forward:

$$\hat{\rho}(t) = \hat{U}\left(t, t_0\right)\hat{\rho}_0\hat{U}\left(t_0, t\right), \tag{2.15}$$

where the time-evolution operator evolves the system with the full Hamiltonian (Eq. 2.1):

$$\hat{U}\left(t, t'\right) = \begin{cases} T\left\{e^{-i\int_{t'}^{t} d\bar{t}\hat{H}(\bar{t})}\right\}, & t > t' \\ \bar{T}\left\{e^{+i\int_{t}^{t'} d\bar{t}\hat{H}(\bar{t})}\right\}, & t < t', \end{cases} \tag{2.16}$$

where T and $\bar{T}$ are the time- and anti-time-ordering respectively. Given the evolution of the density matrix at some time t, we can calculate the ensemble average of a particular operator $\hat{O}(t)$:

$$O(t) = \text{Tr}\left[\hat{\rho}(t)\hat{O}(t)\right] = \text{Tr}\left[\hat{\rho}_0\,\hat{U}\left(t_0, t\right)\hat{O}(t)\hat{U}\left(t, t_0\right)\right] = \text{Tr}\left[\hat{\rho}_0\,\hat{O}_H(t)\right], \tag{2.17}$$

where the Heisenberg representation is given by $\hat{O}_H(t) = \hat{U}\left(t_0, t\right)\hat{O}(t)\hat{U}\left(t, t_0\right)$.

We can go further and cast the initial density matrix as an evolution into the complex plane:

$$e^{-\beta\left(\hat{H}_0 - \mu\hat{N}_{el}\right)} = e^{-i\hat{H}^M(t_0 - i\beta - t_0)} = \hat{U}\left(t_0 - i\beta, t_0\right), \tag{2.18}$$

where we define the Matsubara Hamiltonian as $\hat{H}_M = \hat{H}_0 - \mu\hat{N}_{el}$. This allows us to think about the calculation of our ensemble average as a series of evolutions:

$$O(t) = \frac{\text{Tr}\left[\hat{U}\left(t_0 - i\beta, t_0\right)\,\hat{U}\left(t_0, t\right)\hat{O}(t)\hat{U}\left(t, t_0\right)\right]}{\text{Tr}\left[\hat{U}\left(t_0 - i\beta, t_0\right)\,\hat{U}\left(t_0, t\right)\hat{U}\left(t, t_0\right)\right]}. \tag{2.19}$$

We can read the time-evolution in equation (2.19) as evolving from t_0 to t on a forward branch

C_f, before evolving backward from t to t_0 on a backward branch C_b, and finally evolving along the Matsubara branch C^M from t_0 to $t_0 - i\beta$.

These multiple evolutions can be rolled into one by considering the terms on a single contour $C = C_f \oplus C_b \oplus C_M$. Here, the Hamiltonian needs to be defined for all contour time z, which consists of the times on the forward, backward, and Matsubara sections, which are denoted t^f, t^b and t^M, respectively:

$$\hat{H}(z) = \begin{cases} \hat{H}(t) & z = t^f \in C^f \\ \hat{H}(t) & z = t^b \in C^b \\ \hat{H}^M & z \in C^M \end{cases} . \tag{2.20}$$

This allows us to generalise equation (2.16) to the contour:

$$\hat{U}(z, z') = \begin{cases} T_C \left\{ e^{-i \int_{z'}^{z} d\bar{z} \hat{H}(\bar{z})} \right\}, & z > z' \\ \bar{T}_C \left\{ e^{+i \int_{z}^{z'} d\bar{z} \hat{H}(\bar{z})} \right\}, & z < z' \end{cases}, \tag{2.21}$$

where T_C and $\bar{T}_C$ are the time- and anti-time-ordering on the contour, which sees any series of operators order latest to the left or right for time-ordering or anti-ordering respectively:

$$T_C \left\{ \hat{O}_1(z_1) \hat{O}_2(z_2) \cdots \hat{O}_k(z_k) \right\}$$
$$= \sum_P (\pm)^{\zeta_P} \theta_C(z_{P_1}, z_{P_2}) \theta_C(z_{P_2}, z_{P_3}) ... \theta_C(z_{P_{N-1}}, z_{P_N}) \hat{O}_{P_1}(z_{P_1}) \hat{O}_{P_2}(z_{P_2}) \cdots \hat{O}_{P_N}(z_{P_N}) \tag{2.22}$$

and

$$\bar{T}_C \left\{ \hat{O}_1(z_1) \hat{O}_2(z_2) \cdots \hat{O}_k(z_k) \right\}$$
$$= \sum_P (\pm)^{\zeta_P} \theta_C(z_{P_N}, z_{P_{N-1}}) ... \theta_C(z_{P_3}, z_{P_2}) \theta_C(z_{P_2}, z_{P_1}) \hat{O}_{P_1}(z_{P_1}) \hat{O}_{P_2}(z_{P_2}) \cdots \hat{O}_{P_N}(z_{P_N}) \tag{2.23}$$

where $\pm$ is $+$ for bosons and $-$ for fermions, P is for any permutation and ζ_P is for the number of permutations needed for the initial ordering to that of the permutation P and $\theta_C(z, z')$ is the Heaviside on the contour.

Within the context of the contour, the ensemble average gains the following compact form:

$$O(z) = \langle \hat{O}_H(z) \rangle = \frac{\text{Tr} \left[T_C \left\{ e^{-i \int_C d\bar{z} \hat{H}(\bar{z})} \hat{O}(z) \right\} \right]}{\text{Tr} \left[T_C \left\{ e^{-i \int_C d\bar{z} \hat{H}(\bar{z})} \right\} \right]}, \tag{2.24}$$

which we can extend to consider a string of operators,

$$\langle T_C \left\{ \hat{O}_{1H}(z_1) \hat{O}_{2H}(z_2) \cdots \hat{O}_{kH}(z_k) \right\} \rangle = \frac{\text{Tr} \left[T_C \left\{ e^{-i \int_C d\bar{z} \hat{H}(\bar{z})} \hat{O}_1(z_1) \hat{O}_2(z_2) \cdots \hat{O}_k(z_k) \right\} \right]}{\text{Tr} \left[T_C \left\{ e^{-i \int_C d\bar{z} \hat{H}(\bar{z})} \right\} \right]}. \tag{2.25}$$

Here, the contour Heisenberg picture is defined as

$$\hat{O}_H(z) = \hat{U}(z_i, z)\hat{O}(z)\hat{U}(z, z_i),\tag{2.26}$$

for which we can derive a contour Heisenberg equation of motion:

$$i\frac{d}{dz}\hat{O}_H(z) = \left[\hat{O}_H(z), \hat{H}_H(z)\right]_- + \hat{U}(z_i, z)\left(i\frac{d}{dz}\hat{O}(z)\right)\hat{U}(z, z_i).\tag{2.27}$$

This thesis focuses on dynamics within the long time limit, where information about the initial conditions is lost due to interaction with macroscopically large leads. This can be seen as sending $t_0 \to -\infty$. The consequence of this choice will become apparent at a later stage.

2.3   Green's functions on the Contour

The main objects of interest in our calculations are the nonequilibrium Green's functions, which are time-ordered ensemble averages of correlators of varying complexity. The largest Green's functions (GF) we will deal with is the mixed Green's function:

$$X_{m,n}(\widetilde{1}_{zv}, \cdots, \widetilde{m}_{zv}; 1_{zp}, \cdots, n_{zp}; 1'_{zp}, \cdots, n'_{zp}) =$$

$$\frac{1}{i^{m/2+n}}\frac{\text{Tr}\left[T_C\left\{e^{-i\int_C dz\hat{H}(z)}\hat{\phi}(\widetilde{1}_{zv})\cdots\hat{\phi}(\widetilde{m}_{zv})\hat{d}(1_{zp})\cdots\hat{d}(n_{zp})\hat{d}^\dagger(n'_{zp})\cdots\hat{d}^\dagger(1'_{zp})\right\}\right]}{\text{Tr}\left[T_C\left\{e^{-i\int_C d\underline{z}\hat{H}(z)}\right\}\right]}.\tag{2.28}$$

Here, we use a shorthand that collects related parameters into one parameter; for example, 1_{zxy} refers to parameters z_1, x_1, and y_1. This allows the operators to be written in an abbreviated manner, like $\hat{\phi}(k_{zv}) = \hat{\phi}_{v_k}(z_k)$ and $\hat{d}^{(\dagger)}(1_{zj}) = \hat{d}_{j_1}^{(\dagger)}(z_1)$.

While equation (2.28) suggests the possibility of studying correlation functions of a arbitrary order, for example the two- or three-body electronic Green's functions, we will focus primarily on objects more manageable objects. These include the one-body electronic Green's function,

$$G(1_{zp}, 1'_{zp}) = \frac{1}{i}\frac{\text{Tr}\left[T_C\left\{e^{-i\int_C d\underline{z}\hat{H}(z)}\hat{d}(1_{zp})\hat{d}^\dagger(1'_{zp})\right\}\right]}{\text{Tr}\left[T_C\left\{e^{-i\int_C d\underline{z}\hat{H}(z)}\right\}\right]},\tag{2.29}$$

the phonon amplitude,

$$\phi(\widetilde{1}_{zv}) = \frac{\text{Tr}\left[T_C\left\{e^{-i\int_C d\underline{z}\hat{H}(z)}\hat{\phi}(\widetilde{1}_{zv})\right\}\right]}{\text{Tr}\left[T_C\left\{e^{-i\int_C dz\hat{H}(z)}\right\}\right]},\tag{2.30}$$

the two-field phonon Green's function without fluctuation operators,

$$D_0(\widetilde{1}_{zv}, \widetilde{2}_{zv}) = \frac{1}{i} \frac{\text{Tr}\left[T_C\left\{e^{-i\int_C dz \hat{H}(z)} \hat{\phi}(\widetilde{1}_{zv}) \hat{\phi}(\widetilde{2}_{zv})\right\}\right]}{\text{Tr}\left[T_C\left\{e^{-i\int_C dz \hat{H}(z)}\right\}\right]}, \tag{2.31}$$

and the two-field phonon Green's function with fluctuation operators,

$$D(\widetilde{1}_{zv}, \widetilde{2}_{zv}) = \frac{1}{i} \frac{\text{Tr}\left[T_C\left\{e^{-i\int_C dz \hat{H}(z)} \Delta\hat{\phi}(\widetilde{1}_{zv}) \Delta\hat{\phi}(\widetilde{2}_{zv})\right\}\right]}{\text{Tr}\left[T_C\left\{e^{-i\int_C dz \hat{H}(z)}\right\}\right]}, \tag{2.32}$$

where $\Delta\hat{\phi}(\widetilde{1}_{zv}) = \hat{\phi}(\widetilde{1}_{zv}) - \phi(\widetilde{1}_{zv})$. The need for two different definitions for the phonon Green's functions will become more transparent further on.

It should be noted that the above Green's functions don't include references to the lead self-energies outside of those due to the time-evolution on the contour, i.e., $e^{-i\int_C dz \hat{H}(z)}$. In the following theory, we will disregard the influence of the leads and focus solely on the theory in the context of the interactions. The leads and the tunnelling in and out of the central region by the electrons are described by the equations (2.4) and (2.7), respectively. As these terms are noninteracting, quadratic terms, their influence on the one-body Green's functions will result in a simple modification of the noninteracting one-body Green's function, as seen in section 2.4.8, which in turn will be used in the calculation of the one-body Green's function in the presence of the more complicated interactions.

2.3.1 Martin-Schwinger Hierarchy

We want to generate an equation of motion for the mixed Green's functions. Because our Green's functions consist of ensemble averages of contour time-ordered strings of operators, we can start derivation by investigating contour time-derivatives of equation (2.22):

$$\frac{d}{dz_m} T_C \left\{\hat{O}_1(z_1) \cdots \hat{O}_k(z_k)\right\}$$
$$= \partial^{\theta}_{z_m} T_C \left\{\hat{O}_1(z_1) \cdots \hat{O}_k(z_k)\right\} \tag{2.33}$$
$$+ T_C \left\{\hat{O}_1(z_1) \cdots \left(\frac{d}{dz_m}\hat{O}_m(z_m)\right) \cdots \hat{O}_k(z_k)\right\},$$

where $\partial^{\theta}_{z_m}$ refers to differentiation with respect to the Heaviside terms in equation (2.22). Taking the time-derivative of a contour Heaviside function will give a contour delta function:

$$\delta(z, z') = \partial_z \theta(z, z') = -\partial_{z'} \theta(z, z'). \tag{2.34}$$

This fact will result in the appearance of commutator terms within the strings of operators. Given our interest in the operators found in section (2.1) and their commutator relations, we can restrict ourselves to operators that commute, giving us

$$[O_m(z), O_n(z)]_{\mp} = c_{mn} \tag{2.35}$$

where c_{mn} is a number such that we can write the first term in equation (2.33) as

$$\partial_{z_m}^{\theta} T_C \left\{ \hat{O}_1(z_1) \cdots \hat{O}_k(z_k) \right\} =$$

$$\sum_{l=1}^{m-1} (\pm)^{k-l} \delta(z_m, z_l) [O_m(z_m), O_l(z_m)]_{\mp} T_C \left\{ \hat{O}_1(z_1) \cdots \overset{\sqcap}{\hat{O}_l}(z_l) \cdots \overset{\sqcap}{\hat{O}_m}(z_m) \cdots \hat{O}_k(z_k) \right\}$$

$$+ \sum_{l=k+1}^{n} (\pm)^{l-k-1} \delta(z_m, z_l) [O_m(z_m), O_l(z_m)]_{\mp} T_C \left\{ \hat{O}_1(z_1) \cdots \overset{\sqcap}{\hat{O}_m}(z_m) \cdots \overset{\sqcap}{\hat{O}_l}(z_l) \cdots \hat{O}_k(z_k) \right\},$$

$$\tag{2.36}$$

where $\overset{\sqcap}{\hat{O}}$ denotes the removal of the operator from the string of operators.

We can utilize equations (2.27), (2.33) and (2.36) to generate equations of motion for the mixed Green's function of equation (2.28). The time derivative can be taken with respect to the three different operators. Taking the derivative with respect to a phononic term and making use of the Heisenberg equation of motion

$$i\frac{d}{dz}\hat{\phi}_{kH}(z) = \sum_{mn} \alpha_{km} \Omega_{mn} \hat{\phi}_{nH}(z) + \sum_{m,ij} \alpha_{km} M_{ij}^m \hat{d}_{iH}^\dagger(z) \hat{d}_{jH}(z) \tag{2.37}$$

gives us the first equation of motion for the mixed Green's function:

$$i\frac{d}{dz_{\widetilde{k}}} X_{m,n}(\widetilde{1}_{zv}, \cdots, \widetilde{k}_{zv}, \cdots, \widetilde{m}_{zv}; 1_{zp}, \cdots, n_{zp}; 1'_{zp}, \cdots, n'_{zp}) =$$

$$\sum_{\substack{k \neq l \\ l=1}}^{\widetilde{m}} \delta(z_{\widetilde{k}}, z_{\widetilde{l}}) \alpha_{v_{\widetilde{k}} \bar{v}_{\widetilde{l}}} X_{m-2,n}(\widetilde{1}_{zv}, \cdots, \overset{\sqcap}{\widetilde{k}_{zv}}, \cdots, \overset{\sqcap}{\widetilde{l}_{zv}}, \cdots, \widetilde{m}_{zv}; 1_{zp}, \cdots, n_{zp}; 1'_{zp}, \cdots, n'_{zp})$$

$$+ \sum_{u\zeta} \alpha_{v_{\widetilde{k}}\mu} \Omega_{\mu\zeta} X_{m,n}(\widetilde{1}_{zv}, \cdots, z_{\widetilde{k}}\zeta, \cdots, \widetilde{m}_{zv}; 1_{zp}, \cdots, n_{zp}; 1'_{zp}, \cdots, n'_{zp})$$

$$-i^{1/2} \sum_{wq} \sum_{\mu} \alpha_{v_{\widetilde{k}}\mu} M_{wq}^{\mu} X_{m-1,n+1}\left(\widetilde{1}_{zv}, \cdots, \overset{\sqcap}{\widetilde{k}_{zv}} \cdots, \widetilde{m}_{zv}; 1_{zp}, \cdots, n_{zp}, z_{\widetilde{k}}w; 1'_{zp}, \cdots, n'_{zp}, z_{\widetilde{k}}^+ q\right).$$

$$\tag{2.38}$$

The second equation of motion is given by taking the contour-time derivative of one of the electronic annihilation operators, making use of

$$i\frac{d}{dz}\hat{d}_{kH}(z) = \sum_{l} \epsilon_{kl}(z) \hat{d}_{lH}(z) + \sum_{l\bar{\mu}} M_{kl}^{\bar{\mu}} \hat{\phi}_{\bar{\mu}H}(z) \hat{d}_{lH}(z) + \sum_{qst} w_{kqst} \hat{d}_{qH}^\dagger(z) \hat{d}_{sH}(z) \hat{d}_{tH}(z) \tag{2.39}$$

to give us

$$i\frac{d}{dz_k}X_{m,n}(\widetilde{1}_{zv},\cdots,\widetilde{m}_{zv};1_{zp},\cdots,k_{zp},\cdots,n_{zp};1'_{zp},\cdots,n'_{zp}) =$$

$$\sum_{j'=1}^{n'}(-1)^{k+j'}\delta(k_{zp},j'_{zp})X_{m,n-1}(\widetilde{1}_{zv},\cdots,\widetilde{m}_{zv};1_{zp},\cdots,\overset{\sqcap}{k}_{zp},\cdots,n_{zp};1'_{zp},\cdots,\overset{\sqcap}{j'}_{zp},\cdots,n'_{zp})$$

$$+\sum_{l}\epsilon_{p_k l}(z_k)X_{m,n}(\widetilde{1}_{zv},\cdots,\widetilde{m}_{zv};1_{zp},\cdots,z_k l\cdots,n_{zp};1'_{zp},\cdots,n'_{zp}) \quad (2.40)$$

$$+i^{1/2}\sum_{l\mu}M^{\mu}_{p_k l}X_{m+1,n}(\widetilde{1}_{zv},\cdots,\widetilde{m}_{zv},z_k\mu;1_{zp},\cdots,z_k l\cdots,n_{zp};1'_{zp},\cdots,n'_{zp})$$

$$-i\sum_{qst}w_{p_k qst}X_{m,n+1}(\widetilde{1}_{zv},\cdots,\widetilde{m}_{zv};1_{zp},\cdots,z_k t,\cdots,n_{zp},z_k s;1'_{zp},\cdots,n'_{zp},z_k^+ q).$$

The third equation of motion is given by taking the contour-time derivative of one of the electronic creation operators, making use of

$$-i\frac{d}{dz}\hat{d}^{\dagger}_{kH}(z) = \sum_{l}\hat{d}^{\dagger}_{lH}(z)\epsilon_{lk}(z) + \sum_{l\bar{\mu}}\hat{\phi}_{\bar{\mu}H}(z)\hat{d}^{\dagger}_{lH}(z)M^{\bar{\mu}}_{kl} + \sum_{qst}\hat{d}^{\dagger}_{tH}(z)\hat{d}^{\dagger}_{sH}(z)\hat{d}_{qH}(z)w_{tsqk} \quad (2.41)$$

to gives us

$$-i\frac{d}{dz_{k'}}X_{m,n}(\widetilde{1}_{zv},\cdots,\widetilde{m}_{zv};1,\cdots,n;1',\cdots,k',\cdots,n') =$$

$$\sum_{j=1}^{n}(-1)^{j+k'}\delta(k_{zp},j'_{zp})X_{m,n-1}(\widetilde{1}_{zv},\cdots,\widetilde{m}_{zv};1_{zp},\cdots,\overset{\sqcap}{j}_{zp},\cdots,n_{zp};1'_{zp},\cdots,\overset{\sqcap}{k'}_{zp},\cdots,n'_{zp})$$

$$+\sum_{l}X_{m,n}(\widetilde{1}_{zv},\cdots,\widetilde{m}_{zv};1_{zp},\cdots,n_{zp};1'_{zp},\cdots,z_{k'}l,\cdots,n'_{zp})\epsilon_{lp_{k'}}(z_{k'}) \quad (2.42)$$

$$+i^{1/2}\sum_{l\mu}X_{m+1,n}(\widetilde{1}_{zv},\cdots,\widetilde{m}_{zv},z_{k'}\mu;1_{zp},\cdots,n_{zp};1'_{zp},\cdots,z_{k'}l,\cdots,n'_{zp})M^{\mu}_{lp_{k'}}$$

$$-i\sum_{qst}X_{m,n+1}(\widetilde{1}_{zv},\cdots,\widetilde{m}_{zv};1_{zp},\cdots,z_{k'}q,\cdots,n_{zp},z_{k'}t;1'_{zp},\cdots,n'_{zp},z_{k'}^+ s)w_{tsqp_k}.$$

Equations (2.38), (2.40) and (2.42) are the Martin-Schwinger hierarchy. From these equations, we can make two important observations: firstly, interactions lead to the lower-order Green's functions being dependent on higher-order Green's functions, which makes solving these equations exactly seemingly impossible; secondly, the noninteracting case sees higher-order Green's functions couple only to lower-order Green's functions, via the first term in equations (2.38), (2.40) and (2.42). We now turn our attention to this second fact.

2.3.2 Wick's Theorem

When considering the system as noninteracting, the Martin-Schwinger hierarchy reduces to equations of motion for the noninteracting Green's functions. Taking equation (2.40) as noninteracting and focusing on a purely electronic Green's functions gives us

$$
i\frac{d}{dz_k}g_n(1_{zp},\cdots,k_{zp},\cdots,n_{zp};1'_{zp},\cdots,n'_{zp}) - \sum_l \epsilon_{p_k l}(z_k)g_n(1_{zp},\cdots,z_k l\cdots,n_{zp};1'_{zp},\cdots,n'_{zp})
$$
$$
= \sum_{j'=1}^{n'}(-1)^{k+j'}\delta(k,j')g_{n-1}(1_{zp},\cdots,\overset{\sqcap}{k_{zp}},\cdots,n_{zp};1'_{zp},\cdots,\overset{\sqcap}{j'_{zp}},\cdots,n'_{zp}).
$$

(2.43)

The solution to equation (2.43) turns out to be a determinant made of the single-particle electronic Green's functions [59]:

$$
g_n(1_{zp},\cdots,k_{zp},\cdots,n_{zp};1'_{zp},\cdots,n'_{zp}) = \begin{vmatrix} g(1_{zp},1'_{zp}) & \cdots & g(1_{zp},n'_{zp}) \\ \vdots & & \vdots \\ g(n_{zp},1'_{zp}) & \cdots & g(n_{zp},n'_{zp}) \end{vmatrix}_-
$$
$$
= \sum_P (-)^{\zeta_P}\prod_{i=1}^n g(1_{zp},P(1'_{zp})).
$$

(2.44)

Here, we have used the definition of a determinant in terms of permutations, where ζ_P is the number of permutations for a particular permutation P. For the one-body electronic Green's function, equation (2.43) gives us

$$
i\frac{d}{dz_1}g(1_{zp},1'_{zp}) - \sum_l \epsilon_{p_1 l}(z_1)g(z_1 l,1'_{zp}) = \delta(1_{zp},1'_{zp}).
$$

(2.45)

For the phononic component, taking equation (2.38) as noninteracting gives

$$
\sum_\beta \left[i\alpha_{v_{\tilde{k}}\beta}\frac{d}{dz_{\tilde{k}}} - \Omega_{v_{\tilde{k}}\beta} \right] d_{0;m}(\widetilde{1}_{zv},\cdots,z_{\tilde{k}}\beta,\cdots,\widetilde{1}_{zv})
$$
$$
= \sum_{\substack{\tilde{k}\neq\tilde{l} \\ \tilde{l}=1}}^m \delta(\tilde{k}_{zv},\tilde{l}_{zv})d_{0;m-2}(\widetilde{1}_{zv},\cdots,\overset{\sqcap}{\tilde{k}_{zv}},\cdots,\overset{\sqcap}{\widetilde{1}_{zv}},\cdots,\widetilde{m}_{zv}).
$$

(2.46)

From equation (2.46), we see that the phonon Green's functions couples to diagrams whose order has the same parity: the m-order Green's function couples to $(m-2)$-order Green's functions, skipping the $(m-1)$-order Green's functions. For the 2-order Green's functions,

equation (2.46) reduces to

$$\sum_\beta \left[i\alpha_{\nu_{\tilde{1}}\beta} \frac{d}{dz_{\tilde{1}}} - \Omega_{\nu_{\tilde{1}}\beta} \right] d_{0;2}(z_{\tilde{1}}\beta, \tilde{1}'_{zv}) = \delta(\tilde{1}_{zv}, \tilde{1}'_{zv}). \tag{2.47}$$

However, the equation of motion for the 1-order Green's functions, $\phi(\tilde{1}_{zv}) = i^{1/2} d_{0;1}(\tilde{1}_{zv})$, cannot be calculated from (2.46) and needs to be derived from equation (2.37):

$$\sum_\beta \left[i\alpha_{\nu_{\tilde{1}}\beta} \frac{d}{dz_{\tilde{1}}} - \Omega_{\nu_{\tilde{1}}\beta} \right] \phi(z_{\tilde{1}}\beta) = -i \sum_{ij} M_{ij}^{\nu_{\tilde{1}}} G\left(z_{\tilde{1}}j, z_{\tilde{1}}^{+} i\right), \tag{2.48}$$

which has the solution

$$\phi(\tilde{1}_{zv}) = -i \int_C dz_x \sum_\mu \sum_{ij} d_{0;2}\left(z_{\tilde{1}}\nu_{\tilde{1}}, z_x\mu\right) M_{ij}^{\mu} G\left(z_x j, z_x^{+} i\right). \tag{2.49}$$

Equation (2.49) tells us that, for the noninteracting case, $\phi_0(\tilde{1}_{zv}) = 0$. This tells us that the higher order phonon Green's functions, containing an odd number of operators, will also go to zero, as they all depend on $\phi_0(\tilde{1}_{zv})$. For example,

$$\sum_\beta \left[i\alpha_{\nu_{\tilde{1}}\beta} \frac{d}{dz_{\tilde{1}}} - \Omega_{\nu_{\tilde{1}}\beta} \right] d_{0;3}(z_1\beta, \tilde{2}_{zv}, \tilde{3}_{zv}) = \delta(\tilde{1}_{zv}, \tilde{2}_{zv}) d_{0;1}(\tilde{3}_{zv}) + \delta(\tilde{1}_{zv}, \tilde{2}_{zv}) d_{0;1}(\tilde{2}_{zv}) = 0, \tag{2.50}$$

for which the solution is $d_{0;3}(\tilde{1}_{zv}, \tilde{2}_{zv}, \tilde{3}_{zv}) = 0$.

Focusing now on the even case, $m = 2n$, equations (2.46) and (2.47) can be used to cast the noninteracting phonon Green's function in the form

$$d_{0;2n}(\tilde{1}_{zv}, \cdots, \widetilde{2n}_{zv}) = \sum_{\substack{\tilde{k}\neq\tilde{l} \\ \tilde{l}=1}}^{\widetilde{2n}} d_{0;2}(\tilde{k}_{zv}, \tilde{l}_{zv}) d_{0;2n-2}(\tilde{1}_{zv}, \cdots, \overset{\sqcap}{\tilde{k}_{zv}}, \cdots, \overset{\sqcap}{\tilde{l}_{zv}}, \cdots, \widetilde{2n}_{zv}). \tag{2.51}$$

Equation (2.51) has a recursive form, meaning that $d_{0;2n}$ can be unraveled as all possible pairings of the $2n$ indices. This solution takes the form of a hafnian[66], which can be written in the compact form:

$$d_{0;2n}(\tilde{1}_{zv}, \cdots, \widetilde{2n}_{zv}) = \frac{1}{2^n n!} \sum_P \prod_{i=1}^n d_{0;2}(\widetilde{P(2i-1)}_{zv}, \widetilde{P(2i)}_{zv}). \tag{2.52}$$

2.3.3 Kubo-Martin-Schwinger Boundary Conditions

To solve equations (2.38), (2.40) and (2.42), unique boundary conditions, known as the Kubo-Martin-Schwinger relations, must be met:

$$
\begin{aligned}
& X_{m,n}(\widetilde{1}_{zv}, \cdots, (z_f \widetilde{v}_k), \cdots, \widetilde{m}_{zv}; 1_{zp}, \cdots, n_{zp}; 1'_{zp}, \cdots, n'_{zp}) \\
& = X_{m,n}(\widetilde{1}_{zv}, \cdots, (z_i \widetilde{v}_k), \cdots \widetilde{m}_{zv}; 1_{zp}, \cdots, n_{zp}; 1'_{zp}, \cdots, n'_{zp}),
\end{aligned}
\tag{2.53}
$$

$$
\begin{aligned}
& X_{m,n}(\widetilde{1}_{zv}, \cdots, \widetilde{m}_{zv}; 1_{zp}, \cdots, (z_f, p_k), \cdots, n_{zp}; 1'_{zp}, \cdots, n'_{zp}) \\
& = -X_{m,n}(\widetilde{1}_{zv}, \cdots \widetilde{m}_{zv}; 1_{zp}, \cdots, (z_i, p_k), \cdots, n_{zp}; 1'_{zp}, \cdots, n'_{zp})
\end{aligned}
\tag{2.54}
$$

and

$$
\begin{aligned}
& X_{m,n}(\widetilde{1}_{zv}, \cdots, (z_F \widetilde{v}_k), \cdots, \widetilde{m}_{zv}; 1_{zp}, \cdots, n_{zp}; 1'_{zp}, \cdots, (z_f, p'_k), \cdots, n'_{zp}) \\
& = -X_{m,n}(\widetilde{1}_{zv}, \cdots, (z_i \widetilde{v}_k), \cdots \widetilde{m}_{zv}; 1_{zp}, \cdots, n_{zp}; 1'_{zp}, \cdots, (z_i, p'_k), \cdots, n'_{zp}),
\end{aligned}
\tag{2.55}
$$

where z_i and z_f are the initial and final contour times. These relations follow from equation (2.28), given the cyclic property of the trace and the contour time-ordering.

The KMS relations also allow for the manipulation of the equations of motion for the one-body electronic Green's functions and the two-field phononic Green's functions, removing the differential component:

$$
\int d1_{zp} \sum_l g(1_{zp}, \underline{1}_{zp}) \left[\delta_{p_{\underline{1}}l} i \frac{d}{dz_{\underline{1}}} - \epsilon_{p_{\underline{1}}l}(z_{\underline{1}}) \right] G(z_{\underline{1}}l, 2_{zp}) = G(1_{zp}, 2_{zp})
\tag{2.56}
$$

and

$$
\int d\underline{1}_{zv} \sum_{\bar{v}} d(1_{zv}, \underline{1}_{zv}) \left[i\alpha_{v_{\underline{1}}\bar{v}} \frac{d}{dz_{\underline{1}}} - \Omega_{v_{\underline{1}}\bar{v}} \right] D(z_{\underline{1}}\bar{v}, 2_{zv}) = D(1_{zv}, 2_{zv}).
\tag{2.57}
$$

2.4 Many-Body Perturbation Theory

In section (2.3.1), we saw that deriving an equation of motion for the general mixed Green's function resulted in a Martin-Schwinger hierarchy, which saw Green's functions coupled to other Green's functions of higher order. This fact makes solving the Martin-Schwinger hierarchy for an exact solution seemingly impossible.

Thankfully, if we treat the interactions perturbatively, we can expand Green's functions in terms of the interaction coupling and the noninteracting Green's functions. We can see this

specifically with equation (2.28):

$$X_{m,n}(\widetilde{1}_{zv}, \cdots, \widetilde{m}_{zv}; 1_{zp}, \cdots, n_{zp}; 1'_{zp}, \cdots, n'_{zp}) =$$

$$\frac{Z_0}{Z} \sum_{k,\widetilde{l}=0}^{\infty} \frac{(-)^{\widetilde{l}} i^{\widetilde{l}/2+k}}{2^k k! \widetilde{l}!} \int d\widetilde{1}_{zvpq} \dots d\widetilde{l}_{zvpq} \; d1_{zpq} d1'_{zpq} \dots dk_{zpq} dk'_{zpq}$$

$$M(\widetilde{1}_{zvpq}) \cdots M(\widetilde{l}_{zvpq}) w(1_{zpq}, 1'_{zpq}) \cdots w(\underline{k}_{zpq}, \underline{k}'_{zpq}) \qquad (2.58)$$

$$\times d_{0:m+\widetilde{l}}(\widetilde{1}_{zv}, \cdots, \widetilde{m}_{zv}, \widetilde{1}_{zv} \cdots \widetilde{l}_{zv})$$

$$\times g_{n+\widetilde{l}+2k}(1_{zp}, \cdots, n_{zp}, \widetilde{1}_{zq}, \cdots, \widetilde{l}_{zq}, 1_{zq}, 1'_{zq}, \cdots, \underline{k}_{zq}, \underline{k}'_{zq}$$

$$; 1'_{zp}, \cdots, n'_{zp}, \widetilde{1}^+_{zp}, \cdots, \widetilde{l}^+_{zp}, 1^+_{zp} 1'^+_{zp}, \cdots, \underline{k}^+_{zp} \underline{k}'^+_{zp}),$$

where the partition function can also be expanded perturbatively as

$$Z = \mathrm{Tr}\left[T_C \left\{ e^{-i \int_C dz \hat{H}(z)} \right\} \right] =$$

$$Z_0 \sum_{k,\widetilde{l}=0}^{\infty} \frac{(-)^{\widetilde{l}} i^{\widetilde{l}/2+k}}{2^k k! \widetilde{l}!} \int d\widetilde{1}_{zvpq} \dots d\widetilde{l}_{zvpq} \; d1_{zpq} d1'_{zpq} \dots dk_{zpq} dk'_{zpq}$$

$$M(\widetilde{1}_{zvpq}) \cdots M(\widetilde{l}_{zvpq}) w(1_{zpq}, 1'_{zpq}) \cdots w(\underline{k}_{zpq}, \underline{k}'_{zpq}) \qquad (2.59)$$

$$\times d_{0:\widetilde{l}}(\widetilde{1}_{zv} \cdots \widetilde{l}_{zv})$$

$$\times g_{\widetilde{l}+2k}(\widetilde{1}_{zq}, \cdots, \widetilde{l}_{zq}, 1_{zq}, 1'_{zq}, \cdots, \underline{k}_{zq}, \underline{k}'_{zq}$$

$$; \widetilde{1}^+_{zp}, \cdots, \widetilde{l}^+_{zp}, 1^+_{zp} 1'^+_{zp}, \cdots, \underline{k}^+_{zp} \underline{k}'^+_{zp}).$$

Here, we introduce the shorthand of $\underline{k}^{\pm}_{zp}$, where the addition of a plus/minus in the super-script should be read as an infinitesimal increment/decrement of z_k. We also introduce the shorthand $w(1_{zpq}, 1'_{zpgq}) = w_{p_1 p_{1'} q_{1'} q_1} \delta(z_1, z_{1'})$ and $M(1_{zvpq}) = M^{v_1}_{p_1 q_1}$ for the interaction terms.

Taking to the terms in equation (2.58) with Wick's theorem results in a collection of nonin-teracting single-body electron Green's functions and noninteracting second order phononic Green's functions, sewn together by integrals over connecting interaction terms. These objects are central to the perturbative solutions of the Green's functions and have been studied widely [59–65] and when expressed diagrammatically, they are the well-known Feynman diagrams. Currently, the terms that make up the equation (2.58) are not as tractable as they can be. Three observations can help improve the calculations of our diagrams: the loop rule, the reduction to connected terms, and the reduction to topologically inequivalent diagrams.

2.4.0.1 Loop Rule

The loop rule is concerned with finding the sign for any given Feynman diagram. From equa-tion (2.58), this is given as the $(-)^{\widetilde{l}}(-)^{\zeta_P}$ where $\widetilde{l}$ is the number of electron-phonon interaction terms, denoted by M, and P is associated with a particular permutation that comes from the

determinant we see in the electronic realization of Wick's theorem, as seen in equation (2.44). The term from Wick's theorem that corresponds with the identity permutation and which would be found in equation (2.58) is the following:

$$g(1_{zp}, 1'_{zp}) \cdots g(n_{zp}, n'_{zp}) g(\widetilde{1}_{zq}, \widetilde{1}^+_{zp}) \cdots g(\widetilde{l}_{zq}, \widetilde{l}^+_{zp}) g(\underline{1}_{zq}, \underline{1}^+_{zp}) g(\underline{1}'_{zq}, \underline{1}'^+_{zp}) \cdots g(\underline{k}_{zq}, \underline{k}^+_{zp}) g(\underline{k}'_{zq}, \underline{k}'^+_{zp}).$$

(2.60)

In equation (2.60), the Green's functions that enter due to the interaction terms have the form $g(z, z^+)$, which constitutes a loop. A loop is any chain of Green's functions whose contour times "loop" around to the beginning time, i.e., $g(z_1, z_2) g(z_2, z_3) ... g(z_{x-1}, z_x) g(z_x, z_1)$. The Green's functions that enter into (2.60) that do not come from interaction terms, i.e., $g(1_{zp}, 1'_{zp}) \cdots g(n_{zp}, n'_{zp})$, are open as opposed to closed in a loop. We can imagine closing these open terms by equating z_1 and $z_{1'}$. Then, all the electronic Green's functions in equation (2.60) are closed on themselves to create a loop. We can count the number of loops for the identity permutation as $L_i = n + \widetilde{l} + 2k$ such that $(-)^{\zeta_{P_i}}(-)^{\widetilde{l}} = (-)^{\widetilde{l}} = (-)^{L_i + n}$.

Thinking of equation (2.60) in this closed form is convenient when considering permutations beyond the identity permutation, as the joining of loops or the creation of new loops through the separation of larger loops corresponds with transpositions that result in the different permutations found in equation (2.44). This means that the number of loops relates the parity of a particular permutation by $(-)^{\zeta_P} = (-)^{L - L_i}$.

We can put these observations together to get a final loop rules:

$$(-)^{\zeta_P}(-)^{\widetilde{l}} = (-)^{\zeta_P}(-)^{L_i + n} = (-)^{\zeta_P + L_i}(-)^n = (-)^L(-)^n.$$

(2.61)

This result relates the sign of a diagram to two simple facts: the number of loops, given we close the pairs of open terms by moving z_1 onto z'_1 and the number of open terms.

2.4.0.2 Reduction to connected terms

Equations (2.58) will have terms for a given order of k and $\widetilde{l}$ that will factorize into terms with outgoing parameters and unconnected vacuum diagrams. These terms may contain the same connected components but only differ by a multiplied vacuum diagram, which itself can be made of one or many vacuum diagrams multiplied together. These insights suggest

we express the express equation (2.58) as a series of outgoing and vacuum terms:

$$X_{m,n}(\widetilde{1}_{zv}, \cdots, \widetilde{m}_{zv}; 1_{zp}, \cdots, n_{zp}; 1'_{zp}, \cdots, n'_{zp})$$

$$= \frac{Z_0}{Z} \sum_{k,\widetilde{l}=0}^{\infty} \frac{(-)^{\widetilde{l}} i^{\widetilde{l}/2+k}}{2^k k! \widetilde{l}!} \sum_{k'=0}^{k} \sum_{\widetilde{l}'=0}^{\widetilde{l}} \binom{k}{k!} \binom{\widetilde{l}}{\widetilde{l}'} \sum_{p \in \left\{ \substack{connected \\ diagrams} \right\}} \sum_{q \in \left\{ \substack{vacuum \\ diagrams} \right\}} (-)^{L+j} \tag{2.62}$$

$$X_{out,p}^{(k',\widetilde{l}')}(\widetilde{1}_{zv}, \cdots, \widetilde{m}_{zv}; 1_{zp}, \cdots, n_{zp}; 1'_{zp}, \cdots, n'_{zp}) V_q^{(k-k',\widetilde{l}-\widetilde{l}')},$$

where $X_{out,p}^{(k',\widetilde{l}')}$ is the pth possible connected diagram with k' electron-electron interaction terms and $\widetilde{l}'$ electron-phonon interaction terms and $V_q^{(k-k',\widetilde{l}-\widetilde{l}')}$ is the qth possible realisation of a single or multiple vacuum diagrams with $k - k'$ electron-electron interaction terms and $\widetilde{l} - \widetilde{l}'$ electron-phonon interaction terms. Within equation (2.62), L and j refer to the whole diagram. However, the loop rule is satisfied for each constituent part of the diagram with $L = L_p + L_q$. This allows us to rearrange equation (2.62) for

$$X_{m,n}(\widetilde{1}_{zv}, \cdots, \widetilde{m}_{zv}; 1_{zp}, \cdots, n_{zp}; 1'_{zp}, \cdots, n'_{zp})$$

$$= \frac{Z_0}{Z} \sum_{k,\widetilde{l}=0}^{\infty} \sum_{k'=0}^{k} \sum_{\widetilde{l}'=0}^{\widetilde{l}} \left[\frac{i^{\widetilde{l}'/2+k'}}{2^{k'} k'! \widetilde{l}'!} \sum_{p \in \left\{ \substack{connected \\ diagrams} \right\}} (-)^{L_p-j} X_{out,p}^{(k',\widetilde{l}')}(\cdots) \right]$$

$$\times \left[\frac{i^{(\widetilde{l}-\widetilde{l}')/2+(k-k')}}{2^{(k-k')}(k-k')!(\widetilde{l}-\widetilde{l}')!} \sum_{q \in \left\{ \substack{vacuum \\ diagrams} \right\}} (-)^{L_q+j} V_q^{(k-k',\widetilde{l}-\widetilde{l}')} \right] \tag{2.63}$$

$$= \frac{Z_0}{Z} \sum_{k,\widetilde{l}=0}^{\infty} \sum_{k'=0}^{k} \sum_{\widetilde{l}'=0}^{\widetilde{l}} X_{out}^{(k',\widetilde{l}')}(\cdots) V^{(k-k',\widetilde{l}-\widetilde{l}')},$$

where we have collected all terms relating to the connected and vacuum diagrams into $X_{out}^{(k',\widetilde{l}')}(\cdots)$ and $V^{(k-k',\widetilde{l}-\widetilde{l}')}$ respectively.

Casting the mixed Green's functions in the form of equation (2.63) highlights the points made above: the complete diagrams consist of all possible connected diagrams multiplied on all possible combinations of vacuum diagrams. From here, we can cast all the possible combinations

of vacuum diagrams in terms of the partition function:

$$
X_{m,n}(\widetilde{1}_{zv}, \cdots, \widetilde{m}_{zv}; 1_{zp}, \cdots, n_{zp}; 1'_{zp}, \cdots, n'_{zp})
$$

$$
= \frac{Z_0}{Z} \sum_{k=0}^{\infty} \sum_{\widetilde{l}=0}^{\infty} \sum_{k'=0}^{k} \sum_{\widetilde{l}'=0}^{\widetilde{l}} X_{out}^{(k',\widetilde{l}')}(\cdots) V^{(k-k',\widetilde{l}-\widetilde{l}')}
$$

$$
= \frac{Z_0}{Z} \sum_{k=0}^{\infty} \sum_{\widetilde{l}=0}^{\infty} \sum_{k'=0}^{\infty} \sum_{\widetilde{l}'=0}^{\infty} \delta_{k \geq k'} \delta_{\widetilde{l} \geq \widetilde{l}'} X_{out}^{(k',\widetilde{l}')}(\cdots) V^{(k-k',\widetilde{l}-\widetilde{l}')}
$$

$$
= \frac{Z_0}{Z} \sum_{k'=0}^{\infty} \sum_{\widetilde{l}'=0}^{\infty} \sum_{k=k'}^{\infty} \sum_{\widetilde{l}=\widetilde{l}'}^{\infty} X_{out}^{(k',\widetilde{l}')}(\cdots) V^{(k-k',\widetilde{l}-\widetilde{l}')}
$$

$$
= \frac{Z_0}{Z} \sum_{k'=0}^{\infty} \sum_{\widetilde{l}'=0}^{\infty} \sum_{k=0}^{\infty} \sum_{\widetilde{l}=0}^{\infty} X_{out}^{(k',\widetilde{l}')}(\cdots) V^{(k,\widetilde{l})}
$$

$$
= \frac{Z_0}{Z} \sum_{k'=0}^{\infty} \sum_{\widetilde{l}'=0}^{\infty} X_{out}^{(k',\widetilde{l}')}(\cdots) \left(\sum_{k=0}^{\infty} \sum_{\widetilde{l}=0}^{\infty} V^{(k,\widetilde{l})} \right)
$$

$$
= \frac{Z_0}{Z} \sum_{k'=0}^{\infty} \sum_{\widetilde{l}'=0}^{\infty} X_{out}^{(k',\widetilde{l}')}(\cdots) \left(\frac{Z}{Z_0} \right)
$$

$$
= \sum_{k'=0}^{\infty} \sum_{\widetilde{l}'=0}^{\infty} X_{out}^{(k',\widetilde{l}')}(\cdots).
$$

(2.64)

Here, the substitution $\sum_{k=0}^{\infty} \sum_{\widetilde{l}=0}^{\infty} V^{(k,\widetilde{l})} = Z/Z_0$ is made, which is follows from equation (2.59). This final manipulation shows how the vacuum diagrams generated as a part expansion of the numerator in equation (2.58) cancel those present due to to the denominator term of the Green's function, as seen in equation (2.28).

2.4.0.3 Reduction to topologically inequivalent terms

As laid out in equation (2.58), the expansion of the mixed Green's function contains integrals over the parameters associated with the interaction terms. Some of these dummy variables can be interchanged but do not affect the resultant calculation. The combination of dummy variables that can be interchanged depends on the nature of the interactions.

For the electron-electron interactions, the interchange of terms related to one instance of interaction, given by w, with another, i.e.

$$
\cdots w(1_{zpq}, 1'_{zpq}) w(2_{zpq}, 2'_{zpq}) \cdots \to \cdots w(2_{zpq}, 2'_{zpq}) w(1_{zpq}, 1'_{zpq}) \cdots,
$$

(2.65)

will result in the same calculation. This means that the terms of equation (2.58) with k interactions will have groupings of contributions that are equivalent. These groupings will be $k!$ large as this number of possible permutations of the k interaction lines. The electron-electron

interaction terms also have the property that

$$w(1_{zpq}, 1'_{zpq}) = w(1'_{zpq}, 1_{zpq}). \tag{2.66}$$

This symmetry means that every pair of dummy variables associated with a single interaction can be interchanged. This will result in terms of equation (2.58) with k interactions having groupings of contributions that are equivalent and 2^k large. For the electron-phonon interaction terms, denoted by M, equation (2.58) will $\widetilde{l}!$ terms that will be equivalent given the interchange of dummy variables.

We see that denominators in equation (2.58), the term $2^k k! \widetilde{l}!$, disappears upon observing that many of the terms contribute equally. These diagrams that contribute equally to $X_{m,n}$ are called topological equivalent because if one were to draw these diagrams, specifying the positions of specific interactions terms in the picture, topologically equivalent terms, due to various interchanges and flippings of interaction terms, would result in equivalent contributions to calculations. This makes drawing these diagrams simpler, as we need only worry about drawing diagrams that are topologically inequivalent.

2.4.0.4   Recap

The insights garnered above have significantly simplified the calculation of equation (2.58), which we can now write in the simplified form of

$$X_{m,n}(\widetilde{1}_{zv}, \cdots, \widetilde{m}_{zv}; 1_{zp}, \cdots, n_{zp}; 1'_{zp}, \cdots, n'_{zp}) =$$

$$\sum_{k,\widetilde{l}=0}^{\infty} i^{\widetilde{l}/2+k} \sum_{p \in \left\{ \substack{diagrams \\ (k,\widetilde{l})} \right\}} (-)^{L_p+n} X^p_{m,n\,(t.in.c)}(\widetilde{1}_{zv}, \cdots, \widetilde{m}_{zv}; 1_{zp}, \cdots, n_{zp}; 1'_{zp}, \cdots, n'_{zp}), \tag{2.67}$$

where $X^p_{m,n\,(t.in.c)}$ stands for a particular diagram p, containing k electron-electron interaction terms and $\widetilde{l}$ electron-phonon interaction terms, which is topologically inequivalent and connected and L_p is the number of electronic loops within $X^p_{m,n\,(t.in.c)}$ given we close the n pairs of outgoing electron terms.

We can understand equation (2.67) a simple recipe for calculating the terms for $X_{m,n}$:

1. Draw the diagram.

2. Translate this diagram to algebraic form. Within the text, we use the following diagram-

matic representations of our algebraic objects:

$$g(1_{zp}, 2_{zp}) \equiv \quad \underset{1_{zp} \qquad 2_{zp}}{\longleftarrow} \quad , \tag{2.68}$$

$$d(1_{zp}, 2_{zp}) \equiv \quad \underset{1_{zp} \qquad 2_{zp}}{\wwwww} \quad , \tag{2.69}$$

$$w(1_{zpq}, 2_{zpq}) \equiv \quad \underset{1_{zpq} \qquad 2_{zpq}}{\cdots\cdots} \tag{2.70}$$

and

$$M(\tilde{1}_{zvpq}) \equiv \quad \underset{}{\rangle\!\!\!\!\!\!\wwww} . \tag{2.71}$$

3. Multiply this diagram on the following prefactors:

- Multiply by $i^{\tilde{l}/2}$, where $\tilde{l}$ is the number of times M occurs.

- Multiply by i^k, where k is how many times w occurs.

- Multiply by $(-)^j$, where j is the number of incoming/outcoming electronic pairs.

- Multiply by $(-)^{L_c}$, where L_c is the number of electronic loops given you close all the incoming/outcoming electronic pairs into themselves.

These simple rules allow us to translate any diagrams into algebra to be calculated. However, for this thesis, we focus on two particular Green's functions, equations (2.29), (**??**) and (2.31), for which we can write simplified rules. For both the single-body electronic Green's function and the two-field phononic Green's functions, we have the following rules which follow from the above:

1. Draw the diagram.

2. Translate the diagram to algebraic form.

3. Multiply this diagram on the following prefactors:

- Multiply by $(i)^{\tilde{l}/2}$, where $\tilde{l}$ is the number of times M occurs.

- Multiply by i^k, where k is how many times w occurs.

- Multiply by $(-)^L$, where L is the number of electronic loops.

These rules are best understood when applied to examples. Figure (2.1) can be converted to algebraic following the above rules:

- We transform the diagram to algebraic and get the following:

$$
\begin{aligned}
G^{(2)}(1_{zq}, 1'_{zp}) \sim \int &d\underline{1}_{zpq} d2_{zpq} d\widetilde{\underline{1}}_{zp} d\widetilde{2}_{zp} \\
&g(1_{zq}, \underline{1}_{zp}) g(\underline{1}_{zq}, \widetilde{1}_{zp}) g(\widetilde{1}_{zq}, 1'_{zp}) \\
\times w(\underline{1}_{zpq}, 2_{zpq}) &M(\widetilde{\underline{1}}_{zvpq}) d(\widetilde{\underline{1}}_{zv}, \widetilde{2}_{zv}) M(\widetilde{2}_{zvpq}) \\
&\times g(2_{zq}, \widetilde{2}_{zp}) g(\widetilde{2}_{zq}, 2_{zp}).
\end{aligned}
\tag{2.72}
$$

- We multiply the above on the following prefactors: i for the electron-electron interaction term, $i^{2/2}$ for the two electron-phonon coupling terms and $(-)$ for the electronic loop. This gives us a net prefactor of 1, so we find that

$$
\begin{aligned}
G^{(2)}(1_{zq}, 1'_{zp}) = \int &d\underline{1}_{zpq} d2_{zpq} d\widetilde{\underline{1}}_{zvpq} d\widetilde{2}_{zvpq} \\
&g(1_{zq}, \underline{1}_{zp}) g(\underline{1}_{zq}, \widetilde{1}_{zp}) g(\widetilde{1}_{zq}, 1'_{zp}) \\
\times w(\underline{1}_{zpq}, 2_{zpq}) &M(\widetilde{\underline{1}}_{zvpq}) d(\widetilde{\underline{1}}_{zv}, \widetilde{2}_{zv}) M(\widetilde{2}_{zvpq}) \\
&\times g(2_{zq}, \widetilde{2}_{zp}) g(\widetilde{2}_{zq}, 2_{zp}).
\end{aligned}
\tag{2.73}
$$
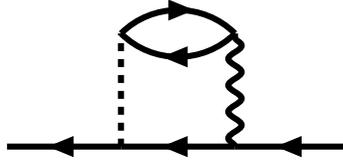
Figure 2.1: An example of a single-body electronic Green's function Feynman diagram.

2.4.1 Self-Energies and dressed Green's functions

The above section introduces the basic building blocks of quantum many-body perturbation theory. However, further manipulation is necessary if one wishes to capture contributions to the perturbation expansion beyond explicitly expressed terms. This can be achieved most notably by the resummation of diagrams.

As seen in figure (2.1), the contributions to the electronic Green's functions, as defined in equation (2.29), have the following form

$$
\tag{2.74}
$$

which we can write algebraically as

$$
\int d\underline{1}_{zp} d2_{zp}\, g(1_{zp}, \underline{1}_{zp}) \Sigma(\underline{1}_{zp}, 2_{zp}) g(2_{zp}, 1'_{zp}).
\tag{2.75}
$$

This object Σ is called the electronic self-energy or self-energy insertion. A self-energy is any diagram that can be separated from the rest of the diagram by cutting two electronic Green's functions. The self-energy allows us to begin summing a series of diagrams of the following form:

$$(2.76)$$

or written algebraically as

$$G(1_{zp}, 2_{zp}) = g(1_{zp}, 2_{zp}) + \int d\underline{1}_{zp} d\underline{2}_{zp} \, g(1_{zp}, \underline{1}_{zp}) \Sigma(\underline{1}_{zp}, \underline{2}_{zp}) g(\underline{2}_{zp}, 2_{zp}) +$$

$$\int d\underline{1}_{zp} d\underline{2}_{zp} d\underline{3}_{zp} d\underline{4}_{zp} \, g(1_{zp}, \underline{1}_{zp}) \Sigma(\underline{1}_{zp}, \underline{2}_{zp}) g(\underline{2}_{zp}, \underline{3}_{zp}) \Sigma(\underline{3}_{zp}, \underline{4}_{zp}) g(\underline{4}_{zp}, 2_{zp}) + \cdots$$

$$= g(1_{zp}, 2_{zp}) + \int d\underline{1}_{zp} d\underline{2}_{zp} \, g(1_{zp}, \underline{1}_{zp}) \Sigma(\underline{1}_{zp}, \underline{2}_{zp}) G(\underline{2}_{zp}, 2_{zp})$$

$$= g(1_{zp}, 2_{zp}) + \int d\underline{1}_{zp} d\underline{2}_{zp} \, G(1_{zp}, \underline{1}_{zp}) \Sigma(\underline{1}_{zp}, \underline{2}_{zp}) g(\underline{2}_{zp}, 2_{zp}),$$

$$(2.77)$$

where we define the full Green's function diagrammatically, as set out in equation (2.29), as

$$G(1_{zp}, 2_{zp}) \quad \equiv \quad \underset{1_{zp} \qquad\quad 2_{zp}}{\text{———◀———}} \quad . \tag{2.78}$$

Equation (2.77) is called the Dyson equation. Given that any contribution to the electronic Green's function can be cast as a self-energy, equation (2.77) is exact when considering the self-energy term to contain all possible self-energy insertions.

A similar analysis can be made for the two-field phononic Green's function, equation (2.31), with contributions that follow the form

$$(2.79)$$

where the object Π is called the phononic self-energy, with the phononic Green's function D_0,

as defined in equation (2.31), having an expansion of the form:

$$D_0 = \text{〜〜〜} + \text{〜〜〜}\Pi_0\text{〜〜}$$

$$+ \text{〜〜〜}\Pi_0\text{〜〜〜}\Pi_0\text{〜〜} + \cdots . \tag{2.80}$$

Among the diagrams within this expansion are diagrams with outgoing phononic Green's functions disconnected from each other. These double "tadpole" diagrams can be shown to sum to $\phi(1_{zv})\phi(1'_{zv})$, where ϕ is the average phonon fields, as seen in equation (2.49):

$$\text{〜〜 ⊙ ⊙〜〜} = \text{〜〜 ○ ○〜〜}$$

$$+ \text{〜〜 ○ ○···○〜〜} + \text{〜〜 ○〜○ ○〜〜} \tag{2.81}$$

$$+ \text{〜〜 ⑧ ○〜〜} + \text{〜〜 ○ ⊙〜〜} + \cdots .$$

If we remove these terms from D_0, we are left with D, as defined in equation (2.32). Moreover, the expansion of D can now be seen to follow a Dyson equation:

$$\text{〰〰〰} = \text{〜〜〜} + \text{〜〜〜}\Pi\text{〜〜}$$

$$+ \text{〜〜〜}\Pi\text{〜〜〜}\Pi\text{〜〜} + \cdots \tag{2.82}$$

$$= \text{〜〜〜} + \text{〜〜〜}\Pi\text{〰〰} ,$$

which can be expressed algebraically as

$$D(1_{zv}, 2_{zv}) = d(1_{zv}, 2_{zv}) + \int d\underline{1}_{zv}d\underline{2}_{zv}\, d(1_{zv}, \underline{1}_{zv})\Pi(\underline{1}_{zv}, \underline{2}_{zv})d(\underline{2}_{zv}, 2_{zv}) +$$

$$\int d\underline{1}_{zv}d\underline{2}_{zv}d\underline{3}_{zv}d\underline{4}_{zv}\, d(1_{zv}, \underline{1}_{zv})\Pi(\underline{1}_{zv}, \underline{2}_{zv})d(\underline{2}_{zv}, \underline{3}_{zv})\Pi(\underline{3}_{zv}, \underline{4}_{zv})d(\underline{4}_{zv}, 2_{zv}) + \cdots$$

$$= d(1_{zv}, 2_{zv}) + \int d\underline{1}_{zv}d\underline{2}_{zv}\, d(1_{zv}, \underline{1}_{zv})\Pi(\underline{1}_{zv}, \underline{2}_{zv})D(\underline{2}_{zv}, 2_{zv}) \tag{2.83}$$

$$= d(1_{zv}, 2_{zv}) + \int d\underline{1}_{zv}d\underline{2}_{zv}\, D(1_{zv}, \underline{1}_{zv})\Pi(\underline{1}_{zv}, \underline{2}_{zv})d(\underline{2}_{zv}, 2_{zv}),$$

where D is expressed diagrammatically as

$$D(1_{zv}, 2_{zv}) \;\equiv\; \underset{1_{zv} \qquad\quad 2_{zv}}{\text{〰〰〰〰}} . \tag{2.84}$$

The phononic self-energies within Π consist of diagrams that cannot be separated from the external vertices by removing two d lines.

In their current forms, the electronic and phononic self-energies are constructed with the non-interacting Green's functions g and d. To include more diagrams self-consistently, replacing the noninteracting Green's functions within these self-energies with full Green's functions is often convenient. To avoid erroneously including some diagrams twice, we must only dress the skeletonic diagrams, which means disregarding self-energy diagrams that contain other self-energies diagrams, called self-energy insertions. This process must be completed for both the electronic self-energies and the phononic self-energies, resulting in $\Sigma[g, d] = \Sigma_{ss}[G, D]$ and $\Pi[g, d] = \Pi_{ss}[G, D]$, where Σ_{ss} and Π_{ss} are the skeletonic electronic and phononic self-energy diagrams for both the electronic and phononic insertions respectively. The Feynman rules for both the electronic and phononic self-energies are the same as those found in section 2.4.0.4, with, in the dressed Green's functions being treated same as the undressed Green's functions.

2.4.2 Kadanoff-Baym Equations

The Dyson equations (2.76) and (2.82) can be rearranged for integro-differential equations of motion by utilizing equations (2.45) and (2.47) to remove the noninteracting Green's functions:

$$\sum_l \left[\delta_{p_1 l} i \frac{d}{dz_1} - \epsilon_{p_1 l}(z_1) \right] G(z_1 l, 2_{zp}) = \delta_{p_1 p_2} \delta(z_1, z_2) + \int d\underline{1}_{zp} \Sigma(1_{zp}, \underline{1}_{zp}) G(\underline{1}_{zp}, 2_{zp}) \tag{2.85}$$

and

$$\sum_\beta \left[i\alpha_{v_1 \beta} \frac{d}{dz_1} - \Omega_{v_1 \beta} \right] D(z_1 \beta, 2_{zv}) = \delta_{v_1 v_2} \delta(z_1, z_2) + \int d\underline{1}_{zv} \Pi(1_{zv}, \underline{1}_{zv}) D(\underline{1}_{zv}, 2_{zv}). \tag{2.86}$$

These are the Kadanoff-Baym equations for the electronic and phononic Green's functions, respectively. They provide an alternative path to solving Dyson's equations, which will be used in the following chapters.

2.4.3 Conserving Approximations

For a given the choice of self-energies, conservation laws need to be satisfied. These include laws for conserving particle number, energy, and momentum within and between the system and the environment. Clear examples are the particle and energy current conservation for the case of a molecular junction:

$$\sum_\alpha I_\alpha(t) = \frac{dN(t)}{dt} \tag{2.87}$$

and

$$\sum_\beta J_\beta(t) = \frac{dE(t)}{dt}. \tag{2.88}$$

$$-\Phi_H[G,D] \;=\; \frac{1}{2}\ \text{<image>}\ +\ \frac{1}{2}\ \text{<image>}$$

Figure 2.2: The diagrams for the Hartree terms of the Luttinger-Ward functional.

$$-\Phi_{xc}[G,D] \;=\; \frac{1}{2}\ \text{<image>}\ +\ \frac{1}{2}\ \text{<image>}\ +\ \cdots$$

Figure 2.3: A sample of diagrams for the exchange terms of the Luttinger-Ward functional.

Here, $I_\alpha(t)$ stands for the particle current, $J_\beta(t)$ the energy current, $N(t)$ the total particle number for the system, $E(t)$ the total energy of the system and α and β stand for the possible pathways through which particles and energy can be exchanged with the environment, respectively.

The satisfying of these conservation laws can be achieved by choosing diagrams such that they are Φ-derivable [59, 60, 67]:

$$\Sigma_{ss}[G,D](1,1') = \frac{\delta\Phi[G,D]}{\delta G(1',1)} \tag{2.89}$$

and

$$\begin{aligned}
\Pi_{ss}[G,D](1,1') &= -2\frac{\delta\Phi_{xc}[G,D]}{\delta D(1,1')}\bigg|_s \\
&= -\frac{\delta\Phi_{xc}[G,D]}{\delta D(1,1')} - \frac{\delta\Phi_{xc}[G,D]}{\delta D(1',1)},
\end{aligned} \tag{2.90}$$

where $\Phi[G,D] = \Phi_H[G,D] + \Phi_{xc}[G,D]$ are the terms of the Luttinger-Ward functionals that contribute the Hartree and exchange diagrams, respectively. Diagrammatically, the process of taking a functional derivative, as seen in equations (2.89) and (2.90), can be understood as the removal of the electronic or phononic line, depending on the functional derivative taken. This can be seen if we compare the second term in figure 2.3 to the self-energies it generates in figure 5.1.

The object Φ is known as the Luttinger-Ward functional and, in the case of both dressed G and D, is all connected, topologically inequivalent G- and D-skeletonic vacuum diagrams multiplied on specific prefactors. These prefactors are the same as those for the electronic self-energies, given in section 2.4.0.4, with an additional minus because of the functional derivative destroying an electronic loop and a further division by the number of symmetries with the vacuum diagram in question, so eliminate the possibility of double-counting diagrams.

A subset of diagrams of the Luttinger-Ward functions can be taken to approximate the dynamics of the system in question, with the electronic and phononic self-energies generated with equations (2.89) and (2.90). There are many popular conserving approximations (Hartree-Fock, self-consistent Born approximation, GW, T-matrix, FLEX, etc.), and their applicability depends on the system under investigation [63, 64]. In addition, the lead and bath self-energy terms (see section 2.4.8 and 2.4.9) can be cast as contributions to Luttinger-Ward functionals, resulting in conserving approximation when added to the contributions due to the correlations.

2.4.4 From the Contour to Real Time

In their current form, the Green's functions are on the Keldysh contour. When completing calculations, it is beneficial to cast the objects of interest, like the Green's functions, in terms of real time. We focus on functions with two contour-time parameters, which have the structure

$$A(z, z') = \theta(z, z') A^>(t, t') + \theta(z', z) A^<(t, t'), \tag{2.91}$$

where the real-time greater projection, $A^>(t, t')$ has the property that $z > z'$, and the lesser projection, $A^<(t, t')$, has the property $z < z'$. We have further projections in the form of the time-ordered projection,

$$A^T(t, t') = \theta(t - t') A^>(t, t') + \theta(t' - t) A^<(t, t'), \tag{2.92}$$

the anti-time-ordered projection,

$$A^{\tilde{T}}(t, t') = \theta(t' - t) A^>(t, t') + \theta(t - t') A^<(t, t'), \tag{2.93}$$

the retarded projection,

$$A^R(t, t') = \theta(t - t') \left[A^>(t, t') - A^<(t, t') \right], \tag{2.94}$$

and the advanced projection

$$A^A(t, t') = \theta(t' - t) \left[A^<(t, t') - A^>(t, t') \right]. \tag{2.95}$$

These projections can be shown to be related via

$$A^T(t, t') + A^{\tilde{T}}(t, t') = A^<(t, t') + A^>(t, t'). \tag{2.96}$$

It is often convenient to express the object $A(z, z')$ in terms of a 2×2 matrix in the Schwinger-

Keldysh space [68]:

$$A(z,z') \rightarrow \hat{A}(t,t') = \begin{pmatrix} A^{--}(t,t') & A^{-+}(t,t') \\ A^{+-}(t,t') & A^{++}(t,t') \end{pmatrix} = \begin{pmatrix} A^T(t,t') & A^<(t,t') \\ A^>(t,t') & A^{\tilde{T}}(t,t') \end{pmatrix}. \tag{2.97}$$

Here, the object A on the contour has two times, z and z', which can exist on the forward branch, denoted by a minus sign, or the backward branch, denoted by a plus sign. Given equation (2.96), only three projections are necessary to describe the dynamics. A popular combination is the advanced, retarded, and lesser projections relatable to equation (2.97)

$$\hat{U}\hat{A}(t,t')\hat{W} = \begin{pmatrix} I & 0 \\ I & -I \end{pmatrix} \begin{pmatrix} A^T(t,t') & A^<(t,t') \\ A^>(t,t') & A^{\tilde{T}}(t,t') \end{pmatrix} \begin{pmatrix} I & 0 \\ -I & I \end{pmatrix}$$

$$= \begin{pmatrix} A^T(t,t') - A^<(t,t') & A^<(t,t') \\ 0 & A^<(t,t') - A^{\tilde{T}}(t,t') \end{pmatrix} = \begin{pmatrix} A^R(t,t') & A^<(t,t') \\ 0 & A^A(t,t') \end{pmatrix}. \tag{2.98}$$

Equation (2.98) also allow us to recast equation (2.96) in terms of the retarded and advanced projections:

$$A^R(t,t') - A^A(t,t') = A^>(t,t') - A^<(t,t'). \tag{2.99}$$

Several important composite objects need to be evaluated in real time:

$$C(z,z') = \int_c d\underline{z}\, A(z,\underline{z}) B(\underline{z},z'), \tag{2.100}$$

$$D(z,z') = A(z,z') B(z,z') \tag{2.101}$$

and

$$E(z,z') = A(z,z') B(z',z). \tag{2.102}$$

Equation (2.100) translates to the Schwinger-Keldysh space as

$$\hat{C}(t,t') = \int d\underline{t}\, \hat{A}(t,\underline{t}) \hat{\sigma}_3 \hat{B}(\underline{t},t'), \tag{2.103}$$

with the Pauli matrix arising from the backward branch of the contour integral. Given $\hat{W}\hat{U} = \hat{\sigma}_3$, we can complete the transform giving us $\hat{C}(t,t')$ in terms of the retarded, advanced, and lesser projections:

$$\hat{U}\hat{C}(t,t')\hat{W} = \int d\underline{t}\, \hat{U}\hat{A}(t,\underline{t})\hat{W}\hat{U}\hat{B}(\underline{t},t')\hat{W}$$

$$= \begin{pmatrix} C^R(t,t') & C^<(t,t') \\ 0 & C^A(t,t') \end{pmatrix} = \int d\underline{t} \begin{pmatrix} A^R(t,\underline{t}) & A^<(t,\underline{t}) \\ 0 & A^A(t,\underline{t}) \end{pmatrix} \begin{pmatrix} B^R(\underline{t},t') & B^<(\underline{t},t') \\ 0 & B^A(\underline{t},t'). \end{pmatrix} \tag{2.104}$$

Using equation (2.104) and the relation $A^R(t,t') - A^A(t,t') = A^>(t,t') - A^<(t,t')$, gives the

following projections for equation (2.100):

$$C^{R/A}(t,t') = \int d\underline{t} \ A^{R/A}(t,\underline{t})B^{R/A}(\underline{t},t')+ \tag{2.105}$$

$$C^{</>}(t,t') = \int d\underline{t} A^{R}(t,\underline{t})B^{</>}(\underline{t},t') + A^{</>}(t,\underline{t})B^{A}(\underline{t},t'). \tag{2.106}$$

For equation (2.101) we have the projections

$$\begin{pmatrix} D^{T}(t,t') & D^{<}(t,t') \\ D^{>}(t,t') & D^{\tilde{T}}(t,t') \end{pmatrix} = \begin{pmatrix} A^{T}(t,t')B^{T}(t,t') & A^{<}(t,t')B^{<}(t,t') \\ A^{>}(t,t')B^{>}(t,t') & A^{\tilde{T}}(t,t')B^{\tilde{T}}(t,t') \end{pmatrix}, \tag{2.107}$$

and

$$D^{R/A}(t,t') = A^{<}(t,t')B^{R/A}(t,t') + A^{R/A}(t,t')B^{<}(t,t') \pm A^{R/A}(t,t')B^{R/A}(t,t')$$
$$= A^{<}(t,t')B^{R/A}(t,t') + A^{A/R}(t,t')B^{>}(t,t'), \tag{2.108}$$

where the last equality follows from $A^{R}(t,t') - A^{A}(t,t') = A^{>}(t,t') - A^{<}(t,t')$ and equations (2.94) and (2.95). Similarly, for equation (2.102) we have the projections

$$\begin{pmatrix} E^{T}(t,t') & E^{<}(t,t') \\ E^{>}(t,t') & E^{\tilde{T}}(t,t') \end{pmatrix} = \begin{pmatrix} A^{T}(t,t')B^{T}(t',t) & A^{<}(t,t')B^{>}(t',t) \\ A^{>}(t,t')B^{<}(t',t) & A^{\tilde{T}}(t,t')B^{\tilde{T}}(t',t) \end{pmatrix} \tag{2.109}$$

and

$$E^{R/A}(t,t') = A^{R/A}(t,t')B^{<}(t',t) + A^{<}(t,t')B^{A/R}(t',t). \tag{2.110}$$

In addition to the convolutions, the derivative with respect to the contouring time and the delta function of the contour times have projections in real time. For the derivative, both the forward and backward branches of the contour have the same projection:

$$\frac{df}{dz} = \lim_{z' \to z} \frac{f(z') - f(z)}{z' - z}$$
$$= \begin{cases} \lim_{\epsilon \to 0} \frac{f(t+\epsilon)-f(t)}{\epsilon} = \frac{df}{dt} & \text{(forward branch)} \\ \lim_{\epsilon \to 0} \frac{f(t-\epsilon)-f(t)}{-\epsilon} = \frac{df}{dt} & \text{(backward branch)}. \end{cases} \tag{2.111}$$

The delta function, $\delta(z,z')$, is understood as the derivative with respect to the contour Heaviside,

$$\theta(z-z') \to \begin{pmatrix} \theta(t-t') & 0 \\ 0 & \theta(t'-t), \end{pmatrix} \tag{2.112}$$

such that

$$\delta(z-z') = \frac{\theta(z-z')}{dz} \to \begin{pmatrix} \delta(t-t') & 0 \\ 0 & -\delta(t-t') \end{pmatrix}, \tag{2.113}$$

where both equations (2.112) and (2.113) are written in the untransformed frame, as seen in

equation (2.97). For the transformed representation in Schwinger-Keldysh space, we get an identity matrix:

$$\hat{U} \begin{pmatrix} \delta(t - t') & 0 \\ 0 & -\delta(t - t') \end{pmatrix} \hat{W} = \begin{pmatrix} \delta(t - t') & 0 \\ 0 & \delta(t - t') \end{pmatrix}. \tag{2.114}$$

2.4.5 Electronic Green's functions' projections

For the single particle electronic Green's functions, equation (2.29), the projections are as follows:

$$G_{pp'}^{>}(t, t') = -i\langle \hat{d}_p(t)\hat{d}_p^{\dagger}(t')\rangle, \tag{2.115}$$

$$G_{pp'}^{<}(t, t') = i\langle \hat{d}_{p'}^{\dagger}(t')\hat{d}_p(t)\rangle, \tag{2.116}$$

$$G_{pp'}^{T}(t, t') = -i\langle \mathrm{T}\left\{\hat{d}_p(t)\hat{d}_{p'}^{\dagger}(t')\right\}\rangle, \tag{2.117}$$

$$G_{pp'}^{\tilde{T}}(t, t') = -i\langle \widetilde{\mathrm{T}}\left\{\hat{d}_p(t)\hat{d}_{p'}^{\dagger}(t)\right\}\rangle, \tag{2.118}$$

$$G_{pp'}^{R}(t, t') = -i\theta(t - t')\langle \left[\hat{d}_p(t), \hat{d}_{p'}^{\dagger}(t')\right]_{+}\rangle \tag{2.119}$$

and

$$G_{pp'}^{A}(t, t') = i\theta(t' - t)\langle \left[\hat{d}_p(t), \hat{d}_{p'}^{\dagger}(t')\right]_{+}\rangle. \tag{2.120}$$

The Dyson equation in the untransformed form in the Schwinger-Keldysh space comes to

$$\hat{G}_{pp'}(t, t') = \hat{g}_{pp'}(t, t') + \int d1_{tp}d2_{tp} \, \hat{g}_{pp_1}(t, t_1)\hat{\sigma}_3\hat{\Sigma}_{p_1p_2}(t_1, t_2)\hat{\sigma}_3\hat{G}_{p_2p'}(t_2, t'), \tag{2.121}$$

whereas the transformed form decouples to give the following equations:

$$G_{pp'}^{R/A}(t, t') = g_{pp'}^{R/A}(t, t') + \int d1_{tp}d2_{tp} \, g_{pp_1}^{R/A}(t, t_1)\Sigma_{p_1p_2}^{R/A}(t_1, t_2)G_{p_2p'}^{R/A}(t_2, t') \tag{2.122}$$

and

$$\begin{aligned} G_{pp'}^{</>}(t, t') = g_{pp'}^{<}(t, t') &+ \int d1_{tp}d2_{tp} \, g_{pp_1}^{</>}(t, t_1)\Sigma_{p_1p_2}^{A}(t_1, t_2)G_{p_2,p'}^{A}(t_2, t') \\ &+ \int d1_{tp}d2_{tp} \, g_{pp_1}^{R}(t, t_1)\Sigma_{p_1p_2}^{</>}(t_1, t_2)G_{p_2,p'}^{A}(t_2, t') \\ &+ \int d1_{tp}d2_{tp} \, g_{pp_1}^{R}(t, t_1)\Sigma_{p_1p_2}^{R}(t_1, t_2)G_{p_2,p'}^{</>}(t_2, t'), \end{aligned} \tag{2.123}$$

where $\int d1_{tp} = \int dt_1 \sum_{p_1}$. The alternate version of the Dyson equation, $G = g + G \circ \Sigma \circ g$, has the same projections, with the switching of G and g in the second term. Equation (2.123) can

be rearranged with the help of equation (2.122) to get the Keldysh equation:

$$G_{pp'}^{</>}(t,t') = \int d1_{tp} d2_{tp} d3_{tp} d4_{tp} \left(\delta_{pp_2}\delta(t-t_2) + G_{pp_1}^R(t,t_1)\Sigma_{p_1,p_2}^R(t_1,t_2) \right) g_{p_2,p_3}^{</>}(t_2,t_3)$$
$$\times \left(\delta_{p_3 p'}\delta(t_3-t') + \Sigma_{p_3 p_4}^A(t_3,t_4)G_{p_4,p'}^A(t_4,t') \right) \quad (2.124)$$
$$+ \int d\underline{1}_{tp} d\underline{2}_{tp} G_{pp_1}^R(t,t_1)\Sigma_{p_1 p_2}^{</>}(t_1,t_2)G_{p_2 p'}^A(t_2,t').$$

When the noninteracting Green's functions situated in the first term, $g_{p_2,p_3}^{</>}(t_2,t_3)$ are defined as the proper noninteracting Green's functions, see equations (2.128) and (2.129), the first term in equation (2.124) will disappear.

Similarly, the Kadanoff-Baym equations in the untransformed form of the Schwinger-Keldysh space are given by

$$\sum_l \left(\hat{I}\delta_{pl}i\frac{d}{dt} - \hat{I}\epsilon_{pl}(t) \right) \hat{G}_{lp'}(t,t') = \hat{\sigma}_3\delta_{pp'}\delta(t-t') + \int d1_{tp}\, \hat{\Sigma}_{pp_1}(t,t_1)\hat{\sigma}_3\hat{G}_{p_1p'}(t_1,t'), \quad (2.125)$$

where $\hat{I}$ is the identity matrix in the Schwinger-Keldysh space. In the transformed form, the equations decouple to give

$$\sum_l \left(\delta_{pl}i\frac{d}{dt} - \epsilon_{pl}(t) \right) G_{lp'}^{R/A}(t,t') = \delta_{pp'}\delta(t-t') + \int d1_{tp} \Sigma_{pp_1}^{R/A}(t,t_1)G_{p_1p'}^{R/A}(t_1,t') \quad (2.126)$$

and

$$\sum_l \left(\delta_{pl}i\frac{d}{dt} - \epsilon_{pl}(t) \right) G_{lp'}^{</>}(t,t') =$$
$$\int d1_{tp} \left[\Sigma_{pp_1}^{</>}(t,t_1)G_{p_1p'}^A(t_1,t') + \Sigma_{pp_1}^R(t,t_1)G_{p_1p'}^{</>}(t_1,t') \right]. \quad (2.127)$$

In the case of unconnected and noninteracting levels, the Green's functions have the following form:

$$g_{pp'}^{<}(t,t') = ie^{-i\int_{t'}^t dt\epsilon_p(t)}f_0\delta_{pp'}, \quad (2.128)$$

$$g_{pp'}^{>}(t,t') = -ie^{-i\int_{t'}^t dt\epsilon_p(t)}(1-f_0)\delta_{pp'}, \quad (2.129)$$

$$g_{pp'}^{R}(t,t') = -i\theta(t-t')e^{-i\int_{t'}^t dt\epsilon_p(t)}\delta_{pp'}, \quad (2.130)$$

and

$$g_{pp'}^{A}(t,t') = i\theta(t'-t)e^{-i\int_{t'}^t dt\epsilon_p(t)}\delta_{pp'}, \quad (2.131)$$

where site p has the energy level $\epsilon_p(t)$ and $f_0 = 1/\left[e^{\beta\epsilon_p(t_0)}+1 \right]$. To calculate $g_{pp'}^{T/\tilde{T}}(t,t')$, equations (2.92) and (2.93) can be utilised. In the case where we take the $\epsilon_p(t)$ to be constant

with time, we can take a Fourier transform with respect to $\tau = t - t'$, giving the results

$$g^<_{pp'}(\omega) = 2\pi i f_0 \delta\left(\omega - \epsilon_p\right) \delta_{pp'}, \tag{2.132}$$

$$g^>_{pp'}(\omega) = -2\pi i (1 - f_0) \delta\left(\omega - \epsilon_p\right) \delta_{pp'}, \tag{2.133}$$

$$g^R_{pp'}(\omega) = \frac{\delta_{pp'}}{\omega - \epsilon_p + i\eta} \tag{2.134}$$

and

$$g^A_{pp'}(\omega) = \frac{\delta_{pp'}}{\omega - \epsilon_p - i\eta}, \tag{2.135}$$

where η is an infinitesimal.

2.4.5.1 Phononic Green's functions' projections

In a similar fashion to the electronic case, the projections of the phononic Green's follow:

$$D^>_{\nu\nu'}(t, t') = D^<_{\nu'\nu}(t', t) = -i\langle \Delta\hat{\phi}_\nu(t) \Delta\hat{\phi}_{\nu'}(t') \rangle, \tag{2.136}$$

$$D^R_{\nu\nu'}(t, t') = -i\theta(t - t')\langle \left[\Delta\hat{\phi}_\nu(t), \Delta\hat{\phi}_{\nu'}(t')\right]_- \rangle \tag{2.137}$$

and

$$D^A_{\nu\nu'}(t, t') = i\theta(t' - t)\langle \left[\Delta\hat{\phi}_\nu(t), \Delta\hat{\phi}_{\nu'}(t')\right]_- \rangle, \tag{2.138}$$

while the time-ordered and anti-time-ordered Green's functions also follow from equation (2.92) and (2.93) respectively.

The Dyson equation in the untransformed form in the Schwinger-Keldysh space comes to

$$\hat{D}_{\nu\nu'}(t, t') = \hat{d}_{\nu\nu'}(t, t') + \int d1_{t\nu} d2_{t\nu} \, \hat{d}_{\nu\nu_1}(t, t_1)\hat{\sigma}_3 \hat{\Pi}_{\nu_1\nu_2}(t_1, t_2)\hat{\sigma}_3 \hat{D}_{\nu_2,\nu'}(t_2, t'), \tag{2.139}$$

whereas the transformed form decouples to give the following equations:

$$D^{R/A}_{\nu\nu'}(t, t') = d^{R/A}_{\nu\nu'}(t, t') + \int d1_{t\nu} d2_{t\nu} \, d^{R/A}_{\nu\nu_1}(t, t_1)\Pi^{R/A}_{\nu_1,\nu_2}(t_1, t_2)D^{R/A}_{\nu_2,\nu'}(t_2, t') \tag{2.140}$$

and

$$\begin{aligned} D^{</>}_{\nu\nu'}(t, t') = d^{</>}_{\nu\nu'}(t, t') &+ \int d1_{t\nu} d2_{t\nu} \, d^{</>}_{\nu\nu_1}(t, t_1)\Pi^A_{\nu_1\nu_2}(t_1, t_2)D^A_{\nu_2\nu'}(t_2, t') \\ &+ \int d1_{t\nu} d2_{t\nu} \, d^R_{\nu\nu_1}(t, t_1)\Pi^{</>}_{\nu_1\nu_2}(t_1, t_2)D^A_{\nu_2\nu'}(t_2, t') \\ &+ \int d1_{t\nu} d2_{t\nu} \, d^R_{\nu\nu_1}(t, t_1)\Pi^R_{\nu_1\nu_2}(t_1, t_2)D^{</>}_{\nu_2\nu'}(t_2, t'). \end{aligned} \tag{2.141}$$

The alternate version of the Dyson equation, $D = d + D \circ \Pi \circ d$, has the same projections,

with the switching of D and d in the second term. Equation (2.141) can be rearranged with the help of equation (2.140) to get the Keldysh equation:

$$D_{\nu\nu'}^{</>}(t,t') = \int d1_{t\nu} d2_{t\nu} d3_{t\nu} d4_{t\nu} \left(\delta(t-t_2)\delta_{\nu\nu_2} + D_{\nu\nu_1}^R(t,t_1)\Pi_{\nu_1\nu_2}^R(t_1,t_2) \right) d_{\nu_2\nu_3}^{</>}(t_2,t_3)$$
$$\times \left(\delta(t_3-t')\delta_{\nu_3\nu'} + \Pi_{\nu_3\nu_4}^A(t_3,t_4) D_{\nu_4\nu'}^A(t_4,t') \right) \quad (2.142)$$
$$+ \int d1_{t\nu} d2_{t\nu} D_{\nu\nu_1}^R(t,t_1)\Pi_{\nu_1\nu_2}^{</>}(t_1,t_2) D_{\nu_2\nu'}^A(t_2,t').$$

In a similar manner to the electronic case, the first term in equation (2.142) will disappear, depending on the how the noninteracting phononic Green's functions have been defined.

Similarly, the Kadanoff-Baym equations in the untransformed form of the Schwinger-Keldysh space are given by

$$\sum_\beta \left[\hat{I} i\alpha_{\nu\beta} \frac{d}{dt} - \hat{I}\Omega_{\nu\beta} \right] \hat{D}_{\beta,\nu}(t,t') = \hat{\sigma}_3 \delta_{\nu\nu'} \delta(t-t') + \int d1_{t\nu} \hat{\Pi}_{\nu,\nu_1}(t,t_1)\hat{\sigma}_3 \hat{D}_{\nu_1,\nu'}(t_1,t'), \quad (2.143)$$

where $\hat{I}$ is the identity matrix in the Schwinger-Keldysh space. In the transformed form, the equations decouple to give

$$\sum_\beta \left[i\alpha_{\nu\beta} \frac{d}{dt} - \Omega_{\nu\beta} \right] D_{\beta\nu'}^{R/A}(t,t') = \delta_{\nu\nu'} \delta(t-t') + \int d1_{t\nu} \Pi_{\nu\nu_1}^{R/A}(t,t_1) D_{\nu_1\nu'}^{R/A}(t_1,t') \quad (2.144)$$

and

$$\sum_\beta \left[i\alpha_{\nu\beta} \frac{d}{dt} - \Omega_{\nu\beta} \right] D_{\beta\nu'}^{</>}(t,t')$$
$$= \int d1_{t\nu} \left[\Pi_{\nu\nu_1}^{</>}(t,t_1) D_{\nu_1\nu'}^A(t_1,t') + \Pi_{\nu\nu_1}^R(t,t_1) D_{\nu_1\nu'}^{</>}(t_1,t') \right] \quad (2.145)$$

So far, the compact notation of equation (2.10) has been utilized. However, given the Hamiltonian of equation (2.9) and (2.13), we observe that $M_{ij}^{\bar{\nu}} = M_{ij}^{n,\nu} = \delta_{1,n}\lambda_{ij}^\nu$, which results in only $D_{\{1,\nu\}\{1\nu'\}}(z,z') = D_{QQ,\nu\nu'}(z,z')$ occuring in our solutions to $\Sigma_{el-ph}[G,D]$ and $\Pi_{\{1,\nu\}\{1,\nu\}}(z,z') = \Pi_{QQ,\nu\nu'}(z,z')\delta_{1n}\delta_{1n'}$. Focusing on the $D_{QQ,\nu\nu'}(z,z')$, we find that

$$D_{QQ,\nu\nu'}(z,z') = d_{QQ,\nu\nu'}(z,z') + \int d1_{z\nu} d2_{z\nu} \, d_{QQ,\nu\nu_1}(z,z_1)\Pi_{QQ,\nu_1\nu_2}(z_1,z_2) D_{QQ,\nu_2\nu'}(z_2,z'), \quad (2.146)$$

which has the projections

$$\hat{D}_{QQ,\nu\nu'}(t,t') = \hat{d}_{QQ,\nu\nu'}(t,t') + \int d1_{t\nu} d2_{t\nu} \, \hat{d}_{QQ,\nu\nu_1}(t,t_1)\hat{\sigma}_3\hat{\Pi}_{QQ,\nu_1\nu_2}(t_1,t_2)\hat{\sigma}_3\hat{D}_{QQ,\nu_2\nu'}(t_2,t'),$$
$$\quad (2.147)$$
$$D_{QQ,\nu\nu'}^{R/A}(t,t') = d_{QQ,\nu\nu'}^{R/A}(t,t') + \int d1_{t\nu} d2_{t\nu} \, d_{QQ,\nu\nu_1}^{R/A}(t,t_1)\Pi_{QQ,\nu_1\nu_2}^{R/A}(t_1,t_2) D_{QQ,\nu_2\nu'}^{R/A}(t_2,t') \quad (2.148)$$

and

$$D_{QQ,vv'}^{</>}(t,t') = d_{QQ,vv'}^{</>}(t,t') + \int d1_{tv} d2_{tv}\, d_{QQ,vv_1}^{</>}(t,t_1)\Pi_{QQ,v_1v_2}^{A}(t_1,t_2)D_{QQ,v_2v'}^{A}(t_2,t')$$

$$+ \int d1_{tv} d2_{tv}\, d_{QQ,vv_1}^{R}(t,t_1)\Pi_{QQ,v_1v_2}^{</>}(t_1,t_2)D_{QQ,v_2v'}^{A}(t_2,t') \quad (2.149)$$

$$+ \int d1_{tv} d2_{tv}\, d_{QQ,vv_1}^{R}(t,t_1)\Pi_{QQ,v_1v_2}^{R}(t_1,t_2)D_{QQ,v_2v'}^{</>}(t_2,t').$$

Again, the alternate version of the Dyson equation, $D = d + D \circ \Pi \circ d$, has the same projections, switching D and d in the second term. Equation (2.149) can be rearranged with the help of equation (2.148) to get the Keldysh equation:

$$D_{QQ,vv'}^{</>}(t,t') = \int d1_{tv} d2_{tv} d3_{tv} d4_{tv} \left(\delta(t-t_2)\delta_{vv_2} + D_{QQ,vv_1}^{R}(t,t_1)\Pi_{QQ,v_1v_2}^{R}(t_1,t_2) \right) d_{QQ,v_2v_3}^{</>}(t_2,t_3)$$

$$\times \left(\delta(t_3-t')\delta_{v_3v'} + \Pi_{QQ,v_3v_4}^{A}(t_3,t_4)D_{QQ,v_4v'}^{A}(t_4,t') \right)$$

$$+ \int d1_{tv} d2_{tv} D_{QQ,vv_1}^{R}(t,t_1)\Pi_{QQ,v_1v_2}^{</>}(t_1,t_2)D_{QQ,v_2v'}^{A}(t_2,t').$$

$$(2.150)$$

Following from equation (2.86), the Kadanoff-Baym equations for $D_{QQ}(1_{zv}, 2_{zv})$ follows as

$$-\frac{1}{\omega_v}\left(\frac{d^2}{dz^2} + \omega_v^2\right)D_{QQ,vv'}(z,z') = \delta_{vv'}\delta(z,z') + \int d1_{zv}\Pi_{QQ,vv_1}(z,z_1)D_{QQ,v_1v'}(z_1,z'), \quad (2.151)$$

with the projections

$$-\frac{1}{\omega_v}\left(\frac{d^2}{dt^2} + \omega_v^2\right)\hat{D}_{QQ,vv'}(t,t') = \hat{\sigma}_3\delta_{vv'}\delta(t-t') + \int d1_{tv}\hat{\Pi}_{QQ,vv_1}(t,t_1)\hat{\sigma}_3\hat{D}_{QQ,v_1v'}(t_1,t'),$$

$$(2.152)$$

$$-\frac{1}{\omega_v}\left(\frac{d^2}{dt^2} + \omega_v^2\right)D_{QQ,vv'}^{R/A}(t,t') = \delta_{v_1v_2}\delta(t-t') + \int d1_{tv}\Pi_{QQ,vv_1}^{R/A}(t,t_1)D_{QQ,v_1v'}^{R/A}(t_1,t') \quad (2.153)$$

and

$$-\frac{1}{\omega_v}\left(\frac{d^2}{dt^2} + \omega_v^2\right)D_{QQ,vv'}^{</>}(t,t')$$

$$= \int d1_{zv}\left[\Pi_{QQ,vv_1}^{</>}(t,t_1)D_{QQ,v_1v'}^{A}(t_1,t') + \Pi_{QQ,vv_1}^{R}(t,t_1)D_{QQ,v_1v'}^{</>}(t_1,t')\right]. \quad (2.154)$$

For the noninteracting case, $D_{QQ,vv'}^{R}$ has the following projections:

$$d_{QQ,vv'}^{R}(t,t') = -\frac{i}{2}\theta(t-t')\left[e^{-i\omega_v(t-t')} - e^{i\omega_v(t-t')}\right]\delta_{vv'}, \quad (2.155)$$

$$d_{QQ,vv'}^{A}(t,t') = \frac{i}{2}\theta(t'-t)\left[e^{-i\omega_v(t-t')} - e^{i\omega_v(t-t')}\right]\delta_{vv'}, \quad (2.156)$$

$$d^<_{QQ,\nu\nu'}(t,t') = -\frac{i}{2}\left[e^{-i\omega_\nu(t-t')}f_B(\omega_\nu) + e^{i\omega_\nu(t-t')}(1+f_B(\omega_\nu))\right]\delta_{\nu\nu'} \qquad (2.157)$$

and

$$d^>_{QQ,\nu\nu'}(t,t') = -\frac{i}{2}\left[e^{-i\omega_\nu(t-t')}(1+f_B(\omega_\nu)) + e^{i\omega_\nu(t-t')}f_B(\omega_\nu)\right]\delta_{\nu\nu'}, \qquad (2.158)$$

where $f_B(\omega) = 1/\left(e^{\omega/T}-1\right)$. We can take a Fourier transform with respect to $\tau = t - t'$, giving the results

$$d^<_{QQ,\nu\nu'}(\omega) = -\pi i\left[f_B(\omega_\nu)\delta(\omega-\omega_\nu) + (1+f_B(\omega_\nu))\delta(\omega+\omega_\nu)\right]\delta_{\nu\nu'}, \qquad (2.159)$$

$$d^>_{QQ,\nu\nu'}(\omega) = -\pi i\left[f_B(\omega_\nu)\delta(\omega+\omega_\nu) + (1+f_B(\omega_\nu))\delta(\omega-\omega_\nu)\right]\delta_{\nu\nu'}, \qquad (2.160)$$

$$d^R_{QQ,\nu\nu'}(\omega) = \left[\frac{\frac{1}{2}}{\omega-\omega_\nu+i\eta} - \frac{\frac{1}{2}}{\omega+\omega_\nu+i\eta}\right]\delta_{\nu\nu'} \qquad (2.161)$$

and

$$d^A_{QQ,\nu\nu'}(\omega) = \left[\frac{\frac{1}{2}}{\omega-\omega_\nu-i\eta} - \frac{\frac{1}{2}}{\omega+\omega_\nu-i\eta}\right]\delta_{\nu\nu'}, \qquad (2.162)$$

where η is an infinitesimal.

2.4.6 Wigner transformation

For objects of the form $A(t,t')$, we can rewrite the time dependence in terms of the central and relative times:

$$T = \frac{t+t'}{2} \quad, \quad \tau = t - t'. \qquad (2.163)$$

This allows us to rearrange a function (say, $A(t,t')$) in terms of the Wigner transformation, which constitutes a Fourier transform in terms of the relative time:

$$A(T,\omega) = \int_{-\infty}^{\infty} d\tau e^{i\omega\tau} A(T+\tau/2, T-\tau/2) \qquad (2.164)$$

and

$$A(T+\tau/2, T-\tau/2) = \int \frac{d\omega}{2\pi} e^{-i\omega\tau} A(T,\omega). \qquad (2.165)$$

As is evident from the equations of motion for the Green's functions, the convolution of the from $A(t,t') = \int d\underline{t}B(t,\underline{t})C(\underline{t},t') = [B \circ C](t,t')$ is of importance. Upon the application of the Wigner transformation to the convolution, we find that

$$A(T,\omega) = e^{-\frac{i}{2}\left(\partial^B_T\partial^C_\omega - \partial^B_\omega\partial^C_T\right)}B(T,\omega)C(T,\omega), \qquad (2.166)$$

where ∂^X_y is a partial derivative with respect to y acting only on X. A limiting case of $B(t,t') =$

$B(t)\delta(t - t')$, where $A(t, t') = B(t)C(t, t')$, we find that

$$A(T, \omega) = e^{-\frac{i}{2}\partial_T^B \partial_\omega^C} B(T, \omega) C(T, \omega). \tag{2.167}$$

In the limiting case, where functions depend upon a relative time only (i.e., $A(t, t') \to A(t - t')$), we retrieve the result that is equivalent to a Fourier transformation of the convolution $A(\omega) = B(\omega)C(\omega)$.

Similarly, the time derivatives of $A(t, t')$ find parallels in Wigner space. Within terms of relative and central time, we have

$$\frac{d}{dt} = \frac{\partial \tau}{\partial t}\frac{d}{d\tau} + \frac{\partial T}{\partial t}\frac{d}{dT} = \frac{d}{d\tau} + \frac{1}{2}\frac{d}{dT} \tag{2.168}$$

such that

$$\frac{d^2}{dt^2} = \left(\frac{d}{d\tau} + \frac{1}{2}\frac{d}{dT}\right)^2 = \frac{d^2}{d\tau^2} + \frac{d}{d\tau}\frac{d}{dT} + \frac{1}{4}\frac{d^2}{dT^2}. \tag{2.169}$$

Utilising integration by parts, the derivatives with respect to the relative time transform under the Wigner transformation gives

$$\int d\tau e^{i\omega\tau}\frac{\partial}{\partial\tau}A\left(T + \tau/2, T - \tau/2\right)$$

$$= \int d\tau \frac{\partial}{\partial\tau}\left(e^{i\omega\tau}A\left(T + \tau/2, T - \tau/2\right)\right) - \int d\tau \left(\frac{\partial}{\partial\tau}e^{i\omega\tau}\right)A\left(T + \tau/2, T - \tau/2\right) \tag{2.170}$$

$$= 0 - i\omega\int d\tau e^{i\omega\tau}A\left(T + \tau/2, T - \tau/2\right) = -i\omega A\left(T, \omega\right),$$

which informs

$$\int d\tau e^{i\omega\tau}\frac{\partial^2}{\partial\tau^2}A\left(T + \tau/2, T - \tau/2\right) = -\omega^2 A\left(T, \omega\right). \tag{2.171}$$

All together, we find that

$$\int d\tau e^{i\omega\tau}\left(\frac{d^2}{d\tau^2} + \frac{d}{d\tau}\frac{d}{dT} + \frac{1}{4}\frac{d^2}{dT^2}\right)A\left(T + \tau/2, T - \tau/2\right)$$

$$= -\omega^2 A\left(T, \omega\right) - i\omega\frac{\partial}{\partial T}A\left(T, \omega\right) + \frac{1}{4}\frac{\partial^2}{\partial T^2}A\left(T, \omega\right) \tag{2.172}$$

$$= \left(-i\omega + \frac{1}{2}\frac{d}{dT}\right)^2 A(T, \omega).$$

2.4.7 Floquet transformation

In addition to the Wigner transformation, for systems that are periodic in time, we can express $A(T, \omega)$ in terms of its Fourier coefficients with respect to the central time:

$$A(T, \omega) = \sum_{n=-\infty}^{\infty} A(\omega, n) e^{\Omega i n T}, \tag{2.173}$$

$$\frac{1}{P} \int_{-P/2}^{P/2} dT e^{-\Omega i m T} A(T, \omega) = A(\omega, m), \tag{2.174}$$

where $P = 2\pi/\Omega$ is the period. For the convolution of type $A(t, t') = \int d\underline{t} B(t, \underline{t}) C(\underline{t}, t') = [B \circ C](t, t')$, assuming periodicity with respect to the central time of A and B gives

$$A(\omega, m) = \sum_n B\left(\omega + \frac{\Omega}{2}(n - m), n\right) C\left(\omega + \frac{\Omega}{2}n, m - n\right). \tag{2.175}$$

With the help of an extra transformation,

$$A(\omega, m, n) = A\left(\omega + \frac{\Omega}{2}(m + n), n - m\right), \tag{2.176}$$

the convolution can be further cast as a matrix multiplication:

$$\begin{aligned} A(\omega, m, n) &= [B \circ C](\omega, m, n) \\ &= \sum_{r=-\infty}^{\infty} B(\omega, m, r) C(\omega, r, n). \end{aligned} \tag{2.177}$$

The subsequent matrix of the Floquet transformation of equation (2.176) is called a Floquet matrix. The Fourier coefficients of the object in question populate the matrix:

$$A(\omega, m, n) = \begin{pmatrix} \cdots & \cdots & \cdots & \cdots & \cdots \\ \cdots & A(\omega - \Omega, 0) & A(\omega - \frac{\Omega}{2}, 1) & A(\omega, 2) & \cdots \\ \cdots & A(\omega - \frac{\Omega}{2}, -1) & A(\omega, 0) & A(\omega + \frac{\Omega}{2}, 1) & \cdots \\ \cdots & A(\omega, -2) & A(\omega + \frac{\Omega}{2}, -1) & A(\omega + \Omega, 0) & \cdots \\ \cdots & \cdots & \cdots & \cdots & \cdots \end{pmatrix}. \tag{2.178}$$

We also have to consider the following limiting case

$$A(t, t') = B(t) C(t, t'), \tag{2.179}$$

which follows from $B(t, t') \to B(t) \delta(t - t')$. Therefore, given the application of equation (2.177), the above has the same form, with the Floquet matrix of B populated with the Fourier coefficient of $B(t)$.

Often, especially when calculating certain interaction self-energies in chapters 5 and 6, we must calculate terms of the form $A_+(t,t') = B(t,t')C(t,t')$ and $A_-(t,t') = B(t,t')C(t',t)$. These terms, when transformed into Fourier coefficients, give a convolution of the following form:

$$
A_\pm(\omega, n) =
$$

$$
\sum_{m=-\infty}^{\infty} \int \frac{d\omega'}{2\pi} B(\omega', m) C(\pm\omega \mp \omega', n - m) \tag{2.180}
$$

$$
= [B \,\square_\pm\, C](\omega, n),
$$

where the use of the symbol $\square_\pm$ is a shorthand.

2.4.8 Electronic Lead Self-Energies

For the junction described by equation (2.1), the influence of the leads can be captured by self-energies. Focusing on a system comprised of just the noninteracting central region and the leads coupled together, described by the sum of equations (2.3),(2.7) and (2.4), we can make use of equation (2.45) and (2.56), to derive equations

$$
G(1_{zc}, 1'_{zc}) = g(1_{zc}, 1'_{zc}) + \int d\underline{1}_{zk\alpha c}\, g(1_{zc}, \underline{1}_{zc}) t_{c_{\underline{1}}k_{\underline{1}}\alpha_{\underline{1}}}(z_{\underline{1}}) G(\underline{1}_{zk\alpha}, 1'_{zc}) \tag{2.181}
$$

and

$$
G(1_{zk\alpha}, 1'_{zc}) = \int d\underline{1}_{zk\alpha c}\, g(1_{zk\alpha}, \underline{1}_{zk\alpha}) t_{k_{\underline{1}}\alpha_{\underline{1}}c_{\underline{1}}}(z_{\underline{1}}) G(\underline{1}_{zk\alpha}, 1'_{zc}) \tag{2.182}
$$

where c refers to sites within the central region, whilst k refers to sites within the α lead. Substituting equation (2.181) and (2.182) gives

$$
G(1_{zc}, 1'_{zc}) = g(1_{zc}, 1'_{zc})
$$

$$
+ \int d\underline{1}_{zc}d\underline{2}_{zc}\, g(1_{zc}, \underline{1}_{zc}) \left[\sum_\alpha \Sigma_\alpha(\underline{1}_{zc}, \underline{2}_{zc}) \right] G(\underline{2}_{zc}, 1'_{zc}). \tag{2.183}
$$

where

$$
\sum_\alpha \Sigma_\alpha(1_{zc}, 2_{zc}) = \sum_{k_{\underline{1}}\alpha_{\underline{1}}} \sum_{k_{\underline{2}}\alpha_{\underline{2}}} t_{c_{\underline{1}}k_{\underline{1}}\alpha_{\underline{1}}}(z_{\underline{1}}) g(\underline{1}_{zk\alpha}, \underline{2}_{zk\alpha}) t_{k_{\underline{2}}\alpha_{\underline{2}}c_{\underline{2}}}(z_{\underline{2}}). \tag{2.184}
$$

For this text, we restrict ourselves to the case where $t_{ck\alpha}$ is time-independent. Furthermore, we assume $\epsilon_{k\alpha}(t) = \epsilon_{k\alpha} + \phi_\alpha(t)$, which suggests a uniform driving of the lead energies. In addition, due to the lead Hamiltonian, (2.4), $g(zk\alpha, z'k'\alpha') = g_{k\alpha}(z, z')\delta_{kk'}\delta_{\alpha\alpha'}$, gives us

$$
\Sigma_{\alpha, cc'}(z, z') = \sum_k t_{ck\alpha} g_{k\alpha}(z, z') t_{k\alpha c'}, \tag{2.185}
$$

which can be projected in real time with

$$
\begin{aligned}
\Sigma_{\alpha,cc'}^{</>/R/A/T/\tilde{T}}(t,t') &= \sum_k t_{ck\alpha} g_{k\alpha}^{</>/R/A/T/\tilde{T}}(t,t') t_{k\alpha c'} \\
&= \sum_k t_{ck\alpha} g_{k\alpha}^{</>/R/A/T/\tilde{T}}(t-t') t_{k\alpha c'} e^{-i\int_{t'}^{t} d\underline{t}\,\phi(\underline{t})} \\
&= \Sigma_{\alpha,cc'}^{</>/R/A/T/\tilde{T}}(t-t') e^{-i\int_{t'}^{t} d\underline{t}\,\phi(\underline{t})},
\end{aligned}
\tag{2.186}
$$

where, here, $\Sigma_{\alpha,cc'}^{</>/R/A/T/\tilde{T}}(t-t')$ is to be understood as the lead self-energy where no driving of the leads is present.

In the case of no driving, the lead self-energies become the following under a Fourier transformation:

$$
\Sigma_{\alpha,cc'}^{<}(\omega) = \sum_k t_{ck\alpha} g_{k\alpha}^{<}(\omega) t_{k\alpha c'} = 2\pi i \sum_k t_{ck\alpha} t_{k\alpha c'} f(\epsilon_{k\alpha} - \mu_\alpha)\delta(\omega - \epsilon_{k\alpha}),
\tag{2.187}
$$

$$
\Sigma_{\alpha,cc'}^{>}(\omega) = \sum_k t_{ck\alpha} g_{k\alpha}^{<}(\omega) t_{k\alpha c'} = -2\pi i \sum_k t_{ck\alpha} t_{k\alpha c'} \left(1 - f(\epsilon_{k\alpha} - \mu_\alpha)\right)\delta(\omega - \epsilon_{k\alpha}),
\tag{2.188}
$$

$$
\Sigma_{\alpha,cc'}^{R}(\omega) = \sum_k t_{ck\alpha} g_{k\alpha}^{R}(\omega) t_{k\alpha c'} = \sum_k \frac{t_{ck\alpha} t_{k\alpha c'}}{\omega - \epsilon_{k\alpha} + i\eta},
\tag{2.189}
$$

and

$$
\Sigma_{\alpha,cc'}^{A}(\omega) = \sum_k t_{ck\alpha} g_{k\alpha}^{A}(\omega) t_{k\alpha c'} = \sum_k \frac{t_{ck\alpha} t_{k\alpha c'}}{\omega - \epsilon_{k\alpha} - i\eta}.
\tag{2.190}
$$

We can examine the real and imaginary components of the retarded and advanced lead self-energies:

$$
\begin{aligned}
\Sigma_{\alpha,cc'}^{R/A}(\omega) &= \sum_k \frac{t_{ck\alpha} t_{k\alpha c'}}{\omega - \epsilon_{k\alpha} \pm i\eta} \\
&= \sum_k \frac{t_{ck\alpha} t_{k\alpha c'}(\omega - \epsilon_{k\alpha})}{(\omega - \epsilon_{k\alpha})^2 + \eta^2} \mp i\sum_k \frac{t_{ck\alpha} t_{k\alpha c'}\eta}{(\omega - \epsilon_{k\alpha})^2 + \eta^2} \\
&= \sum_k \frac{t_{ck\alpha} t_{k\alpha c'}(\omega - \epsilon_{k\alpha})}{(\omega - \epsilon_{k\alpha})^2 + \eta^2} \mp i\pi \sum_k t_{ck\alpha} t_{k\alpha c'}\delta(\omega - \epsilon_{k\alpha}),
\end{aligned}
\tag{2.191}
$$

where we make use of the relation

$$
\lim_{\eta \to 0} \frac{\eta}{x^2 + \eta^2} = \pi\delta(x).
\tag{2.192}
$$

We collect details of the lead coupling in the imaginary part into the level-width function,

$$
\Gamma_{\alpha,cc'}(\omega) = 2\pi \sum_k t_{ck\alpha} t_{k\alpha c'}\delta(\omega - \epsilon_{k\alpha})
\tag{2.193}
$$

and $t_{c\alpha}(\epsilon_{k\alpha}) = t_{k\alpha c}$, and the level-shift function,

$$\Lambda_{\alpha,cc'}(\omega) = \lim_{\eta \to 0} \sum_k \frac{t_{ck\alpha}t_{k\alpha c'}(\omega - \epsilon_{k\alpha})}{(\omega - \epsilon_{k\alpha}) + \eta}. \tag{2.194}$$

We introduce a density of states for the lead, $\rho_\alpha(\omega) = \sum_k \delta(\omega - \epsilon_{k\alpha})$, such that any object of the form $\sum_k q_{k\alpha}$ can be expressed as an integral:

$$\begin{aligned}
\sum_k q_{k\alpha} &= \int d\omega q_\alpha(\omega) \sum_k \delta(\omega - \epsilon_{k\alpha}) \\
&= \int d\omega q_\alpha(\omega)\rho(\omega).
\end{aligned} \tag{2.195}$$

This result allows for the express the line-width function as

$$\begin{aligned}
\Gamma_{\alpha,cc'}(\omega) &= 2\pi \sum_k t_{ck\alpha}t_{k\alpha c'}\delta(\omega - \epsilon_{k\alpha}) \\
&= 2\pi t_{c\alpha}^*(\omega)t_{c\alpha}(\omega)\rho_\alpha(\omega),
\end{aligned} \tag{2.196}$$

Here, we introduce $t_{c\alpha}(\omega)$, such that $t_{c\alpha}(\epsilon_{k\alpha}) = t_{k\alpha c}$ otherwise $t_{c\alpha}(\omega) = 0$. This allows us to recast the self-energies as follows:

$$\Sigma_{\alpha,cc'}^<(\omega) = if_\alpha(\omega)\Gamma_{\alpha,cc'}(\omega), \tag{2.197}$$

$$\Sigma_{\alpha,cc'}^>(\omega) = -i\left(1 - f_\alpha(\omega)\right)\Gamma_{\alpha,cc'}(\omega), \tag{2.198}$$

and

$$\Sigma_{\alpha,cc'}^{R/A}(\omega) = \Lambda_{\alpha,cc'}(\omega) \mp \frac{i}{2}\Gamma_{\alpha,cc'}(\omega). \tag{2.199}$$

From the relations of equations (2.98) and (2.99) we find the time-ordered and anti-time-ordered self-energies:

$$\Sigma_{\alpha,cc'}^{T/\tilde{T}}(\omega) = \pm\Lambda_{\alpha,cc'}(\omega) - i\left(1/2 - f_\alpha(\omega)\right)\Gamma_{\alpha,cc'}(\omega). \tag{2.200}$$

To solve for equations (2.193) and (2.194), we assume that $t_{k\alpha c} = t_{\alpha c}$ and that the density of states of the lead is constant within the band $[\omega_1, \omega_2]$ and zero elsewhere. This gives us the results

$$\Gamma_{\alpha,cc'}(\omega) = \begin{cases} 2\pi t_{\alpha c}^* t_{\alpha c'}\rho & \omega_1 \le \omega \le \omega_2 \\ 0 & otherwise \end{cases} \tag{2.201}$$

and

$$
\begin{aligned}
\Lambda_{\alpha,cc'}(\omega) &= \lim_{\eta\to 0} \sum_k \frac{t_{ck\alpha}t_{k\alpha c'}(\omega - \epsilon_{k\alpha})}{(\omega - \epsilon_{k\alpha})^2 + \eta} \\
&= \lim_{\eta\to 0} \int d\underline{\omega}\, \frac{\rho(\underline{\omega})t^*_{\alpha c}(\underline{\omega})t_{\alpha c'}(\underline{\omega})(\omega - \underline{\omega})}{(\omega - \underline{\omega})^2 + \eta} \\
&= t^*_{\alpha c}t_{\alpha c'}\rho \int_{\omega_1}^{\omega_2} \frac{d\underline{\omega}}{(\omega - \underline{\omega})} \\
&= t^*_{\alpha c}t_{\alpha c'}\rho \ln\left|\frac{\omega_1 - \omega}{\omega_2 - \omega}\right| = \frac{\Gamma_{\alpha,cc'}}{2\pi} \ln\left|\frac{\omega_1 - \omega}{\omega_2 - \omega}\right|.
\end{aligned}
\tag{2.202}
$$

Within the text, we will utilize the wide-band limit, meaning $\omega_1 \to -\infty$ and $\omega_2 \to \infty$, in which the line-width function becomes constant, and the line-shift function disappears, resulting in the following self-energies:

$$
\Sigma^<_{\alpha,cc'}(\omega) = if_\alpha(\omega)\Gamma_{\alpha,cc'},
\tag{2.203}
$$

$$
\Sigma^>_{\alpha,cc'}(\omega) = -i\left(1 - f_\alpha(\omega)\right)\Gamma_{\alpha,cc'},
\tag{2.204}
$$

and

$$
\Sigma^{R/A}_{\alpha,cc'}(\omega) = \mp\frac{i}{2}\Gamma_{\alpha,cc'}.
\tag{2.205}
$$

From the relations of equations (2.98) and (2.99) we find the time-ordered and anti-time-ordered self-energies to be as follows:

$$
\Sigma^{T/\tilde{T}}_{\alpha,cc'}(\omega) = -i\left(1/2 - f_\alpha(\omega)\right)\Gamma_{\alpha,cc'}.
\tag{2.206}
$$

Within this thesis, we assume sinusoidal driving within the leads:

$$
\varepsilon_{k\alpha}(t) = \varepsilon_{k\alpha} + \Delta_\alpha \cos(\Omega_\alpha t).
\tag{2.207}
$$

Substituting this result into equation (2.186), we find

$$
\begin{aligned}
\Sigma_{\alpha,cc'}(t,t') &= \Sigma'_{\alpha,cc'}(t - t')e^{-i\int_{t'}^{t} dt_1 \Delta_\alpha \cos(\Omega_\alpha t_1)} \\
&= e^{-i\frac{\Delta_\alpha}{\Omega_\alpha}\sin(\Omega_\alpha t)}\Sigma'_{\alpha,cc'}(t - t')e^{i\frac{\Delta_\alpha}{\Omega_\alpha}\sin(\Omega_\alpha t')},
\end{aligned}
\tag{2.208}
$$

where $\Sigma'_{\alpha,cc'}(t - t')$ is to be understood as the lead self-energy where no driving of the leads is present. We see that the above follows a pattern similar to equation convolution of type $A(t,t') = \int d\underline{t}B(t,\underline{t})C(\underline{t},t') = [B \circ C](t,t')$ and, following a similar analysis as section 2.4.7, can be expressed as the matrix multiplication of three Floquet matrices:

$$
\Sigma_{\alpha,cc'} = \left[S_\alpha \circ \Sigma'_{\alpha,cc'} \circ S_\alpha^\dagger\right](\omega,m,n).
\tag{2.209}
$$

Here, $S_\alpha^\dagger(m,n) = S_\alpha^\dagger(n,m)$, where $S_\alpha(m,n)$ is found with the use of the Jacobi-Anger expan-

sion,

$$e^{iz\sin(\theta)} = \sum_{n=-\infty}^{n=\infty} J_n(z)e^{in\theta},$$ (2.210)

as $S_\alpha(m,n) = J_{m-n}(\Delta_\alpha/\Omega_\alpha)$. Here, $J_r(x)$ are Bessel functions of the first kind.

2.4.9 Phononic Bath Self-Energies

To capture the effects of a phonon bath on the central phonons, instead of letting η_α be infinitesimals, as in equations (2.161) and (2.162), we take them as finite:

$$D^R_{vv'}(\omega) = \left[\frac{\frac{1}{2}}{\omega - \omega_v + i\eta_v} - \frac{\frac{1}{2}}{\omega + \omega_v + i\eta_v}\right]\delta_{vv'}$$ (2.211)

and

$$D^A_{vv'}(\omega) = \left[\frac{\frac{1}{2}}{\omega - \omega_v - i\eta_v} - \frac{\frac{1}{2}}{\omega + \omega_v - i\eta_v}\right]\delta_{vv'}.$$ (2.212)

Making use of fluctuation-dissipation relations [69], we can introduce η_α into the lesser and greater phonon Green's functions:

$$d^<_\alpha(\omega) = \left(d^R_\alpha(\omega) - d^A_\alpha(\omega)\right)f_B(\omega)$$
$$= \left(-\frac{i\eta_\alpha}{(\omega - \omega_\alpha)^2 + \eta_\alpha^2} + \frac{i\eta_\alpha}{(\omega + \omega_\alpha)^2 + \eta_\alpha^2}\right)f_B(\omega)$$ (2.213)

and

$$d^>_\alpha(\omega) = \left(d^R_\alpha(\omega) - d^A_\alpha(\omega)\right)(1 + f_B(\omega))$$
$$= \left(-\frac{i\eta_\alpha}{(\omega - \omega_\alpha)^2 + \eta_\alpha^2} + \frac{i\eta_\alpha}{(\omega + \omega_\alpha)^2 + \eta_\alpha^2}\right)(1 + f_B(\omega)),$$ (2.214)

where taking the limit of η,

$$\lim_{\eta \to 0^+}\left[\frac{\eta}{(\omega - \omega_0)^2 + \eta^2}\right] \to \pi\delta(\omega - \omega_0),$$ (2.215)

and substituting for $f^0_B(-\omega) = -\left(f^0_B(\omega) + 1\right)$, gives us back the equations (2.159) and (2.160).

For the lesser and greater phonon Green's functions, we can use the fluctuation-dissipation rules to cast the effects due to the infinitesimals as self-energies. Equating equations (2.213) and (2.214) to the associated Keldysh equation, equation (2.150) where the first term disappears, gives us:

$$\Pi^{</>}_\alpha(\omega) = \mp 4i\eta_\alpha\left(\frac{\omega}{\omega_\alpha}\right)f_B(\pm\omega).$$ (2.216)

This phonon self-energy can be used to incorporate the effects of a bath into self-consistent calculations. For the retarded and advanced terms, the bath effects can enter into the interacting calculations via the left-hand side of the Kadanoff-Baym equations. In the context of equation (2.211) and (2.212), we have

$$-\frac{1}{\omega_\nu} \left(\frac{d^2}{dt^2} + \omega_\nu^2 \right) D_{QQ,\nu\nu'}^{R/A} \left(t, t' \right) = \delta_{\nu_1\nu_2} \delta(t - t'), \tag{2.217}$$

which transform under Fourier transform to gives

$$-\frac{1}{\omega_\nu} \left(\omega_\nu^2 - (\omega \pm i\eta_\nu)^2 \right) D_{QQ,\nu\nu'}^{R/A} \left(\omega \right) = \delta_{\nu_1\nu_2}, \tag{2.218}$$

where the addition of $\pm i\eta_\nu$ captures bath's effects.

2.4.10 Calculating ϕ

To calculate the average position and momentum of a phonon mode, we start with equation (2.48):

$$\sum_\beta \left[i\alpha_{\nu\beta} \frac{d}{dz} - \Omega_{\nu\beta} \right] \phi_\beta(z) = -i \sum_{ij} M_{ij}^\nu G_{ji} \left(z, z^+ \right).$$

We can expand and rearrange the above for

$$-\frac{1}{\omega_\nu} \left(\frac{d^2}{dz^2} + \omega_\nu^2 \right) Q_\nu(z) = -i \sum_{ij} \lambda_{ij}^\nu G_{ji}(z, z^+) \tag{2.219}$$

and

$$P_\nu(z) = \frac{1}{\omega_\nu} \frac{dQ_\nu(z)}{dz}. \tag{2.220}$$

Using the KMS relation $\phi_\nu(z_f) = \phi_\nu(z_i)$, see section 2.3.3, we can rearrange equation (2.48) for

$$\phi_\nu(z) = -i \int_C d\bar{z} \sum_\mu \sum_{ij} d_{\nu\mu} \left(z, \bar{z} \right) M_{ij}^\mu G_{ji} \left(\bar{z}, \bar{z}^+ \right), \tag{2.221}$$

which expands to give

$$Q_\nu(z) = -i \int_c d\bar{z} \sum_\mu \sum_{ij} d_{QQ,\nu\mu} \left(z, \bar{z} \right) \lambda_{ij}^\mu G_{ji} \left(\bar{z}, \bar{z}^+ \right). \tag{2.222}$$

Moving to real time, take $z \to t^-$, such that

$$
\begin{aligned}
Q_\nu(t^-) &= -i \int_c dz \sum_\mu \sum_{ij} d_{QQ,\nu\mu} \left(t^-, z\right) \lambda_{ij}^\mu G_{ji} \left(z, z^+\right) \\
&= -i \int_{-\infty}^\infty dt^- \sum_\mu \sum_{ij} d_{QQ,\nu\mu} \left(t^-, t^-\right) \lambda_{ij}^\mu G_{ji}^< \left(t^-, t^-\right) \\
&\quad -i \int_\infty^{-\infty} dt^+ \sum_\mu \sum_{ij} d_{QQ,\nu\mu} \left(t^-, t^+\right) \lambda_{ij}^\mu G_{ji}^< \left(t^+, t^+\right) \\
&= -i \int_{-\infty}^\infty dt \sum_\mu \sum_{ij} \left(d_{QQ,\nu\mu}^T \left(t, t\right) - d_{QQ,\nu\mu}^< \left(t, t\right)\right) \lambda_{ij}^\mu G_{ji}^< \left(t, t\right) \\
Q_\nu(t) &= -i \int_{-\infty}^\infty dt \sum_\mu \sum_{ij} d_{QQ,\nu\mu}^R \left(t, t\right) \lambda_{ij}^\mu G_{ji}^< \left(t, t\right).
\end{aligned}
\tag{2.223}
$$

In addition to the average position, the average momentum follows simply as

$$
P_\nu(t) = \frac{1}{\omega_\nu} \frac{dQ_\nu(t)}{dt}.
\tag{2.224}
$$

To include the effects of a phonon bath, as set out in section 2.4.9, we calculate equation (2.223) with the additional bath, as set out in (2.211).

2.4.11 Observables

Given the calculation of the electronic and phononic Green's functions, we can calculate several observables important for investigating the dynamics in the system.

2.4.11.1 Electronic occupation

The occupation of the electronic levels within the central region can be calculated with the use of the lesser Green's functions:

$$
n_i^{el}(t) = \langle d_i^\dagger(t) d_i(t) \rangle = -i G_{ii}^< (t, t).
\tag{2.225}
$$

2.4.11.2 Electronic current

For the current through the junction, change in the α lead's occupation (i.e. $N_\alpha = \sum_k c_{k\alpha}^\dagger c_{k\alpha}$) over time. In the investigation, we consider the current from electrode α,

$$J_\alpha(t) = -\left\langle \frac{dN_\alpha}{dt} \right\rangle = -i\left\langle [H, N_\alpha] \right\rangle = 2Re\left[\sum_{k,c} t_{k\alpha,c}(t) G_{c,k\alpha}^<(t,t) \right], \qquad (2.226)$$

given that Here, we have that

$$\left[H(t), c_{k\alpha}^\dagger(t) c_{k\alpha}(t) \right]_- = \sum_j -t_{k\alpha,j} c_{k\alpha}^\dagger(t) d_j(t) + t_{k\alpha,j}^* d_j^\dagger(t) c_{k\alpha}(t). \qquad (2.227)$$

Substitution of the Dyson equation, using the alternate definition,

$$G_{c,k\alpha}^<(t,t')$$
$$= \int d1_{tc} \left[G_{cc_1}^<(t,t_1) t_{c_1 k\alpha} g_{ka,k\alpha}^A(t_1,t') + G_{cc_1}^R(t,t_1) t_{c_1 k\alpha} g_{ka,k\alpha}^<(t_1,t') \right], \qquad (2.228)$$

into Eq. (2.226) and encapsulation of the terms referring to the leads into the lead self-energies gives

$$J_\alpha = 2Re\left[\int dt_1 \sum_{c,c'} \left(G_{cc'}^<(t,t_1) \Sigma_{\alpha,c'c}^A(t_1,t) + G_{cc'}^R(t,t_1) \Sigma_{\alpha,c'c}^<(t_1,t) \right) \right]. \qquad (2.229)$$

2.4.11.3 Energy current

In addition to the current due to the flow of electrons from a lead, we can also calculate the energy carried by said electrons in terms of the energy current. To calculate the energy that leaves one of the leads via the movement of particles, we use the following:

$$\begin{aligned} I_\alpha^E(t) &= -\langle \frac{dH_\alpha(t)}{dt} \rangle\big|_{particles} = -\sum_k \epsilon_{k\alpha}(t) \langle \frac{d}{dt}\left(c_{k\alpha}^\dagger(t) c_{k\alpha}(t) \right) \rangle \\ &= -i\sum_{k\alpha} \epsilon_{k\alpha}(t) \langle \left[H(t), c_{k\alpha}^\dagger(t) c_{k\alpha}(t) \right]_- \rangle. \end{aligned} \qquad (2.230)$$

This can be manipulated for

$$\begin{aligned} I_\alpha^E(t) &= \sum_{kc} \epsilon_{k\alpha}(t) t_{ka,c}\left[i\langle c_{k\alpha}^\dagger(t) d_c(t) \rangle \right] - \epsilon_{k\alpha}(t) t_{ka,c}^*\left[i\langle d_c^\dagger(t) c_{k\alpha}(t) \rangle \right] \\ &= \sum_{kc} \epsilon_{k\alpha}(t) t_{ka,c} G_{cka}^<(t,t) - \epsilon_{k\alpha}(t) t_{ka,c}^* G_{k\alpha c}^<(t,t) \\ &= -2\,Re\left\{ \sum_{kc} \epsilon_{k\alpha}(t) t_{k\alpha c}^* G_{k\alpha c}^<(t,t) \right\}, \end{aligned} \qquad (2.231)$$

where substitution of the Dyson equation,

$$G_{k\alpha c}(t, t') = \int dt_1 \sum_{c'} g_{k\alpha}^<(t, t_1) t_{k\alpha c'} G_{c'c}^A(t_1, t') + g_{k\alpha}^R(t, t_1) t_{k\alpha c'} G_{c'c}^<(t_1, t'), \qquad (2.232)$$

allows for further rearrangement to

$$\begin{aligned}
I_\alpha^E(t) &= -2 \operatorname{Re} \left\{ \sum_{kc} \epsilon_{k\alpha}(t) t_{k\alpha c}^* G_{k\alpha c}^<(t, t) \right\} \\
&= -2 \operatorname{Re} \left\{ \int dt_1 \sum_{cc'} \sum_k \epsilon_{k\alpha}(t) t_{k\alpha c}^* g_{k\alpha}^<(t, t_1) t_{k\alpha c'} G_{c'c}^A(t_1, t') \right. \\
&\qquad \left. + \sum_k \epsilon_{k\alpha}(t) t_{k\alpha c}^* g_{k\alpha}^R(t, t_1) t_{k\alpha c'} G_{c'c}^<(t_1, t') \right\} \\
&= -2 \operatorname{Re} \left\{ \int dt_1 \sum_{cc'} \Phi_{\alpha, cc'}^<(t, t_1) G_{c'c}^A(t_1, t) + \Phi_{\alpha, cc'}^R(t, t_1) G_{c'c}^<(t_1, t) \right\},
\end{aligned} \qquad (2.233)$$

where we have defined

$$\Phi_{\alpha, cc'}^{A/R/</>}(t, t') = \sum_k \epsilon_{k\alpha}(t) t_{k\alpha c}^* g_{k\alpha}^{A/R/</>}(t, t') t_{k\alpha c'}. \qquad (2.234)$$

To calculate this new object, we note that the projections of equation (2.45) are

$$\left(i\frac{d}{dt} - \epsilon_{k\alpha}(t) \right) g_{k\alpha}^R(t, t') = \delta(t, t') \qquad (2.235)$$

and

$$\left(i\frac{d}{dt} - \epsilon_{k\alpha}(t) \right) g_{k\alpha}^<(t, t') = 0. \qquad (2.236)$$

This allows us to write the lesser new objects as

$$\Phi_{\alpha, cc'}^<(t, t') = \sum_k t_{k\alpha c}^* i\frac{d}{dt} g_{k\alpha}^<(t, t') t_{k\alpha c'} = i\frac{d}{dt} \Sigma_{\alpha, cc'}^<(t, t'). \qquad (2.237)$$

The retarded term has a further step:

$$\begin{aligned}
\Phi_{\alpha, cc'}^R(t, t') &= \sum_k \epsilon_{k\alpha}(t) t_{k\alpha c}^* g_{k\alpha}^R(t, t') t_{k\alpha c'} \\
&= \sum_k t_{k\alpha c}^* i\frac{d}{dt} g_{k\alpha}^R(t, t') t_{k\alpha c'} - \sum_k t_{k\alpha c}^* t_{k\alpha c'} \delta(t - t').
\end{aligned} \qquad (2.238)$$

We can show that the last term comes to zero when substituted into the equation for energy current:

$$\text{Re} \left\{ \int dt_1 \sum_{cc'} (-) \sum_k t^*_{k\alpha c} t_{k\alpha c'} \delta(t - t_1) G^<_{c'c}(t_1, t) \right\}$$

$$= \text{Re} \left\{ (-i) \sum_{cc'} \sum_k t^*_{k\alpha c} t_{k\alpha c'} n_{c'c}(t) \right\} = \text{Im} \left\{ \sum_{cc'} \sum_k t^*_{k\alpha c} t_{k\alpha c'} n_{c'c}(t) \right\}, \quad (2.239)$$

however, rather simply, we can prove that the object above has only a real part:

$$\sum_{cc'} \sum_k t^*_{k\alpha c} t_{k\alpha c'} n_{c'c}(t) = \sum_{c'c} \sum_k t^*_{k\alpha c'} t_{k\alpha c} n_{cc'}(t) = \sum_{cc'} \sum_k t_{k\alpha c} t^*_{k\alpha c'} n^*_{c'c}(t), \quad (2.240)$$

where we use $n^*_{cc'}(t) = n_{c'c}(t)$. This means that this terms disappears and we can define the new term's retarded projection as

$$\Phi^R_{\alpha,cc'}(t, t') = \sum_k t^*_{k\alpha c} i \frac{d}{dt} g^R_{k\alpha}(t, t') t_{k\alpha c'} = i \frac{d}{dt} \Sigma^R_{cc'}(t, t'). \quad (2.241)$$

2.4.11.4 Phonon occupation

To calculate the occupation of a phonon mode, we must evaluate the following terms:

$$\begin{aligned} n^{ph}_\nu(t) &= \left\langle \hat{a}^\dagger_\nu(t) \hat{a}_\nu(t) \right\rangle \\ &= \frac{1}{2} \left[\langle \hat{P}_\nu(t)^2 \rangle + \langle \hat{Q}_\nu(t)^2 \rangle \right] - \frac{1}{2} \\ &= \frac{1}{2} \left[i D^<_{QQ,\nu\nu}(t, t) + (Q_\nu(t))^2 + i D^<_{PP,\nu\nu}(t, t) + (P_\nu(t))^2 \right] - \frac{1}{2}. \end{aligned} \quad (2.242)$$

Here, the equations of motion for $D^<_{QQ,\nu\nu}(t, t)$, $Q_\nu(t)$ and $P_\nu(t)$ have been set out above. To calculate $D^<_{PP,\nu\nu}(t, t)$, we have, on the Keldysh contour, that

$$\frac{d^2}{dz dz'} \left[\text{T}_c \left(\Delta Q_\nu(z) \Delta Q_{\nu'}(z') \right) \right]$$

$$= \frac{d}{dz} \left[\frac{d}{dz'} \left(\theta(z, z') \Delta \hat{Q}_\nu(z) \Delta \hat{Q}_{\nu'}(z') + \theta(z', z) \Delta \hat{Q}_{\nu'}(z') \Delta \hat{Q}_\nu(z) \right) \right]$$

$$= \frac{d}{dz} \left[\delta(z, z') \left[\Delta \hat{Q}_{\nu'}(z'), \Delta \hat{Q}_\nu(z) \right]_- + \Omega_{\nu'} \text{T}_c \left(\Delta \hat{Q}_\nu(z) \Delta \hat{P}_{\nu'}(z') \right) \right] \quad (2.243)$$

$$= \Omega_{\nu'} \frac{d}{dz} \left[\theta(z, z') \Delta \hat{Q}_\nu(z) \Delta \hat{P}_{\nu'}(z') + \theta(z', z) \Delta \hat{P}_{\nu'}(z') \Delta \hat{Q}_\nu(z) \right]$$

$$= \Omega_{\nu'} \delta(z, z') \left[\Delta \hat{Q}_\nu(z), \Delta \hat{P}_{\nu'}(z') \right]_- + \Omega_\nu \Omega_{\nu'} \text{T}_c \left(\Delta \hat{P}_\nu(z) \Delta \hat{P}_{\nu'}(z') \right)$$

$$= \Omega_{\nu'} \delta(z, z') i \delta_{\nu\nu'} + \Omega_\nu \Omega_{\nu'} \text{T}_c \left(\Delta \hat{P}_\nu(z) \Delta \hat{P}_{\nu'}(z') \right),$$

where we use $\left[\hat{Q}_\nu, \hat{Q}_\mu\right]_- = \left[\hat{P}_\nu, \hat{P}_\mu\right]_- = 0$ and $\left[\hat{Q}_\nu, \hat{P}_\mu\right]_- = i\delta_{\nu\mu}$, to give us the following equation of motion of the contour:

$$\frac{d}{dzdz'}D_{\nu\nu'}(z,z') = \Omega_\nu\delta_{\nu\nu'}\delta(z,z') + \Omega_\nu\Omega_{\nu'}D_{\nu\nu'}^{PP}(z,z'). \tag{2.244}$$

This gives us the following lesser projection, which we can utilize to calculate equation (2.242):

$$\frac{d}{dtdt'}D_{\nu\nu'}^<(t,t') = \Omega_\nu\Omega_{\nu'}D_{\nu\nu'}^{PP,<}(t,t'). \tag{2.245}$$

2.4.12 Full Counting Statistics

So far, the observables considered have been calculable from the single-particle electronic Green's functions and two-field phononic Green's functions. In this section, we set out how to access current noise and higher cumulants of the current with the help of full counting statistics [70, 71].

2.4.12.1 General considerations

We begin by defining the generating function, $\chi(\lambda_\alpha, t_c, t_0)$, and the probability that q charge will be transferred from lead α to the central region from the time t_0 to the time t_c, $P(q, t_c, t_0)$:

$$\chi(\lambda_\alpha, t_c, t_0) = \sum_q e^{iq\lambda_\alpha} P(q, t_c, t_0) \tag{2.246}$$

and

$$P(q, t_c, t_0) = \int_0^{2\pi} \frac{d\lambda_\alpha}{2\pi} \chi(\lambda_\alpha, t_c, t_0) e^{-iq\lambda_\alpha}. \tag{2.247}$$

We can find the cumulants $\langle \delta^n q \rangle$, i.e. the irreducible moments of P_q, with the following definition:

$$\langle \delta^n q \rangle = (-i)^n \frac{\partial^n}{\partial \lambda_\alpha^n} \ln \chi(\lambda_\alpha) \Big|_{\lambda_\alpha = 0}. \tag{2.248}$$

We can define the generating function for counting the change in the number of electrons in lead α between times t_c and t_0 as follows:

$$\chi(\lambda_\alpha, t_c, t_0) = \left\langle e^{-i\lambda_\alpha N_\alpha(t_c)} e^{i\lambda_\alpha N_\alpha(t_0)} \right\rangle. \tag{2.249}$$

When we insert the above into equation (2.248), the cumulants of the change in occupation of the lead are generated:

$$\langle \delta q \rangle = \langle N_\alpha(t_c) \rangle - \langle N_\alpha(t_0) \rangle |_{\lambda=0} \tag{2.250}$$

and

$$\langle \delta^2 q \rangle = \left. \langle (N_\alpha(t_c) - N_\alpha(t_0))^2 \rangle - (\langle N_\alpha(t_c) \rangle - \langle N_\alpha(t_0) \rangle)^2 \right|_{\lambda=0}. \tag{2.251}$$

In our calculations, we assume that the first observation at t_0 is completed at the moment the central region and the surrounding leads are connected. This means that the system and reservoirs are decoupled at equilibrium at time t_0. Specifically, we make use of the fact that $[\rho(t_0), N_L(t_0)] = 0$ when the above is assumed. This allows us to, while making use of the cyclical properties of the trace, manipulate the generating function:

$$\begin{aligned}
\chi(\lambda_\alpha, t_c, t_0) &= \langle e^{-i\lambda_\alpha N_\alpha(t_c)} e^{i\lambda_\alpha N_\alpha(t_0)} \rangle \\
&= \text{Tr}\left[\rho(t_0) e^{-i\lambda_\alpha N_\alpha(t_c)} e^{i\lambda_\alpha N_\alpha(t_0)}\right] \\
&= \text{Tr}\left[\rho(t_0) U(t_0, t_c) e^{-i\lambda_\alpha N_\alpha(t_0)} U(t_c, t_0) e^{i\lambda_\alpha N_\alpha(t_0)}\right] \\
&= \text{Tr}\left[\rho(t_0) e^{\frac{i}{2}\lambda_\alpha N_\alpha(t_0)} U(t_0, t_c) e^{-\frac{i}{2}\lambda_\alpha N_\alpha(t_0)}\right. \\
&\qquad \left. e^{-\frac{i}{2}\lambda_\alpha N_\alpha(t_0)} U(t_c, t_0) e^{\frac{i}{2}\lambda_\alpha N_\alpha(t_0)}\right] \\
&= \text{Tr}\left[\rho(t_0) U_{\lambda_\alpha}^\dagger U(t_0, t_c) U_{\lambda_\alpha} U_{\lambda_\alpha} U(t_c, t_0) U_{\lambda_\alpha}^\dagger\right],
\end{aligned} \tag{2.252}$$

where we utilise the fact that $N_\alpha(t_c) = U(t_0, t_c) N_\alpha(t_0) U(t_c, t_0)$. We see that we have a unitary transformation of the evolution operators, where we define $U_{\lambda_\alpha} = e^{-\frac{i}{2}\lambda_\alpha N_\alpha(t_0)}$.

We open up the evolution operator to investigate the resulting transformation:

$$\begin{aligned}
U_{\lambda_\alpha} U(t_c, t_0) U_{\lambda_\alpha}^\dagger &= U_{\lambda_\alpha} \text{T}\left\{e^{-i\int_{t_0}^{t_c} dt H(t)}\right\} U_{\lambda_\alpha}^\dagger \\
&= \sum_{n=0}^\infty \frac{(-i)^n}{n!} U_{\lambda_\alpha} \text{T}\left\{\int_{t_0}^{t_c} dt_1 ... \int_{t_0}^{t_c} dt_n H(t_1) ... H(t_n)\right\} U_{\lambda_\alpha}^\dagger \\
&= \sum_{n=0}^\infty \frac{(-i)^n}{n!} \text{T}\left\{\int_{t_0}^{t_c} dt_1 ... \int_{t_0}^{t_c} dt_n U_{\lambda_\alpha} H(t_1) U_{\lambda_\alpha}^\dagger ... U_{\lambda_\alpha} H(t_n) U_{\lambda_\alpha}^\dagger\right\}.
\end{aligned} \tag{2.253}$$

With respect to $U_{\lambda_\alpha} H(t) U_{\lambda_\alpha}^\dagger$, all the terms in the Hamiltonian commute with U_{λ_α} but the coupling between lead α and the central region, $H_{\alpha C}$, as seen in equation (2.7). Of $H_{\alpha C}$, the following operators for lead α do not commute with U_{λ_α}:

$$\begin{aligned}
U_{\lambda_\alpha} c_{k\alpha}^\dagger U_{\lambda_\alpha}^\dagger &= e^{-\frac{i}{2}\lambda_\alpha N_\alpha(t_0)} c_{k\alpha}^\dagger e^{\frac{i}{2}\lambda_\alpha N_\alpha(t_0)} \\
&= \left(1 - \frac{i}{2}\lambda_\alpha N_\alpha(t_0)...\right) c_{k\alpha}^\dagger \left(1 + \frac{i}{2}\lambda_\alpha N_\alpha(t_0)...\right) \\
&= \left(1 - \frac{i}{2}\lambda_\alpha...\right) c_{k\alpha}^\dagger (1 + 0...) \\
&= e^{-\frac{i}{2}\lambda_\alpha} c_{k\alpha}^\dagger,
\end{aligned} \tag{2.254}$$

and similarly

$$U_{\lambda_\alpha} c_{k\alpha} U_{\lambda_\alpha}^\dagger = e^{\frac{i}{2}\lambda_\alpha} c_{k\alpha}. \tag{2.255}$$

We see that the transformation has the effect of adding the counting field into $H_{\alpha C}$:

$$H_{\alpha C}^{\lambda_\alpha}(t) = \sum_{i,k\alpha} t_{k\alpha,i}(t) e^{-\frac{i}{2}\lambda_\alpha} c_{k\alpha}^\dagger d_i + t_{k\alpha,i}^*(t) e^{\frac{i}{2}\lambda_\alpha} d_i^\dagger c_{k\alpha}. \tag{2.256}$$

With the counting field now within the Hamiltonian, labelled as $H^{\lambda_\alpha}(t)$, the time evolution operator can be bundled back up:

$$U_{\lambda_\alpha} U(t_c, t_0) U_{\lambda_\alpha}^\dagger = U_{\lambda_\alpha}(t_c, t_0) = \mathrm{T}\left\{ e^{-i\int_{t_0}^{t_c} dt H^{\lambda_\alpha}(t)} \right\}. \tag{2.257}$$

We can complete a similar assessment of the other term in Eq. (2.252); however, the counting field must be negated (i.e., $\lambda_\alpha \to -\lambda_\alpha$):

$$e^{\frac{i}{2}\lambda_\alpha N_\alpha(t_0)} U(t_0, t_c) e^{-\frac{i}{2}\lambda_\alpha N_\alpha(t_0)} = U_{-\lambda_\alpha} U(t_0, t_c) U_{-\lambda_\alpha}^\dagger = U_{-\lambda_\alpha}(t_0, t_c). \tag{2.258}$$

Putting all the above together, we find that the generating function is given in terms of our evolution operators:

$$\chi(\lambda_\alpha, t_c, t_0) = \langle U_{-\lambda_\alpha}(t_0, t_c) U_{\lambda_\alpha}(t_c, t_0) \rangle. \tag{2.259}$$

We invoke the contour and define $\lambda_\alpha(z) = \lambda_\alpha$ on the forward branch (i.e. C_f) and $\lambda(z) = -\lambda_\alpha$ on the backward branch (i.e. C_b). Hence, we arrive at the desired result for a generating function:

$$\chi(\lambda_\alpha, t_c, t_0) = \langle \mathrm{T_c}\left(e^{-i\int_c H^{\lambda_\alpha(z)}(z)dz} \right) \rangle, \tag{2.260}$$

where

$$H_{\alpha C}^{\lambda_\alpha(z)}(z) = \sum_{i,k} t_{k\alpha i}(z) e^{-\frac{i}{2}\lambda_\alpha(z)} c_{k\alpha}^\dagger d_i + t_{k\alpha i}^*(z) e^{\frac{i}{2}\lambda_\alpha(z)} d_i^\dagger c_{k\alpha}, \tag{2.261}$$

or

$$H_{\alpha C}^{\lambda_\alpha}(t) = \sum_{i,k} t_{k\alpha i}(t) e^{-\frac{i}{2}\lambda_\alpha} c_{k\alpha}^\dagger d_i + t_{k\alpha i}^*(t) e^{\frac{i}{2}\lambda_\alpha} d_i^\dagger c_{k\alpha} \tag{2.262}$$

and

$$H_{\alpha C}^{-\lambda_\alpha}(t) = \sum_{i,k} t_{k\alpha i}(t) e^{\frac{i}{2}\lambda_\alpha} c_{k\alpha}^\dagger d_i + t_{k\alpha i}^*(t) e^{-\frac{i}{2}\lambda_\alpha} d_i^\dagger c_{k\alpha}, \tag{2.263}$$

for the forward and backward branches of the contour, respectively.

2.4.12.2 Moving to NEGF

Equation (2.259) can be further manipulated to generate a result in terms of the electronic Green's functions and self-energies. To begin, we cast the problem in terms of the interaction

picture, which will help with the derivation of the final result:

$$H_{\lambda_\alpha}(t) = h(t) + V_{\lambda_\alpha}(t), \tag{2.264}$$

such that

$$U_{\lambda_\alpha}(t,t') = P(t,t_0)S_{\lambda_\alpha}(t,t')P^\dagger(t',t_0), \tag{2.265}$$

where

$$P(t,t') = \begin{cases} \mathrm{T}\left\{e^{-i\int_{t'}^{t} dt\, h(t)}\right\} & t > t' \\ \widetilde{\mathrm{T}}\left\{e^{i\int_{t}^{t'} dt\, h(t)}\right\} & t < t' \end{cases}. \tag{2.266}$$

Here, $h(t)$ is the term of the complete Hamiltonian without counting field, while $V_{\lambda_\alpha}(t)$ is the term containing the counting field, in this case $H_{\alpha C}^{\pm\lambda_\alpha}(t)$. With some investigation, we find that

$$S_{\lambda_\alpha}(t,t') = \begin{cases} \mathrm{T}\left\{e^{-i\int_{t'}^{t} dt\, V_h^{\lambda_\alpha}(t)}\right\} & t > t' \\ \widetilde{\mathrm{T}}\left\{e^{i\int_{t}^{t'} dt\, V_h^{\lambda_\alpha}(t)}\right\} & t < t', \end{cases} \tag{2.267}$$

where

$$V_h^{\lambda_\alpha}(t) = P^\dagger(t,t_0)V_{\lambda_\alpha}(t)P(t,t_0). \tag{2.268}$$

We begin by considering the generating function in the interacting picture:

$$\begin{aligned}
\chi(\lambda_\alpha, t_c, t_0) &= \langle U_{-\lambda_\alpha}(t_0, t_c)\, U_{\lambda_\alpha}(t_c, t_0)\rangle \\
&= \langle P(t_0, t_0)S_{-\lambda_\alpha}(t_0, t_c)\, P^\dagger(t_c, t_0)P(t_c, t_0)S_{\lambda_\alpha}(t_c, t_0)\, P^\dagger(t_0, t_0)\rangle \\
&= \langle S_{-\lambda_\alpha}(t_0, t_c)\, S_{\lambda_\alpha}(t_c, t_0)\rangle \\
&= \langle \mathrm{T_c}\left(e^{-i\int_c V_h^{\lambda_\alpha(z)}(z)dz}\right)\rangle.
\end{aligned} \tag{2.269}$$

To cast the problem in terms of Green's functions, we now take the first cumulant without setting the measuring field to zero:

$$-i\frac{\partial}{\partial\lambda_\alpha}\ln\left(\chi(\lambda_\alpha, t_c, t_0)\right) = -i\frac{\frac{\partial}{\partial\lambda_\alpha}\chi(\lambda_\alpha, t_c, t_0)}{\chi(\lambda_\alpha, t_c, t_0)}. \tag{2.270}$$

Focusing on the numerator, we have that

$$\begin{aligned}
\frac{\partial}{\partial\lambda_\alpha}\chi(\lambda_\alpha, t_c, t_0) &= \frac{\partial}{\partial\lambda_\alpha}\langle \mathrm{T_c}\left(e^{-i\int_c V_h^{\lambda_\alpha(z)}(z)dz}\right)\rangle \\
&= -i\int_c dz\langle \mathrm{T_c}\left(\frac{\partial V_h^{\lambda_\alpha(z)}(z)}{\partial\lambda_\alpha}e^{-i\int_c V_h^{\lambda_\alpha(z)}(z)dz}\right)\rangle,
\end{aligned} \tag{2.271}$$

where

$$\frac{\partial V_h^{\lambda_\alpha(z)}(z)}{\partial \lambda_\alpha} = \sum_{c,k} \frac{\partial \lambda_\alpha(z)}{\partial \lambda_\alpha} \left(-\frac{i}{2} t_{k\alpha c}(z) e^{-\frac{i}{2}\lambda_\alpha(z)} c_{k\alpha,h}^\dagger(z) d_{c,h}(z) + \frac{i}{2} t_{k\alpha c}^*(z) e^{\frac{i}{2}\lambda_\alpha(z)} d_{c,h}^\dagger(z) c_{k\alpha,h}(z) \right),$$

(2.272)

hence

$$-i\frac{\partial}{\partial \lambda_\alpha} \ln\left(\chi\left(\lambda_\alpha, t_c, t_0\right)\right)$$

$$= \frac{i}{2} \frac{1}{\chi\left(\lambda_\alpha, t_c, t_0\right)} \sum_{c,k} \int_c dz \frac{\partial \lambda_\alpha(z)}{\partial \lambda_\alpha} \left[t_{k\alpha c}(z) e^{-\frac{i}{2}\lambda_\alpha(z)} \langle T_c \left(e^{-i\int_c V_h^{\lambda(z)}(z)dz} c_{k\alpha,h}^\dagger(z) d_{c,h}(z) \right) \rangle \right.$$

$$\left. - t_{k\alpha c}^*(z) e^{\frac{i}{2}\lambda_\alpha(z)} \langle T_c \left(e^{-i\int_c V_h^{\lambda_\alpha(z)}(z)dz} d_{c,h}^\dagger(z) c_{k\alpha,h}(z) \right) \rangle \right] \quad (2.273)$$

$$= -\frac{i}{2} \frac{1}{\chi\left(\lambda_\alpha, t_c, t_0\right)} \sum_{c,k} \int_c dz \frac{\partial \lambda_\alpha(z)}{\partial \lambda_\alpha} \left[t_{k\alpha c}(z) e^{-\frac{i}{2}\lambda_\alpha(z)} \langle T_c \left(e^{-i\int_c V_h^{\lambda_\alpha(z)}(z)dz} d_{c,h}(z) c_{k\alpha,h}^\dagger(z) \right) \rangle \right.$$

$$\left. - t_{k\alpha c}^*(z) e^{\frac{i}{2}\lambda_\alpha(z)} \langle T_c \left(e^{-i\int_c V_h^{\lambda_\alpha(z)}(z)dz} c_{k\alpha,h}(z) d_{c,h}^\dagger(z) \right) \rangle \right].$$

Collecting the above, we have that

$$-i\frac{\partial}{\partial \lambda_\alpha} \ln\left(\chi\left(\lambda_\alpha, t_c, t_0\right)\right)$$

$$= \frac{i}{2} \frac{1}{\chi\left(\lambda_\alpha, t_c, t_0\right)} \sum_{c,k} \int_c dz \frac{\partial \lambda_\alpha(z)}{\partial \lambda_\alpha} \left[t_{k\alpha c}(z) e^{-\frac{i}{2}\lambda_\alpha(z)} \langle T_c \left(e^{-i\int_c H^{\lambda_\alpha(z)}(z)dz} c_{k\alpha}^\dagger(z) d_i(z) \right) \rangle \right.$$

$$\left. - t_{k\alpha c}^*(z) e^{\frac{i}{2}\lambda_\alpha(z)} \langle T_c \left(e^{-i\int_c H^{\lambda_\alpha(z)}(z)dz} d_c^\dagger(z) c_{k\alpha}(z) \right) \rangle \right] \quad (2.274)$$

$$= -\frac{i}{2} \frac{1}{\chi\left(\lambda_\alpha, t_c, t_0\right)} \sum_{c,k} \int_c dz \frac{\partial \lambda_\alpha(z)}{\partial \lambda_\alpha} \left[t_{k\alpha c}(z) e^{-\frac{i}{2}\lambda_\alpha(z)} \langle T_c \left(e^{-i\int_c H^{\lambda_\alpha(z)}(z)dz} d_c(z) c_{k\alpha}^\dagger(z) \right) \rangle \right.$$

$$\left. - t_{k\alpha c}^*(z) e^{\frac{i}{2}\lambda_\alpha(z)} \langle T_c \left(e^{-i\int_c H^{\lambda_\alpha(z)}(z)dz} c_{k\alpha}(z) d_c^\dagger(z) \right) \rangle \right].$$

Here, the last step is due to the rearranging of the operators within the contour-time average. We can cast the above in terms of the electronic Green's functions of the system, with the addition of the counting field. Here, it is important to remember that the Green's functions need to be calculated on a contour that goes up to t_c, as you cannot remove (or add) the once redundant extra part to the contour.

The Green's functions allows us to rewrite the generating function as follows:

$$-i\frac{\partial}{\partial \lambda_\alpha} \ln\left(\chi\left(\lambda_\alpha, t_c, t_0\right)\right)$$

(2.275)

$$= \frac{1}{2} \sum_{c,k} \int_c dz \frac{\partial \lambda_\alpha(z)}{\partial \lambda_\alpha} \left[t_{k\alpha c}(z) e^{-\frac{i}{2}\lambda_\alpha(z)} G_{ck\alpha}\left(z^+, z\right) - t_{k\alpha c}^*(z) e^{\frac{i}{2}\lambda_\alpha(z)} G_{k\alpha c}\left(z^+, z\right) \right].$$

We can cast the above in terms of lead self-energies. In a similar way to sections 2.4.11.2 and

we make use of the Dyson equations for the contour Green's functions,

$$G_{k\alpha c}\left(z,z'\right) = \sum_{c',k'}\int_c dz_1 \; g_{k\alpha,k'\alpha}\left(z,z_1\right) t_{k'\alpha c'}(z_1) e^{-\frac{i}{2}\lambda_\alpha(z)} G_{c'c}\left(z_1,z'\right) \tag{2.276}$$

and

$$G_{ck\alpha}\left(z,z'\right) = \sum_{c',k'}\int_c dz_1 \; G_{cc'}\left(z,z_1\right) t^*_{k'\alpha c'}(z_1) e^{\frac{i}{2}\lambda_\alpha(z)} g_{k'\alpha,k\alpha}\left(z_1,z'\right) \tag{2.277}$$

to acquire the following result:

$$-i\frac{\partial}{\partial\lambda_\alpha}\ln\left(\chi\left(\lambda_\alpha,t_c,t_0\right)\right)$$
$$= \frac{1}{2}\sum_{c,k}\int_c dz \sum_{c',k'}\int_c dz_1 \frac{\partial\lambda_\alpha(z)}{\partial\lambda_\alpha}\left[G_{cc'}\left(z,z_1\right)e^{-\frac{i}{2}(\lambda_\alpha(z)-\lambda_\alpha(z_1))}t^*_{k'\alpha c'}(z_1)g_{k'\alpha,k\alpha}\left(z_1,z\right)t_{k\alpha c}(z)\right. \tag{2.278}$$
$$\left. - e^{-\frac{i}{2}(\lambda_\alpha(z_1)-\lambda_\alpha(z))}t^*_{k\alpha c}(z)\,g_{k\alpha,k'\alpha}\left(z,z_1\right)t_{k'\alpha,i'}(z_1)G_{c'c}\left(z_1,z\right)\right],$$

which allows us to define the self-energy for lead α:

$$\Sigma_{\alpha,cc'}(z,z') = \sum_{k,k'}e^{\frac{i}{2}(\lambda_\alpha(z)-\lambda_\alpha(z'))}t^*_{k\alpha c}(z)\,g_{k\alpha,k'\alpha}\left(z,z'\right)t_{k'\alpha c'}(z'). \tag{2.279}$$

This allows us to write the above as follows:

$$-i\frac{\partial}{\partial\lambda_\alpha}\ln\left(\chi\left(\lambda_\alpha,t_c,t_0\right)\right)$$
$$= -\frac{1}{2}\sum_{c,c'}\int_c dz \int_c dz_1 \frac{\partial\lambda_\alpha(\tau)}{\partial\lambda_\alpha}\left[\Sigma_{\alpha,cc'}(z,z_1)G_{c'c}\left(z_1,z\right) - G_{cc'}\left(z,z_1\right)\Sigma_{\alpha,c'c}(z_1,z)\right]. \tag{2.280}$$

Utilising the results from section 2.4.4, we move from the Keldysh contour to a real-time result. We begin by expanding the first integral into its forward and backward branches, using the

notation of section 2.4.4:

$$-\frac{1}{2}\sum_{c,c'}\int_c dz \int_c dz_1 \frac{\partial \lambda_\alpha(z)}{\partial \lambda_\alpha}\left[\Sigma_{\alpha,cc'}(z,z_1)G_{i'i}(z_1,z) - G_{ii'}(z,z_1)\Sigma_{\alpha,c'c}(z_1,z)\right]$$

$$= -\frac{1}{2}\sum_{c,c'}\int_c dz_1 \left[\int_{t_0}^{t_c} dt \frac{\partial \lambda_\alpha(t^-)}{\partial \lambda_a \alpha}\left[\Sigma_{\alpha,cc'}^-(t,z_1)G_{c'c}^-(z_1,t) - G_{cc'}^-(t,z_1)\Sigma_{\alpha,c'c}^-(z_1,t)\right]\right.$$

$$\left. - \int_{t_0}^{t_c} dt \frac{\partial \lambda(t^+)}{\partial \lambda}\left[\Sigma_{\alpha,cc'}^+(t,z_1)G_{c'c}^+(z_1,t) - G_{cc'}^+(t,z_1)\Sigma_{\alpha,c'c}^+(z_1,t)\right]\right]$$

$$= -\frac{1}{2}\sum_{c,c'}\int_{t_0}^{t_c} dt_1 \int_{t_0}^{t_c} dt\, \Sigma_{\alpha,cc'}^{--}(t,t_1)G_{c'c}^{--}(t_1,t) - \Sigma_{\alpha,cc'}^{-+}(t,t_1)G_{c'c}^{+-}(t_1,t)$$

$$-G_{cc'}^{--}(t,t_1)\Sigma_{\alpha,c'c}^{--}(t_1,t) + G_{cc'}^{-+}(t,t_1)\Sigma_{\alpha,c'c}^{+-}(t_1,t) \qquad (2.281)$$

$$+\Sigma_{\alpha,cc'}^{+-}(t,t_1)G_{c'c}^{-+}(t_1,t) - \Sigma_{\alpha,cc'}^{++}(t,t_1)G_{c'c}^{++}(t_1,t)$$

$$-G_{cc'}^{+-}(t,t_1)\Sigma_{\alpha,c'c}^{-+}(t_1,t) + G_{cc'}^{++}(t,t_1)\Sigma_{\alpha,c'c}^{++}(t_1,t)$$

$$= -\frac{1}{2}\sum_{i,i'}\int_{t_0}^{t_c} dt_1 \int_{t_0}^{t_c} dt\, \mathrm{Tr}\left[\Sigma_\alpha^{--}(t,t_1)G^{--}(t_1,t) - \Sigma_\alpha^{-+}(t,t_1)G^{+-}(t_1,t)\right.$$

$$-G^{--}(t,t_1)\Sigma_\alpha^{--}(t_1,t) + G^{-+}(t,t_1)\Sigma_\alpha^{+-}(t_1,t)$$

$$+\Sigma_\alpha^{+-}(t,t_1)G^{-+}(t_1,t) - \Sigma_\alpha^{++}(t,t_1)G^{++}(t_1,t)$$

$$\left. - G^{+-}(t,t_1)\Sigma_\alpha^{-+}(t_1,t) + G^{++}(t,t_1)\Sigma_\alpha^{++}(t_1,t)\right].'$$

Here, $t^\mp$ refers to time on the forward and backward branches of the Keldysh contour, respectively. We take the above and, using the cyclic properties of the trace, combine and remove terms to acquire the final result:

$$-i\frac{\partial}{\partial \lambda_\alpha}\ln\left(\chi\left(\lambda_L, t_c, t_0\right)\right)$$

$$= \int_{t_0}^{t_c} dt \int_{t_0}^{t_c} dt'\, \mathrm{Tr}\left[\Sigma_\alpha^{-+}(t,t')G^{+-}(t',t) - G^{-+}(t,t')\Sigma_\alpha^{+-}(t',t)\right] \qquad (2.282)$$

$$= \int_{t_0}^{t_c} dt \int_{t_0}^{t_c} dt'\, \mathrm{Tr}\left[\Sigma_\alpha^<(t,t')G^>(t',t) - G^<(t,t')\Sigma_\alpha^>(t',t)\right].$$

From equation (2.279), we find that, within the wide-band approximation, the lead self-energies have the following projections:

$$\Sigma_{\alpha,cc'}^<(t,t') = \bar{\Sigma}_{\alpha,cc'}^<(t,t')\, e^{i\lambda_\alpha}, \qquad (2.283)$$

and

$$\Sigma_{\alpha,cc'}^>(t,t') = \bar{\Sigma}_{\alpha,cc'}^>(t,t')\, e^{-i\lambda_\alpha}, \qquad (2.284)$$

where the bar signifies no counting field. The $\Sigma_{\alpha,cc'}^{T/\tilde{T}}(t,t')$ self-energies will not change. Due to this we have that $\Sigma_{\alpha,cc'}^T(t,t') + \Sigma_{\alpha,cc'}^{\tilde{T}}(t,t') \neq \Sigma_{\alpha,cc'}^<(t,t') + \Sigma_{\alpha,cc'}^>(t,t')$. This means that the transformation of equation (2.98) will not remove a term from the Keldysh-Schwinger matrix, making it unnecessary when using full counting statistics.

Timescale-Separation for Time Dependent Transport

3.1 Introduction

A nanoscale electronic junction is typically a single molecule attached to two macroscopic leads. In the standard scenario, the static voltage bias is applied to the lead electrodes and the electric current across the molecule is measured. Whilst interest in time-dependent quantum transport phenomena has a long history [36], recently, microwave or optical irradiation of the molecular scale electronic junctions have been used to control electronic properties of the system[72–74]. Access to the optical range is of particular importance, since the frequencies of the time-dependent driving become comparable to molecular vibrational frequencies, which suggests the opportunity to stir the electron-vibrational dynamics in molecular junctions. These recent experimental advances have resulted in an increase in the ongoing development and application of time-dependent quantum transport theories tailored specifically to the properties of molecular electronic junctions [75–79].

Historically, Tien and Gordon proposed their seminal qualitative theory to describe the effects of harmonic time-dependent potential on electronic tunnel junctions as early as 1963[34]. Since this work, further more sophisticated approaches, based on Floquet and scattering theories[80–88], quantum master equations[76, 77], and notably nonequilibrium Green's functions (NEGF) based approaches[78, 89–106] have been developed to deal with time dependent trans-

port in driven quantum systems. The use of NEGF allows for the possibility of a systematic treatment of correlations in time-dependent electron transport. In particular, the effects of electron-phonon interactions with time-dependent junctions have been investigated[107–113]. However, this often comes with a considerable increase in complexity, computationally and theoretically, with the helpful simplifications of the noninteracting case being inapplicable.

In this chapter, we develop an approach which algebraically solves the Kadanoff-Baym equations for a molecular electronic junction in time-dependent fields using the separation of time-scales between fast electronic tunnelling and slow oscillations of driving external fields. It enables us to produce analytic expressions for dynamical corrections to adiabatic (instantaneous) Green's functions and, consequently, dynamical corrections to adiabatic expressions for observable quantities such as time-dependent electric current. The approach follows the ideas of Arrachea and Moskalets in that it makes use of adiabatic approximations to solve the NEGF Dysons equations [90].

3.2   Theory

We begin with the Kadanoff-Baym equations of motion for the retarded, advanced and lesser Green's functions, as set out in section 2.4.5:

$$\left(i\partial_t - \mathbf{h}(t)\right)\mathcal{G}^<(t,t') = \int dt_1 \left[\mathbf{\Sigma}_{\text{tot}}^R(t,t_1)\mathcal{G}^<(t_1,t') + \mathbf{\Sigma}_{\text{tot}}^<(t,t_1)\mathcal{G}^A(t_1,t')\right] \tag{3.1}$$

and

$$\left(i\partial_t - \mathbf{h}(t)\right)\mathcal{G}^{R/A}(t,t') = \mathbf{I}\delta(t-t') + \int dt_1 \mathbf{\Sigma}_{\text{tot}}^{R/A}(t,t_1)\mathcal{G}^{R/A}(t_1,t'). \tag{3.2}$$

We have chosen to work with the Kadanoff-Baym equations in matrix form where the Green's functions $\mathcal{G}$, self-energies $\mathbf{\Sigma}$ and Hamiltonian $\mathbf{h}$ are matrices in the molecular single-particle space, as seen in equation (2.3). Here $\mathbf{I}$ is the identity matrix in molecular space. We introduced the total self-energy

$$\mathbf{\Sigma}_{\text{tot}}^{R/A/<} = \mathbf{\Sigma}^{R/A/<} + \mathbf{\Sigma}_c^{R/A/<}, \tag{3.3}$$

where $\mathbf{\Sigma}_c$ is the self-energy from correlations in the central region and the choice of the particular form is not relevant for our immediate discussion in this section.

Transforming the Kadanoff-Baym equations (3.1,3.2) to the Wigner representation removes all time-integrals via an infinite series of time and energy derivatives collected in the exponential

operators:

$$\left[\frac{i}{2}\partial_T + \omega - e^{-\frac{i}{2}\partial_\omega^{\mathcal{G}}\partial_T^{h}}h(T)\right]\widetilde{\mathcal{G}}^{<}(T,\omega) =$$

$$e^{-\frac{i}{2}\left(\partial_T^{\Sigma}\partial_\omega^{\mathcal{G}} - \partial_\omega^{\Sigma}\partial_T^{\mathcal{G}}\right)}\left(\widetilde{\boldsymbol{\Sigma}}_{\text{tot}}^{<}(T,\omega)\widetilde{\mathcal{G}}^{A}(T,\omega) + \widetilde{\boldsymbol{\Sigma}}_{\text{tot}}^{R}(T,\omega)\widetilde{\mathcal{G}}^{<}(T,\omega)\right)$$

(3.4)

and

$$\left[\frac{i}{2}\partial_T + \omega - e^{-\frac{i}{2}\partial_\omega^{\mathcal{G}}\partial_T^{h}}h(T)\right]\widetilde{\mathcal{G}}^{A/R}(T,\omega) = \mathbf{I} + e^{-\frac{i}{2}\left(\partial_T^{\Sigma}\partial_\omega^{\mathcal{G}} - \partial_\omega^{\Sigma}\partial_T^{\mathcal{G}}\right)}\widetilde{\boldsymbol{\Sigma}}_{\text{tot}}^{A/R}(T,\omega)\widetilde{\mathcal{G}}^{A/R}(T,\omega). \quad (3.5)$$

In contrast to section 2.4.8, the lead self-energies can be calculated with an alternative method, starting with the harmonic modulation of the leads' single-particle energies

$$\epsilon_{k\alpha}(t) = \epsilon_{k\alpha} + \Delta_\alpha \cos\left(\Omega_\alpha t + \phi_\alpha\right). \tag{3.6}$$

The self-energies of leads are, as seen in equation (2.186),

$$\Sigma_{\alpha ij}^{R,A,<}(t,t') = \sum_k t_{k\alpha i}^* g_{k\alpha}^{R,A,<}(t,t') t_{k\alpha j}, \tag{3.7}$$

where, making use of definitions for the noninteracting Green's functions as in section (2.4.5), the Green's functions for leads can be cast as

$$g_{k\alpha}^{<}(t,t') = if_{k\alpha}e^{-i\epsilon_{k\alpha}(t-t')}e^{\frac{-2i\Delta_\alpha}{\Omega_\alpha}\cos(\Omega_\alpha(t+t')/2+\phi_\alpha)\sin(\Omega_\alpha(t-t')/2)} \tag{3.8}$$

$$g_{k\alpha}^{A}(t,t') = i\theta(t'-t)e^{-i\epsilon_{k\alpha}(t-t')}e^{\frac{-2i\Delta_\alpha}{\Omega_\alpha}\cos(\Omega_\alpha(t+t')/2+\phi_\alpha)\sin(\Omega_\alpha(t-t')/2)}, \tag{3.9}$$

and

$$g_{k\alpha}^{R}(t,t') = g_{k\alpha}^{A}(t',t)^*. \tag{3.10}$$

Introducing relative $\tau = t - t'$ and central $T = (t+t')/2$ times and using the Jacobi-Anger expansion,

$$e^{iz\cos(\theta)} = \sum_{n=-\infty}^{\infty} i^n J_n(z)e^{in\theta}, \tag{3.11}$$

we bring free leads Green's function to the form

$$g_{k\alpha}^{A/R/<}(T,\tau) = g_{k\alpha}^{A/R/<}(\tau) \times \sum_{n=-\infty}^{\infty} (-1)^n J_n\left(\psi_\alpha(T)\right)e^{\frac{i}{2}n\Omega_\alpha\tau}, \tag{3.12}$$

where

$$\psi_\alpha(T) = \frac{2\Delta_\alpha}{\Omega_\alpha}\cos(\Omega_\alpha T + \phi_\alpha) \tag{3.13}$$

and $g_{k\alpha}^{A/R/<}(\tau)$ are standard advanced, retarded, and lesser leads Green's function which

depend on relative time only and are computed for static leads:

$$g_{k\alpha}^{<}(\tau) = if_{k\alpha}e^{-i\epsilon_{k\alpha}(\tau)}, \tag{3.14}$$

$$g_{k\alpha}^{A}(\tau) = i\theta(-\tau)e^{-i\epsilon_{k\alpha}(\tau)}, \tag{3.15}$$

$$g_{k\alpha}^{R}(\tau) = g_{k\alpha}^{A}(-\tau)^{*}. \tag{3.16}$$

The substitution of these Green's functions into the definition of lead self-energies gives us

$$\boldsymbol{\Sigma}_{\alpha}^{A/R/<}(T,\tau) = \boldsymbol{\Sigma}_{\alpha}^{A/R/<}(\tau) \times \sum_{n=-\infty}^{\infty} (-1)^{n} J_{n}\left(\psi_{\alpha}(T)\right) e^{\frac{i}{2}n\Omega_{\alpha}\tau} \tag{3.17}$$

where $\boldsymbol{\Sigma}_{\alpha}^{A/R/<}(\tau)$ is again the standard self-energy matrix computed for static leads. For the solutions of the Kadanoff-Baym equations we will need self-energies computed in Wigner space

$$\widetilde{\boldsymbol{\Sigma}}_{\alpha}^{A/R/<}(T,\omega) = \int_{-\infty}^{\infty} d\tau e^{i\omega\tau}\boldsymbol{\Sigma}_{\alpha}^{A/R/<}(T,\tau). \tag{3.18}$$

The direct calculation gives the lesser self-energy

$$\widetilde{\boldsymbol{\Sigma}}_{\alpha}^{<}(T,\omega) = i\sum_{n=-\infty}^{\infty} (-1)^{n} f_{\alpha}(\omega + n\Omega_{\alpha}/2)\boldsymbol{\Gamma}_{\alpha}(\omega + n\Omega_{\alpha}/2) \times J_{n}\left(\psi_{\alpha}(T)\right). \tag{3.19}$$

and advanced/retarded lead self-energies:

$$\widetilde{\boldsymbol{\Sigma}}_{\alpha}^{A/R}(T,\omega) = \sum_{n=-\infty}^{\infty} (-1)^{n} \left[\boldsymbol{\Lambda}_{\alpha}\left(\omega + \frac{n}{2}\Omega_{\alpha}\right) \pm \frac{i}{2}\boldsymbol{\Gamma}_{\alpha}\left(\omega + \frac{n}{2}\Omega_{\alpha}\right)\right] J_{n}\left(\psi_{\alpha}(T)\right). \tag{3.20}$$

The level-width functions are

$$\Gamma_{\alpha ij}(\omega) = 2\pi \sum_{k} \delta(\omega - \epsilon_{k\alpha})t_{k\alpha i}^{*}t_{k\alpha j}. \tag{3.21}$$

The level-shift functions $\Lambda_{\alpha ij}(\omega)$ can be computed from $\Gamma_{\alpha ij}(\omega)$ via Kramers-Kronig relation. To simplify analysis, we make the wide-band approximation. This gives us the following self-energies:

$$\widetilde{\boldsymbol{\Sigma}}_{\alpha}^{<}(T,\omega) = i\boldsymbol{\Gamma}_{\alpha}\sum (-)^{n} f_{\alpha}(\omega + n\Omega_{\alpha}/2)J_{n}\left(\psi_{\alpha}(T)\right), \tag{3.22}$$

$$\widetilde{\boldsymbol{\Sigma}}_{\alpha}^{A}(T,\omega) = \frac{i}{2}\boldsymbol{\Gamma}_{\alpha} \tag{3.23}$$

and

$$\widetilde{\boldsymbol{\Sigma}}_{\alpha}^{R}(T,\omega) = -\frac{i}{2}\boldsymbol{\Gamma}_{\alpha}. \tag{3.24}$$

The time and energy derivatives of the lesser leads self-energy in Wigner space, which are

required for the gradient expansion of Kadanoff-Baym equation, are

$$\partial_T \Sigma_\alpha^< = i\mathbf{\Gamma}_\alpha \Delta_\alpha \sin\left(\Omega_\alpha T\right) \sum_{n=-\infty}^{\infty} (-)^n f_\alpha(\omega + n\Omega_\alpha/2) \times \left[J_{n+1}\left(\psi_\alpha(T)\right) - J_{n-1}\left(\psi_\alpha(T)\right)\right] \quad (3.25)$$

and

$$\partial_\omega \mathbf{\Sigma}_\alpha^< = -i\frac{\mathbf{\Gamma}_\alpha}{\zeta_\alpha} \sum_{n=-\infty}^{\infty} (-)^n \left[f_\alpha\left(\omega + \frac{1}{2}n\Omega_\alpha\right)\right]^2 \times e^{\left(\omega + \frac{1}{2}n\Omega_\alpha - \mu_\alpha\right)/\zeta_\alpha} J_n\left(\psi_\alpha(T)\right), \quad (3.26)$$

where ζ_α is the temperature in the α-th lead. The equations of motion (3.4, 3.5) are governed by an explicitly time-dependent Hamiltonian and describes the exact evolution of the lesser, advanced and retarded Green's functions. The direct numerical solution of Kadanoff-Baym equation with an explicitly time-dependent Hamiltonian represents a formidable computational challenge and possible only for very simplified systems[59]. Our goal is to develop an approximate theory employing the separation of time-scales and assuming that the rate of change of the system Hamiltonian due to external driving is smaller than the electronic tunneling time across the junction. That means that the small parameter is

$$\Omega/\Gamma \ll 1, \quad (3.27)$$

where Ω is a characteristic external driving frequency and Γ is the molecular level broadening due to the coupling to the leads.

The fast and slow timescales in a driven molecular junction are easily detectable in the Wigner representation. The external driving is associated with explicit central time dependence, whereas electronic dynamics is linked with relative time variations. This means that for all Green's functions $\mathcal{G}(t, t')$, the slow time-dependent external field implies that $\mathcal{G}(T + \tau/2, T - \tau/2)$ varies slowly with the central time T, but oscillates fast with the relative time τ. This idea has been often used to separate classical (slow) and quantum (fast) degrees of freedom using NEGF theory[71, 114–121].

To solve Kadanoff-Baym equations approximately, we expand the exponent, keeping the first order terms in central time derivatives:

$$\left[\frac{i}{2}\partial_T + \omega - h\right] \widetilde{\mathcal{G}}^< + \frac{i}{2}\partial_T h \partial_\omega \widetilde{\mathcal{G}}^< = \widetilde{\mathbf{\Sigma}}_{\text{tot}}^R \widetilde{\mathcal{G}}^< + \widetilde{\mathbf{\Sigma}}_{\text{tot}}^< \widetilde{\mathcal{G}}^A$$

$$-\frac{i}{2}\left(\partial_T^\Sigma \partial_\omega^\mathcal{G} - \partial_\omega^\Sigma \partial_T^\mathcal{G}\right) \widetilde{\mathbf{\Sigma}}_{\text{tot}}^R \widetilde{\mathcal{G}}^< - \frac{i}{2}\left(\partial_T^\Sigma \partial_\omega^\mathcal{G} - \partial_\omega^\Sigma \partial_T^\mathcal{G}\right) \widetilde{\mathbf{\Sigma}}_{\text{tot}}^< \widetilde{\mathcal{G}}^A \quad (3.28)$$

$$\left[\frac{i}{2}\partial_T + \omega - h\right]\widetilde{\mathcal{G}}^{A/R} + \frac{i}{2}\partial_T h \partial_\omega \widetilde{\mathcal{G}}^{A/R} = I + \widetilde{\Sigma}_{\text{tot}}^{A/R}\widetilde{\mathcal{G}}^{A/R} - \frac{i}{2}\left(\partial_T^\Sigma\partial_\omega^\mathcal{G} - \partial_\omega^\Sigma\partial_T^\mathcal{G}\right)\widetilde{\Sigma}_{\text{tot}}^{A/R}\widetilde{\mathcal{G}}^{A/R} \quad (3.29)$$

For brevity, we omit the functional dependence on T and ω in the Green's functions, Hamiltonian matrix and self-energies.

All Wigner space molecular Green's functions are expanded with respect its change with time

$$\widetilde{\mathcal{G}} = \widetilde{\mathcal{G}}_{(0)} + \widetilde{\mathcal{G}}_{(1)} + O((\Omega/\Gamma)^2), \quad (3.30)$$

such that $\widetilde{\mathcal{G}}_{(1)}$ is linear in ∂_T, and the remaining terms involves the higher order derivatives with respect to central time T. Here, we truncate the expansion to the first order. Considering the correlation self-energy as a functional of Green's function, we expand it up to the first order as well

$$\widetilde{\Sigma}_c[\widetilde{\mathcal{G}}] \approx \underbrace{\widetilde{\Sigma}_c[\widetilde{\mathcal{G}}_{(0)}]}_{\widetilde{\Sigma}_{c(0)}} + \underbrace{\left(\widetilde{\Sigma}_c[\widetilde{\mathcal{G}}_{(0)} + \widetilde{\mathcal{G}}_{(1)}] - \widetilde{\Sigma}_c[\widetilde{\mathcal{G}}_{(0)}]]\right)}_{\widetilde{\Sigma}_{c(1)}}. \quad (3.31)$$

Making expansions (3.30) and (3.31) for Green's functions and self-energies in Eq. (3.29) and collecting the zeroth order terms, we get

$$\widetilde{\mathcal{G}}_{(0)}^{A/R} = \left[\omega - h - \widetilde{\Sigma}^{A/R} - \widetilde{\Sigma}_{c(0)}^{A/R}\right]^{-1} \quad (3.32)$$

Therefore, the zeroth order term is the standard Green's function computed adiabatically for time-dependent molecular Hamiltonian $\mathbf{h}(T)$ and time-dependent leads self-energies $\widetilde{\Sigma}_{\text{tot}}^{A/R}(T,\omega)$. Notice that the zeroth order correction is not static, it changes adiabatically in time, instantaneously following the external time-dependent perturbation.

Similarly, we collect the first order terms to obtain the dynamical corrections for advanced/retarded Green's functions:

$$\widetilde{\mathcal{G}}_{(1)}^{A/R} = \widetilde{\mathcal{G}}_{(0)}^{A/R}\widetilde{\Sigma}_{c(1)}^{A/R}\widetilde{\mathcal{G}}_{(0)}^{A/R} - \frac{i}{2}\widetilde{\mathcal{G}}_{(0)}^{A/R}\partial_T\widetilde{\mathcal{G}}_{(0)}^{A/R} - \frac{i}{2}\widetilde{\mathcal{G}}_{(0)}^{A/R}\partial_T h \partial_\omega\widetilde{\mathcal{G}}_{(0)}^{A/R}$$
$$- \frac{i}{2}\widetilde{\mathcal{G}}_{(0)}^{A/R}\partial_T\left(\widetilde{\Sigma}^{A/R} + \widetilde{\Sigma}_{c(0)}^{A/R}\right)\partial_\omega\widetilde{\mathcal{G}}_{(0)}^{A/R} + \frac{i}{2}\widetilde{\mathcal{G}}_{(0)}^{A/R}\partial_\omega\left(\widetilde{\Sigma}^{A/R} + \widetilde{\Sigma}_{c(0)}^{A/R}\right)\partial_T\widetilde{\mathcal{G}}_{(0)}^{A/R} \quad (3.33)$$

for which we computed explicitly the central-time derivatives,

$$\partial_T\widetilde{\mathcal{G}}_{(0)}^{A/R} = \widetilde{\mathcal{G}}_{(0)}^{A/R}\partial_T\left(h + \widetilde{\Sigma}^{A/R} + \widetilde{\Sigma}_{c(0)}^{A/R}\right)\widetilde{\mathcal{G}}_{(0)}^{A/R}, \quad (3.34)$$

and also the derivatives with respect to energy

$$\partial_\omega\widetilde{\mathcal{G}}_{(0)}^{A/R} = -\left(\widetilde{\mathcal{G}}_{(0)}^{A/R}\right)^2 + \widetilde{\mathcal{G}}_{(0)}^{A/R}\partial_\omega\left(\widetilde{\Sigma}^{A/R} + \widetilde{\Sigma}_{c(0)}^{A/R}\right)\widetilde{\mathcal{G}}_{(0)}^{A/R}. \quad (3.35)$$

Similarly, using the expansions (3.30) and (3.31) in the truncated Kadanoff-Baym equation (3.28), we arrive at the zeroth order lesser Green's function

$$\widetilde{\mathcal{G}}_{(0)}^{<} = \widetilde{\mathcal{G}}_{(0)}^{R} \widetilde{\Sigma}^{<} \widetilde{\mathcal{G}}_{(0)}^{A} + \widetilde{\mathcal{G}}_{(0)}^{R} \widetilde{\Sigma}_{c(0)}^{<} \widetilde{\mathcal{G}}_{(0)}^{A}. \tag{3.36}$$

The zeroth order corrections constitute the adiabatic solution to the problem, which is equivalent to imbuing the static solution with time-dependent parameters.

For the first order terms, we find,

$$\begin{aligned}
\widetilde{\mathcal{G}}_{(1)}^{<} = &-\frac{i}{2}\widetilde{\mathcal{G}}_{(0)}^{R}\partial_{T}\widetilde{\mathcal{G}}_{(0)}^{<} - \frac{i}{2}\widetilde{\mathcal{G}}_{(0)}^{R}\partial_{T}h\partial_{\omega}\widetilde{\mathcal{G}}_{(0)}^{<} + \widetilde{\mathcal{G}}_{(0)}^{R}\left(\widetilde{\Sigma}^{<} + \widetilde{\Sigma}_{c(0)}^{<}\right)\widetilde{\mathcal{G}}_{(1)}^{A} \\
&-\frac{i}{2}\widetilde{\mathcal{G}}_{(0)}^{R}\partial_{T}\left(\widetilde{\Sigma}^{<} + \widetilde{\Sigma}_{c(0)}^{<}\right)\partial_{\omega}\widetilde{\mathcal{G}}_{(0)}^{A} + \frac{i}{2}\widetilde{\mathcal{G}}_{(0)}^{R}\partial_{\omega}\left(\widetilde{\Sigma}^{<} + \widetilde{\Sigma}_{c(0)}^{<}\right)\partial_{T}\widetilde{\mathcal{G}}_{(0)}^{A} \\
&-\frac{i}{2}\widetilde{\mathcal{G}}_{(0)}^{R}\partial_{T}\left(\widetilde{\Sigma}^{R} + \widetilde{\Sigma}_{c(0)}^{R}\right)\partial_{\omega}\widetilde{\mathcal{G}}_{(0)}^{<} + \frac{i}{2}\widetilde{\mathcal{G}}_{(0)}^{R}\partial_{\omega}\left(\widetilde{\Sigma}^{R} + \widetilde{\Sigma}_{c(0)}^{R}\right)\partial_{T}\widetilde{\mathcal{G}}_{(0)}^{<}.
\end{aligned} \tag{3.37}$$

The Eqs. (3.32),(3.33),(3.36) and (3.37) represent solutions for the Kadanoff-Baym equations under the assumption that the characteristic period of the external time-dependent driving is slower than the time spent by the electron in the central region.

3.2.1 Dynamical corrections to time-dependent electric current

Having obtained the non-adiabatic corrections to the retarded, advanced and lesser Green's functions, we are now ready to calculate the time-dependent electric current. Using the equation for particle current derived in section 2.4.11.2,

$$J_{\alpha}(t) = 2\mathrm{Re}\int dt_{1}\mathrm{Tr}\left\{\mathcal{G}^{<}(t,t_{1})\Sigma_{\alpha}^{A}(t_{1},t) + \mathcal{G}^{R}(t,t_{1})\Sigma_{\alpha}^{<}(t_{1},t)\right\}., \tag{3.38}$$

we find that

$$J_{\alpha}(t) = 2\,\mathrm{Re}\int_{-\infty}^{\infty}\frac{d\omega}{2\pi}\,\mathrm{Tr}[\mathbf{C}_{\alpha}(t,\omega)], \tag{3.39}$$

where $\mathbf{C}_{\alpha}(t,\omega)$ is defined as

$$\mathbf{C}_{\alpha}(t,\omega) = e^{-\frac{i}{2}\left(\partial_{t}^{G}\partial_{\omega}^{\Sigma} - \partial_{\omega}^{G}\partial_{t}^{\Sigma}\right)}\left(\widetilde{\mathcal{G}}^{<}(t,\omega)\widetilde{\Sigma}_{\alpha}^{A}(t,\omega) + \widetilde{\mathcal{G}}^{R}(t,\omega)\widetilde{\Sigma}_{\alpha}^{<}(t,\omega)\right). \tag{3.40}$$

As before, we truncate the exponential terms, assuming slow variation with respect to central time of the Green's functions and self-energies in Wigner representation:

$$\mathbf{C}_{\alpha} = \widetilde{\mathcal{G}}^{<}\widetilde{\Sigma}_{\alpha}^{A} + \widetilde{\mathcal{G}}^{R}\widetilde{\Sigma}_{\alpha}^{<} - \frac{i}{2}\partial_{t}\widetilde{\mathcal{G}}^{<}\partial_{\omega}\widetilde{\Sigma}_{\alpha}^{A} + \frac{i}{2}\partial_{\omega}\widetilde{\mathcal{G}}^{<}\partial_{T}\widetilde{\Sigma}_{\alpha}^{A} - \frac{i}{2}\partial_{t}\widetilde{\mathcal{G}}^{R}\partial_{\omega}\widetilde{\Sigma}_{\alpha}^{<} + \frac{i}{2}\partial_{\omega}\widetilde{\mathcal{G}}^{R}\partial_{T}\widetilde{\Sigma}_{\alpha}^{<}. \tag{3.41}$$

Splitting the zeroth and first order contributions, we calculate the adiabatic current and first order dynamical corrections to it. For the zeroth order, the adiabatic current, we find that

$$J_{L,(0)}(t) = 2\,\text{Re} \int_{-\infty}^{\infty} \frac{d\omega}{2\pi}\,\text{Tr}\left[\widetilde{\mathcal{G}}_{(0)}^{<}\widetilde{\Sigma}_{L}^{A} + \widetilde{\mathcal{G}}_{(0)}^{R}\widetilde{\Sigma}_{L}^{<}\right]. \tag{3.42}$$

The first order correction to the electric current is

$$\begin{aligned}
J_{\alpha,(1)}(t) = 2\,\text{Re} \int_{-\infty}^{\infty} \frac{d\omega}{2\pi}\,\text{Tr}\Big[&\widetilde{\mathcal{G}}_{(1)}^{<}\widetilde{\Sigma}_{\alpha}^{A} + \widetilde{\mathcal{G}}_{(1)}^{R}\widetilde{\Sigma}_{\alpha}^{<} - \frac{i}{2}\partial_{T}\widetilde{\mathcal{G}}_{(0)}^{<}\partial_{\omega}\widetilde{\Sigma}_{\alpha}^{A} + \frac{i}{2}\partial_{\omega}\widetilde{\mathcal{G}}_{(0)}^{<}\partial_{T}\widetilde{\Sigma}_{\alpha}^{A})\\
&-\frac{i}{2}\partial_{T}\widetilde{\mathcal{G}}_{(0)}^{R}\partial_{\omega}\widetilde{\Sigma}_{\alpha}^{<} + \frac{i}{2}\partial_{\omega}\widetilde{\mathcal{G}}_{(0)}^{R}\partial_{T}\widetilde{\Sigma}_{\alpha}^{<}\Big].
\end{aligned} \tag{3.43}$$

Taking the wide-band approximation, the first order correction to the current reduces to the following:

$$J_{\alpha,(1)}(t) = 2\,\text{Re} \int_{-\infty}^{\infty} \frac{d\omega}{2\pi}\,\text{Tr}\left[\widetilde{\mathcal{G}}_{(1)}^{<}\widetilde{\Sigma}_{\alpha}^{A} + \widetilde{\mathcal{G}}_{(1)}^{R}\widetilde{\Sigma}_{\alpha}^{<} - \frac{i}{2}\partial_{T}\widetilde{\mathcal{G}}_{(0)}^{R}\partial_{\omega}\widetilde{\Sigma}_{\alpha}^{<} + \frac{i}{2}\partial_{\omega}\widetilde{\mathcal{G}}_{(0)}^{R}\partial_{T}\widetilde{\Sigma}_{\alpha}^{<}\right]. \tag{3.44}$$

3.3   Results

3.3.1   AC current through single resonant-level

Let us first consider the simple case of a single resonant-level connected to two leads with harmonically driven chemical potentials. In this case the molecular Hamiltonian is

$$H_M = (\epsilon + V(t))d^{\dagger}d, \tag{3.45}$$

where ϵ is the energy of the resonant-level, $V(t)$ is the external time-depending potential, and $d^{\dagger}(d)$ are creation(annihilation) operators for a resonant-level electron. The harmonic modulations of the leads' single-particle energies is given by

$$\epsilon_{k\alpha}(t) = \epsilon_{k\alpha} + \Delta_{\alpha}\cos\Omega t, \tag{3.46}$$

where Δ_{α} is the amplitude of the oscillations of the energy levels and Ω is the modulation frequency. We assume that the energy of resonant-level is also shifted in time with the same frequency due to the time-oscillating voltage drop between the leads or due to a time-dependent gate

$$V(t) = \Delta\cos\Omega t. \tag{3.47}$$

Under this approximation, the exact solution for the model is known[95] and the proposed theory will be benchmarked against this available exact result.
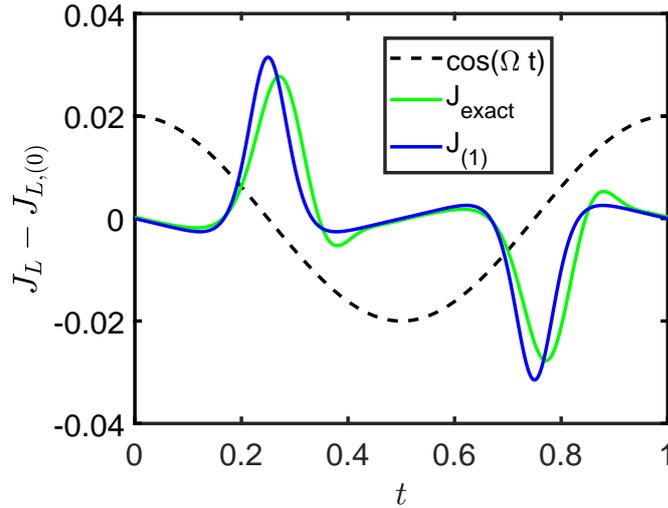
Figure 3.1: Comparison between the first order correction to current and the difference between the exact and zeroth order currents. The parameters are $\Gamma_L = \Gamma_R = 0.5\Gamma$, $\Delta_L = \Gamma$, $\Delta_R = -\Gamma$, $\Delta = 0$, $\epsilon = 0$, $\Omega = 0.1\Gamma$, $\mu_L = \mu_R = 0$ and $T = 0.001\Gamma$. The current is measured in units of Γ and time is given in periods of the external driving $2\pi/\Omega$.

We assess the adiabatic, zeroth order, electric current $J_{(0)}(t)$ given by Eq.(3.42) along with the first order dynamical correction $J_{(1)}(t)$ given by Eq.(3.44) against the exact time-dependent current $J_{\text{exact}}(t)$ from literature[95]. It is difficult to visually judge the performance of the method from the comparison of the total currents, since it is dominated by the adiabatic contribution in both cases. In order to eliminate this bulk trivial term, we subtract $J_{(0)}$ from $J_{\text{exact}}(t)$ and plot it along with our first order dynamical correction $J_{(1)}(t)$. the result is shown in figure 3.1. One can see that the first order correction captures the essential dynamical features of the exact solution which is associated with the retardation of the filling and emptying of the resonant level when it crosses the Fermi level of leads.

Figure 3.2 shows that in certain situations the first order dynamical correction plays a critical role. Let us consider the case when the left lead is grounded at all time, a small AC voltage is applied to the right lead whilst a much larger harmonically oscillating gate voltage is applied to the central region. The adiabatic current does not show any dynamical characters and fails to reproduce the exact time behavior; it simply follows instantaneously the applied time dependent voltage bias. The first order dynamical correction significantly improves the results by bringing the value of the current close to the exact value.

3.3.2   Holstein model in time-dependent Hartree approximation

Having checked the proposed theoretical approach by the comparison with exact results, we turn our attention to electron transport through the molecular junction with electron-vibration
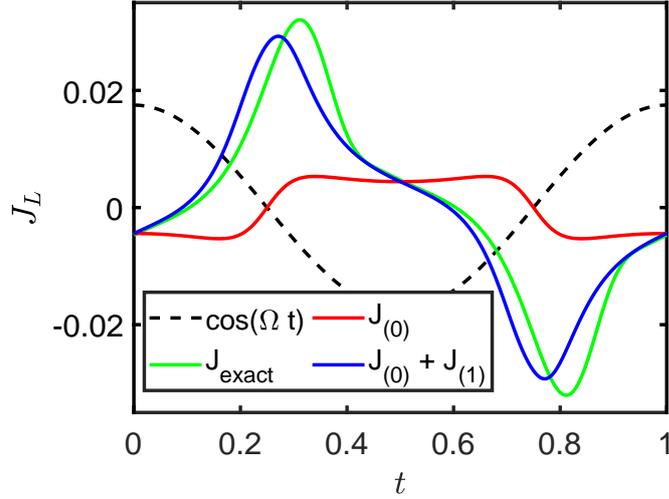
Figure 3.2: Current through a single-resonant level as a function of time. The parameters are $\Gamma_L = \Gamma_R = 0.5\Gamma$, $\Delta_L = 0$, $\Delta_R = 0.125\Gamma$, $\Delta = 1$, $\epsilon = 0$, $\Omega = 0.1\Gamma$, $\mu_L = \mu_R = 0$ and $T = 0.1\Gamma$. The current is measured in units of Γ and time is given in periods of the external driving $2\pi/\Omega$.

interaction. The molecule is described by the Holstein model Hamiltonian:

$$H_M(t) = \epsilon d^\dagger d + \lambda (a^\dagger + a) d^\dagger d + \omega a^\dagger a, \tag{3.48}$$

where ϵ molecular orbital energy, ω is molecular vibrational energy, and λ is the strength of the electron-vibration coupling. The operator $d^\dagger$ (d) creates (annihilates) an electron on molecular orbital, and $a^\dagger$ (a) is the bosonic creation (annihilation) operator for the molecular vibrations. The electronic spin does not play any physical role in this section and will not be included explicitly into the equations. Similar to the single resonant-level considered in section 3.3.1, the single particle energies of the leads depend on time harmonically as given in Eq.(3.46).

Assuming that the vibration is slower than the characteristic electron tunnelling time $\omega \ll \Gamma$, meaning that at any given time moment a tunnelling electron interacts with a constant, static molecular vibration, the correlation self-energy can be written in Hartree approximation as [69, 122]

$$\Sigma_c^{A/R}(t, t') = \chi n(t) \delta(t - t'), \tag{3.49}$$

$$\Sigma_c^<(t, t') = 0, \tag{3.50}$$

where

$$\chi = -\frac{2\lambda^2}{\omega} \tag{3.51}$$

and $n(t)$ is the time-dependent molecular population given by

$$n(t) = \mathrm{Im}\left[\int_{-\infty}^{\infty} \frac{d\omega}{2\pi} \widetilde{\mathcal{G}}^<(t, \omega)\right]. \tag{3.52}$$
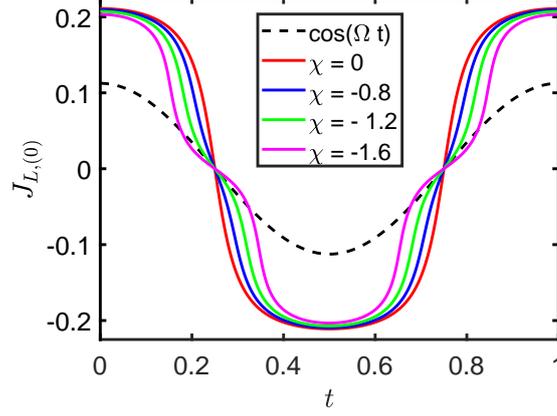
Figure 3.3: The adiabatic time-dependent current computed with varying values for χ. The other parameters are $\Gamma_L = \Gamma_R = 0.5\Gamma$, $\Delta_L = 2\Gamma$, $\Delta_R = -2\Gamma$, $\epsilon = 0$, $\Omega = 0.05\Gamma$, $\mu_L = \mu_R = 0$ and $T = 0.001\Gamma$. The current is measured in units of Γ and time is given in periods of the external driving $2\pi/\Omega$.
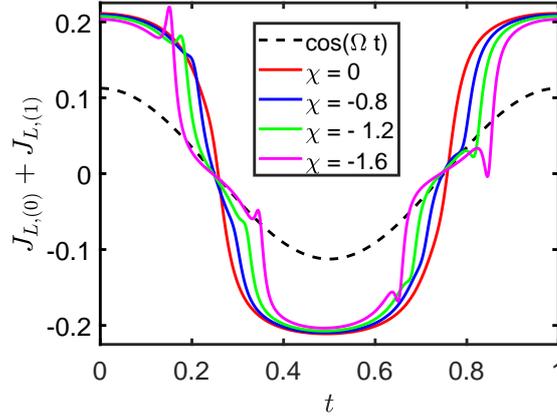
Figure 3.4: Time-dependent current with the first order dynamical corrections computed with varying values for χ. The parameters are the same as in Fig. (3.3).

The assumption that $\omega \ll \Gamma$ does not effect or is related to the gradient expansion, as unlike Ω, the phonon frequency ω does not dictate the time-dependent variation of the system. It is required for the validity of the Hartree approximation.

The corresponding correlation self-energies in the Wigner space representation become

$$\widetilde{\Sigma}_c^{A/R}(T,\omega) = \chi n(T), \tag{3.53}$$

$$\widetilde{\Sigma}_c^{<}(T,\omega) = 0. \tag{3.54}$$

In order to compute the self-energies, and consequently the Green's functions, we need to know the adiabatic molecular electronic population $n_{(0)}(t)$ and its first order dynamical correction $n_{(1)}(t)$. The adiabatic molecular population is obtained from the solution of the fol-

lowing equation

$$n_{(0)}(t) = \mathrm{Im}\left[\int_{-\infty}^{\infty}\frac{d\omega}{2\pi}\widetilde{\mathcal{G}}_{(0)}^{<}(t,\omega)\right]. \tag{3.55}$$

This equation is nonlinear since the expression for the lesser Green's function under the integral depends on adiabatic electronic population $n_{(0)}(t)$; it is solved numerically by the bisection method. It is known that depending on the parameters of the system, there can be several solutions to the zeroth order correction to the occupation [122]. We restrict ourselves to the situations with a single solutions. The first order dynamical correction to the electronic occupation is obtained from a similar equation

$$n_{(1)}(t) = \mathrm{Im}\left[\int_{-\infty}^{\infty}\frac{d\omega}{2\pi}\widetilde{\mathcal{G}}_{(1)}^{<}(t,\omega)\right], \tag{3.56}$$

where $\mathcal{G}_{(1)}^{<}$ depends on $n_{(1)}$ and on the already computed value of $n_{(0)}$. Eq. (3.56) is linear and can be resolved analytically. The first correction to the occupation can be related to the adiabatic result. Making use of Eqs. (3.52) and (3.37), we find

$$n_{(1)}(T) = \int_{-\infty}^{\infty}\frac{d\omega}{2\pi}\,\mathrm{Im}\left[-\frac{i}{2}\widetilde{\mathcal{G}}_{(0)}^{R}\partial_{T}\widetilde{\mathcal{G}}_{(0)}^{<} - \frac{i}{2}\widetilde{\mathcal{G}}_{(0)}^{R}\partial_{T}\widetilde{\Sigma}^{<}\partial_{\omega}\widetilde{\mathcal{G}}_{(0)}^{A} + \frac{i}{2}\widetilde{\mathcal{G}}_{(0)}^{R}\partial_{\omega}\widetilde{\Sigma}^{<}\partial_{T}\widetilde{\mathcal{G}}_{(0)}^{A}\right.$$
$$\left. -\frac{i}{2}\widetilde{\mathcal{G}}_{(0)}^{R}\chi\partial_{T}n_{(0)}\partial_{\omega}\widetilde{\mathcal{G}}_{(0)}^{<} + \widetilde{\mathcal{G}}_{(0)}^{R}\widetilde{\Sigma}^{<}\widetilde{\mathcal{G}}_{(1)}^{A}\right]. \tag{3.57}$$

Here, the first correction to the advanced Green's function is given as

$$\widetilde{\mathcal{G}}_{(1)}^{A/R} = \widetilde{\mathcal{G}}_{(0)}^{A/R}\chi n_{(1)}\widetilde{\mathcal{G}}_{(0)}^{A/R}. \tag{3.58}$$

For Eq. (3.57), we observe that the result can be split into contributions that depend on the adiabatic solution only and the term containing $n_{(1)}$ itself. Hence making use of the Eqs. (3.57) and (3.58), we find a linear equation such that:

$$n_{(1)}(T) = \frac{A(T)}{1 - B(T)}, \tag{3.59}$$

where

$$A(T) = \int_{-\infty}^{\infty}\frac{d\omega}{2\pi}\,\mathrm{Im}\left[-\frac{i}{2}\widetilde{\mathcal{G}}_{(0)}^{R}\partial_{T}\widetilde{\mathcal{G}}_{(0)}^{<} - \frac{i}{2}\widetilde{\mathcal{G}}_{(0)}^{R}\partial_{T}\widetilde{\Sigma}^{<}\partial_{\omega}\widetilde{\mathcal{G}}_{(0)}^{A}\right.$$
$$\left. +\frac{i}{2}\widetilde{\mathcal{G}}_{(0)}^{R}\partial_{\omega}\widetilde{\Sigma}^{<}\partial_{T}\widetilde{\mathcal{G}}_{(0)}^{A} - \frac{i}{2}\widetilde{\mathcal{G}}_{(0)}^{R}\chi\partial_{T}n_{(0)}\partial_{\omega}\widetilde{\mathcal{G}}_{(0)}^{<}\right], \tag{3.60}$$

$$B(T) = \chi\int_{-\infty}^{\infty}\frac{d\omega}{2\pi}\,\mathrm{Im}\left[\widetilde{\mathcal{G}}_{(0)}^{R}\widetilde{\Sigma}^{<}\left(\widetilde{\mathcal{G}}_{(0)}^{A}\right)^{2}\right]. \tag{3.61}$$

Having computed time-dependent electronic occupation number

$$n(t) = n_{(0)}(t) + n_{(1)}(t), \tag{3.62}$$

we calculate the correlation adiabatic (zeroth order) advanced or retarded self-energies

$$\widetilde{\Sigma}^{A/R}_{c(0)}(T,\omega) = \chi n_{(0)}(T), \tag{3.63}$$

and the first order dynamical corrections

$$\widetilde{\Sigma}^{A/R}_{c(1)}(T,\omega) = \chi n_{(1)}(T). \tag{3.64}$$

Next, we calculate Green's functions, adiabatic electric current $J_{(0)}(t)$ using Eq.(3.42) and first order dynamical correction $J_{(1)}(t)$ using Eq.(3.44). Figure 3.3 shows the adiabatic, zeroth order current; the current instantaneously follows the applied voltage and, as expected, does not demonstrate any dynamical features associated with non-adiabatic transport. The polaron shift of the molecular orbital away from the voltage window, which depends quadratically on strength of the electron-vibration interaction λ, leads to the current blockade around zero voltage.

Figure 3.4 shows the time-dependent current computed with first-order dynamical corrections. The current shows a negative differential resistance behaviour, with spikes in the current-time profile. These are observed to occur around when the oscillating right and left chemical potentials become equal. The effect becomes more pronounced as the strength of the electron-vibration interaction λ increases.

To understand the behavior of the time-dependent current, we turn our attention to the time-evolution of the electronic population in the molecular junction. Figure 3.5 shows adiabatic electronic populations $n_{(0)}(t)$, total electronic population $n(t) = n_{(0)}(t) + n_{(1)}(t)$ and first order corrections to electronic population $n_{(1)}(t)$. From Figure 3.5, we see that, just before the chemical potentials of the leads meet, there is a dip within the electronic population, followed by a peak of equal magnitude whilst the lead's chemical potentials increase again. This dynamical effect becomes more noticeable if the strength of the electron-vibration coupling is increased, as it is demonstrated in Figure 3.6.

Within the approximation employed to compute the correlation self-energy, the electronic energy level is shifted downward by the electron-vibrational coupling

$$\epsilon(t) = \epsilon - \frac{2\lambda^2}{\omega}\left(n_{(0)}(t) + n_{(1)}(t)\right). \tag{3.65}$$

In figure 3.7 we plot side by side the first order dynamical corrections to electronic occupation
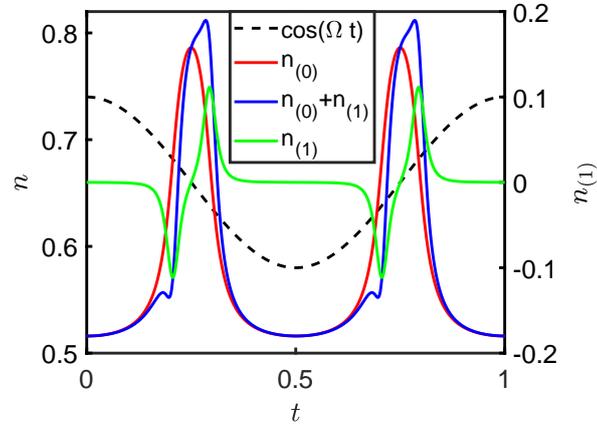
Figure 3.5: Time-dependence of the adiabatic electronic occupation, electronic occupation with first order dynamical correction, and first order correction. Here $\chi = -0.8$, and the other parameters are the same as in Fig. (3.3).
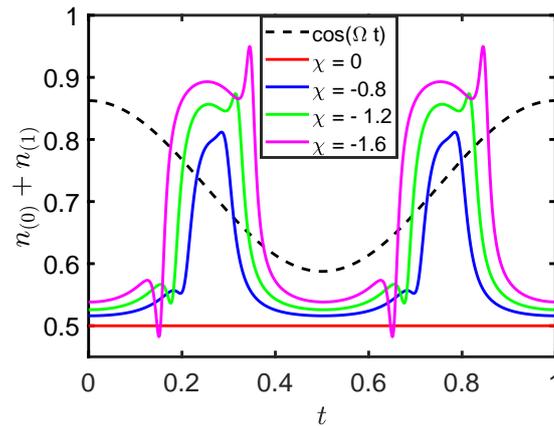
Figure 3.6: Time-dependence of electronic occupation computed with first order dynamical correction for various values of $\chi = -\frac{2\lambda^2}{\omega}$. The other parameters are the same as in Fig. (3.3).
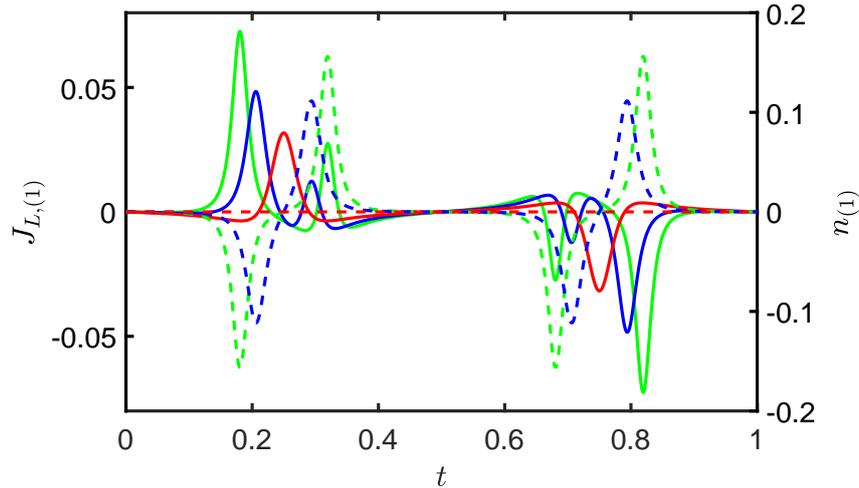
Figure 3.7: Time-dependence of the first order dynamical corrections to the electronic population (dotted line) and to the current (full line). Here, the red lines correspond to $\chi = 0$; the blue to $\chi = -0.8$; and the green to $\chi = -1.2$. The other parameters are the same as in Fig. (3.3).

numbers $n_{(1)}(t)$ and electric current $J_{(1)}(t)$. One can see that the peaks and dips in dynamical corrections to the electronic populations are mirrored by corresponding dips and peaks in the time-dependence of the first order corrections to the current. This behavior can be easily interpreted with the use of Eq.(3.65), noticing that the dip in the electronic population temporarily brings the energy level into the voltage bias window, and therefore results in an increase in current. Conversely, the peak in the electronic population pushes the electronic level down, out of resonance, thus resulting in the reduction in current.

3.4 Conclusion

In this chapter, we have developed a time-dependent transport theory for molecular junctions. The theory uses nonequilibrium Green's functions to separate time-scales on slow driving and fast electron tunneling. The gradient expansion of the Wigner space Kadanoff-Baym equations in terms of the slow time variable enabled us to convert the nonlocal in time integro-differential equations into a set of algebraic equations at each order of the gradient expansion. We found the solution of these equations, and consequently produced analytic expressions for the first order dynamical corrections to the adiabatic Green's functions. The dynamical corrections to time-dependent electric current is obtained as well. The derived expressions are applicable to the general case of an AC electric current through a correlated central region. We applied the theory to two transport scenarios: a single-resonant level coupled to leads with harmonically oscillating chemical potentials; and a periodically driven molecular junction coupled to a vibrational mode described by the Holstein model.

For the noninteracting case, we found that the model agrees well with the exact results, within the realm of applicability. Upon the model's application to the Holstein model using time-dependent Hartree-approximation to treat electron-vibration interactions, we found that the variation of the junction's electronic population in time, due to nonadiabatic effects, induced small peaks and dips within the current. This suggests that dynamical, nonlinear effects may have a significant influence on the current, depending on the central region's correlations and the operating frequency of the junctions.

Given the approximate nature of our approach, the conservation of charge deserves special attention. Any meaningful theoretical approach should preserve, at each moment in time, the continuity equation

$$\frac{dn(t)}{dt} = J_R(t) + J_L(t), \tag{3.66}$$

where

$$n(t) = \text{Im}\left[\text{Tr}\left[\int_{-\infty}^{\infty} \frac{d\omega}{2\pi} \widetilde{\mathcal{G}}^{<}(t,\omega)\right]\right] \tag{3.67}$$

is the occupation of the central region. We have that $\mathcal{G}^{<} \approx \mathcal{G}^{<}_{(0)} + \mathcal{G}^{<}_{(1)}$. In the continuity equations, we disregard $\frac{d\mathcal{G}^{<}_{(1)}}{dt} \sim \mathcal{G}^{<}_{(2)}$ and take into account that the adiabatic current is conserved $J_{R,(0)}(t) + J_{L,(0)}(t) = 0$, leaving the following continuity equation for the first order dynamical corrections to the current:

$$J_{R,(1)}(t) + J_{L,(1)}(t) = \text{Im}\left[\text{Tr}\left[\int_{-\infty}^{\infty} \frac{d\omega}{2\pi} \frac{d\mathcal{G}^{<}_{(0)}}{dt}\right]\right]. \tag{3.68}$$

In all considered cases we checked numerically that continuity equation (3.68) is satisfied.

Floquet Nonequilibrium Green's Functions with Full Counting Statistics

This chapter contains material that has been previously published in the following journal article:

Full counting statistics for electron transport in periodically driven quantum dots,

T. D. Honeychurch and D. S. Kosov, Phys. Rev. B **102**, 195409 (2020)

4.1 Introduction

Time-dependent phenomena play an important part in the investigation and application of nanoscale electronics. The dynamical response of a junction to the modulation of a voltage or to the irradiation by a light source offers intriguing means of probing and controlling the system's dynamics [36]. Applications include optically irradiated nanoscale junctions [73, 74], electron pumping [71, 123, 124], pump-probe spectroscopy [79, 125], and AC current rectification [72, 126]. The exploration of time-dependent phenomena has a long history [34, 36], which mostly centers on periodic drivings, typically induced with microwave radiation. For periodic driving, the explanation of photon-assisted transport (PAT) is often invoked: electrons, moving between regions under periodic driving, are observed to undergo inelastic tunneling events, with the absorption and emission of quanta of energy given by the driving frequency [36]. PAT has been realized within many systems [35, 73, 74], and has undergone extensive theoretical investigation [36].

The discrete nature of the charge carrier results in irrepressible current fluctuations. These current fluctuations can contain information about the nature of the junction. For systems with explicit time dependence, understanding current fluctuations is crucial for metrological and performance reasons [56, 77]. Full counting statistics (FCS) allows the calculation of higher cumulants of the current in a rather concise and systematic manner. The theory of

FCS was first introduced by Levitov and Lesovik [127, 128] in a scattering theory framework via the explicit inclusion of a measuring device in the theoretical setup, which has since been extended to a general quantum mechanical variable[129] and applied to various transport scenarios [130]. For periodically driven systems, FCS has been coupled within scattering theory [131–133] and master-equation approaches [123, 134, 135] with various investigated periodically driven systems.

In this chapter, the AC driving of a single resonant level and a T-shaped double-level system, both noninteracting, with the help of full counting statistics as realised in nonequilibrium Green's functions[70, 71], was investigated. In both cases, the left lead underwent the sinusoidal driving of its energies. This results in photon-assisted transport being observed within the current cumulants, most notably resulting in additional noise in particular cases. For the T-shaped junction, Fano-resonance effects were found to manifest in the peaks generated by the driving. This was explained by considering the bonding and anti-bonding levels of the central molecule.

4.2 Theory

4.2.1 General considerations

Within the investigation, the Hamiltonian for a central region (i.e., the molecule) connected to two macroscopic leads is given by

$$H(t) = H_C(t) + H_L(t) + H_R(t) + H_{CL}(t) + H_{CR}(t), \tag{4.1}$$

where H_C is the Hamiltonian of the molecule, H_L and H_R are the Hamiltonians of the left and right leads, and $H_{CL/R}$ is the interaction between the central region and the left/right lead, respectively.

We consider the electrons within the central region to be noninteracting:

$$H_C = \sum_{ij} h_{ij}(t) d_i^\dagger d_j, \tag{4.2}$$

where $d_i^\dagger$ (d_i) creation (annihilation) operators are for an electron in the single-particle state i.

The left and right leads are modeled as macroscopic reservoirs of noninteracting electrons,

$$H_L + H_R = \sum_{k,\alpha=L,R} \epsilon_{k\alpha}(t) c_{k\alpha}^\dagger c_{k\alpha}, \tag{4.3}$$

where $c_{k\alpha}^{\dagger}(c_{k\alpha})$ creates (annihilates) an electron in the single-particle state k of either the left ($\alpha = L$) or the right ($\alpha = R$) lead. The coupling between the central region and left and right leads is given by the tunneling interaction

$$H_{CL} + H_{CR} = \sum_{i,k,\alpha=L,R} \left[t_{k\alpha i}(t) c_{k\alpha}^{\dagger} d_i + \text{H.c.} \right], \tag{4.4}$$

where $t_{k\alpha i}(t)$ is the time-dependent tunneling amplitude between leads and central single-particle states.

Utilizing full counting statistics, we follow the procedure set out in section 2.4.12.2. with the generating function,

$$\chi\left(\lambda_L, t_c, t_0\right) = \langle e^{-i\lambda_L N_L(t_c)} e^{i\lambda_L N_L(t_0)} \rangle, \tag{4.5}$$

allows for the calculation of the charge that leaves the left lead between times t_0 and t_c. Here, $N_L(t)$ is the occupation of the left lead within the Heisenberg picture. The cumulants of the above are given by

$$\langle \delta^n q(t_c, t_0) \rangle = (-i)^n \frac{\partial^n}{\partial \lambda_L^n} \ln \chi\left(\lambda_L, t_c, t_0\right) \Big|_{\lambda_L=0}. \tag{4.6}$$

By taking the first derivative with respect to the counting field, this result can be recast:

$$-i \frac{\partial}{\partial \lambda_L} \ln\left[\chi\left(\lambda_L, t_c, t_0\right)\right] = \int_{t_0}^{t_c} dt \int_{t_0}^{t_c} dt' \ \text{Tr}\left[\boldsymbol{\Sigma}_{<}^{L}(t, t')\boldsymbol{G}_{>}\left(t', t\right) - \boldsymbol{G}_{<}\left(t, t'\right)\boldsymbol{\Sigma}_{>}^{L}(t', t)\right], \tag{4.7}$$

where the Hamiltonian is modified by the appropriate counting field

$$H_{CL}^{\lambda_L}(t) = \sum_{i,k} t_{kL,i}(t) e^{-\frac{i}{2}\lambda_L(\tau)} c_{k\alpha}^{\dagger} d_i + t_{kL,i}^*(t) e^{\frac{i}{2}\lambda_L(\tau)} d_i^{\dagger} c_{k\alpha}, \tag{4.8}$$

and where $\lambda(\tau) = \pm\lambda_L$ on the forward and backward branches of the contour, respectively.

Moving to real time, the contour Green's function is expressed in Schwinger-Keldysh space, as in equation (2.97),

$$\hat{G}(t, t') = \begin{pmatrix} G^T(t, t') & G^<(t, t') \\ G^>(t, t') & G^{\tilde{T}}(t, t') \end{pmatrix}, \tag{4.9}$$

with the Kadanoff-Baym equation, manipulated from the definition of equation (2.125) to take the following form:

$$\left(i\frac{\partial}{\partial t} - \boldsymbol{h}(t)\right) \check{\boldsymbol{G}}\left(t, t'\right) - \int_{t_0}^{t_c} dt_1 \check{\boldsymbol{\Sigma}}\left(t, t_1\right) \check{\boldsymbol{G}}\left(t_1, t'\right) = \delta\left(t - t'\right), \tag{4.10}$$

with $\check{A}_{2,j}\left(t, t'\right) = -\hat{A}_{2,j}\left(t, t'\right)$. [68]

Solving the Kadanoff-Baym equations by invoking a Floquet approach restricts the method

to considering time-averaged statistics: the points of measurement are moved to the infinities to ensure the periodicity of the system (i.e., $t_0 \to -\infty$ and $t_c \to \infty$). Following the above considerations, the Kadanoff-Baym equation can be transformed into a matrix equation:

$$\left[\begin{pmatrix} \omega\mathbf{I} & 0 \\ 0 & \omega\mathbf{I} \end{pmatrix} + \begin{pmatrix} \Omega\mathbf{D} & 0 \\ 0 & \Omega\mathbf{D} \end{pmatrix} - \begin{pmatrix} \mathbf{H} & 0 \\ 0 & \mathbf{H} \end{pmatrix} - \begin{pmatrix} \boldsymbol{\Sigma}^T & \boldsymbol{\Sigma}^< \\ -\boldsymbol{\Sigma}^> & -\boldsymbol{\Sigma}^{\tilde{T}} \end{pmatrix} \right] \check{\mathcal{G}} \quad = \quad \begin{pmatrix} \mathbf{I} & 0 \\ 0 & \mathbf{I} \end{pmatrix}, \quad (4.11)$$

where $(\mathbf{D})_{a,b} = a\delta_{a,b}$, $(\mathbf{H})_{a,b} = \mathbf{h}(b-a)$, and the projections of the self-energy are given as

$$(\boldsymbol{\Sigma})_{a,b} = \boldsymbol{\Sigma}\left(\omega + (a+b)\Omega/2, b-a\right), \quad (4.12)$$

for a given projection. Here, the time-dependence of the self-energies are handled as in section 2.4.8, with the addition of counting fields, as set out in section 2.4.12.2, such that $\boldsymbol{\Sigma}_L^< \to \boldsymbol{\Sigma}_L^< e^{i\lambda_L}$ and $\boldsymbol{\Sigma}_L^> \to \boldsymbol{\Sigma}_L^> e^{-i\lambda_L}$.

One can recast Eq. (4.7) in terms of Floquet matrices, giving us

$$C_n = \lim_{t_c,t_0 \to \pm\infty} \left(\frac{(-i)^n \frac{\partial^n}{\partial \lambda_L^n} \ln\left[\chi\left(\lambda_L, t_c, t_0\right) \right]}{t_c - t_0} \right) = (-i)^{n-1} \frac{\partial^{n-1}}{\partial \lambda^{n-1}} \int_{-\infty}^{\infty} \frac{d\omega}{2\pi} \operatorname{Tr}\left[X(\omega, 0) \right], \quad (4.13)$$

where $n \geq 1$ and $X(\omega, 0)$ is the zeroth Fourier component, calculated from the Floquet matrix equation

$$X = \boldsymbol{\Sigma}_L^< \mathcal{G}^> - \mathcal{G}^< \boldsymbol{\Sigma}_L^>. \quad (4.14)$$

This result corresponds to calculating the time-averaged cumulants of the current, with $C_1 = I$ and $C_2 = S_{LL}(\omega = 0)$ [136, 137].

4.3 Results

4.3.1 Resonant level

We begin by considering a central region consisting of a single resonant level. The central region and leads are both taken to have sinusoidal driving. The central region Hamiltonian is

$$H_C(t) = \left[\epsilon_0 + \Delta_0 \cos\left(\Omega t\right)\right] d^\dagger d, \quad (4.15)$$

and the leads' energy levels are

$$\epsilon_{k\alpha}(t) = \epsilon_{k\alpha} + \Delta_\alpha \cos\left(\Omega t\right). \quad (4.16)$$

Considering the current, one can turn off the counting field and rearrange Eq. (4.13) to find

$$I = \sum_{k=-\infty}^{\infty} \int_{-\infty}^{\infty} \frac{d\omega}{2\pi} \quad T(\omega - k\Omega) \left(f_L(\omega) J_k^2 \left(\frac{\Delta_0 - \Delta_L}{\Omega} \right) - f_R(\omega) J_k^2 \left(\frac{\Delta_0 - \Delta_R}{\Omega} \right) \right) \quad (4.17)$$

where

$$T(\omega) = \frac{\Gamma_L \Gamma_R}{(\omega - \epsilon_0)^2 + \frac{\Gamma^2}{4}}, \quad (4.18)$$

in agreement with the literature [95, 138]. We see the established phenomena of photon-assisted transport, where the sinusoidal driving of regions results in an effective splitting of the transmission between pictures which can be interpreted as the absorption or emission of photons of $\hbar\Omega$ [36].

The results of these calculations are given in Figs. 4.1 and 4.2. Within all the calculations completed, the matrices were truncated to consider 41 of the Fourier coefficients of each object (i.e., from $n = -20$ to $n = 20$). We see that the higher cumulants also display characteristics surrounding the positions of the photopeaks. With the photopeaks entering into the voltage window, the cumulants C_2 and C_3 decrease in magnitude, suggesting that the moving of the photopeaks into resonance decreases the variability within the average current. Indeed, as the photopeaks move into the resonance, the ratio C_2/C_1, an appropriate indicator for the clarity of the current, decreases. This is expected, with increasing voltage, moving the effects of the driving further away, as the level moves further into resonance.

For C_3, as the photopeak approaches the voltage window, we see an increase, followed by a decrease, when the photopeak has entered into the voltage window. The above suggests that, around voltages where photopeaks are entering resonance, the current suffers an increased skewness in its distribution. This can be seen with the ratio of C_3/C_1, which is larger than in the static case (see Fig. 4.2), within the region before the first photopeak enters resonance.

4.3.2 Quantum interference

Here, we investigate a simple manifestation of Fano interference due to a secondary offset level coupled to our primary site but uncoupled from the electrodes. The introduction of this secondary site results in interference between the two paths through the system, those being straight through the connecting sites and via the additional secondary site. The Hamiltonian for the central region is

$$H_C = \epsilon_1 d_1^\dagger d_1 + \epsilon_0 d_0^\dagger d_0 + t(d_1^\dagger d_0 + d_0^\dagger d_1), \quad (4.19)$$
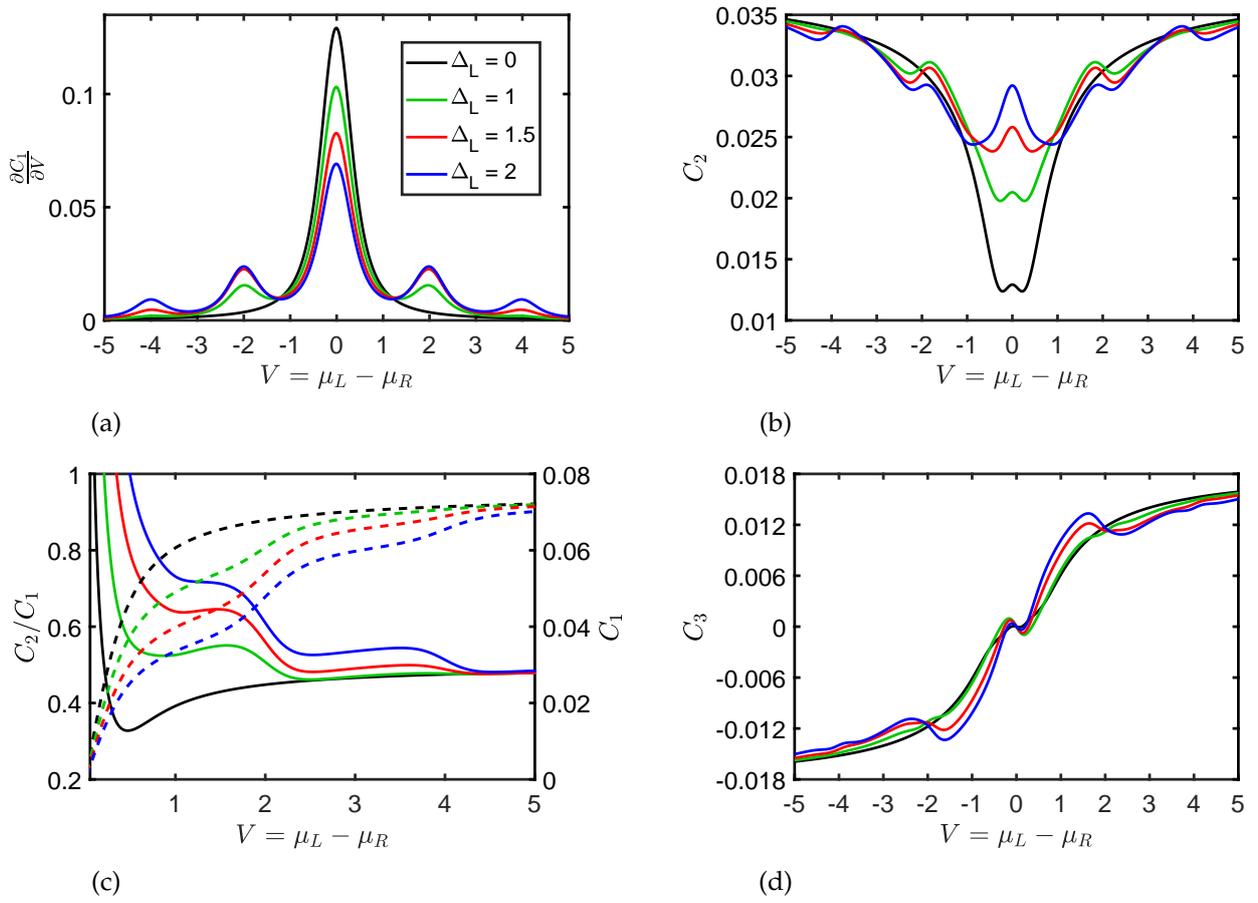
Figure 4.1: Cumulants of the current plotted against increasing voltage ($\mu_L = -\mu_R$) for a single level. The left lead's driving is increased, revealing the effects of the photopeaks. Dashed lines shows C_1, and solid lines show C_2/C_1 in (c). The parameters are $\Gamma_L = \Gamma_R = 0.15$, $\varepsilon_1 = 0$, $T = 0.05$, $\Omega = 1$, $\Delta_0 = 0$, and $\Delta_R = 0$.
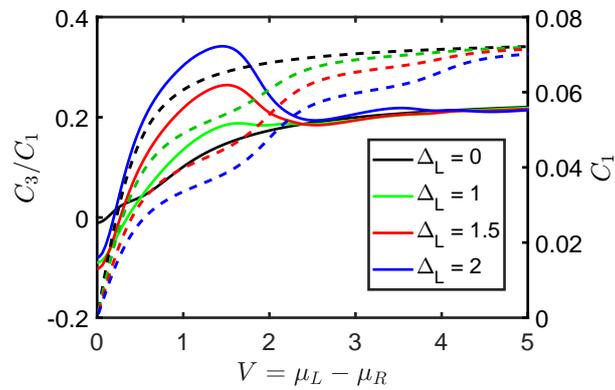
Figure 4.2: The ratio of cumulants, C_3/C_1 plotted against increasing voltage ($\mu_L = -\mu_R$) for a single level. Dashed lines shows C_1, and solid lines show C_3/C_1. The left lead's driving is increased, revealing the effects of the photopeaks. The parameters are those of Fig. 4.1.

(a)

(b)

(c)

(d)
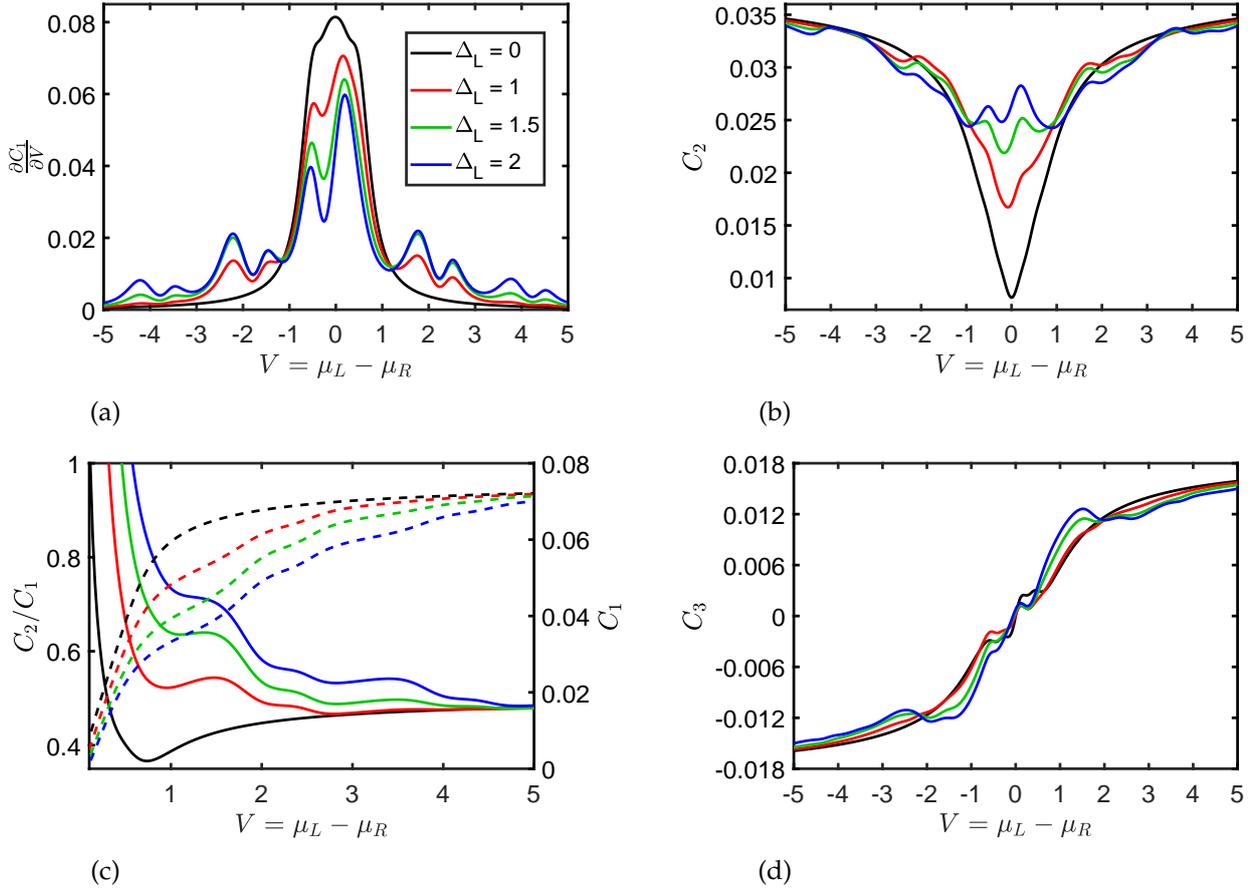
Figure 4.3: Cumulants of the current plotted against increasing voltage ($\mu_L = -\mu_R$). The leads are connected to the first level, which is further connected to the isolated second level. Dashed lines shows C_1, and solid lines show C_2/C_1 in (c). Here, the left lead's driving is increased to reveal the effects of the Fano interference on the photopeaks and higher cumulants. The parameters are $\Gamma_L = \Gamma_R = 0.15$, $\varepsilon_0 = 0$, $\varepsilon_1 = 0.15$, $t = 0.15$, $T = 0.05$, $\Omega = 1$, and $\Delta_R = 0$.

and the central region is connected to the leads through level ϵ_0

$$H_{CL} + H_{CR} = \sum_{i,k,\alpha=L,R} (t_{k\alpha} c_{k\alpha}^\dagger d_0 + \text{H.c.}). \tag{4.20}$$

The leads are sinusoidally driven as in the resonant level case considered before Eq. (4.16), and the central region Hamiltonian remains static all the time.

Calculations for the current concur with theory [Eq. (4.17)], with the transmission undergoing well-known changes due to the introduction of the second level [8]:

$$T(\omega) = \frac{\Gamma_L \Gamma_R}{\left[\omega - \epsilon_0 - t^2/(\omega - \epsilon_1)\right]^2 + \frac{\Gamma^2}{4}}. \tag{4.21}$$

The results of the calculations are given in Fig. 4.3. With the introduction of the secondary level, the photon-assisted sidebands in the current acquire pronounced asymmetrical interfer-
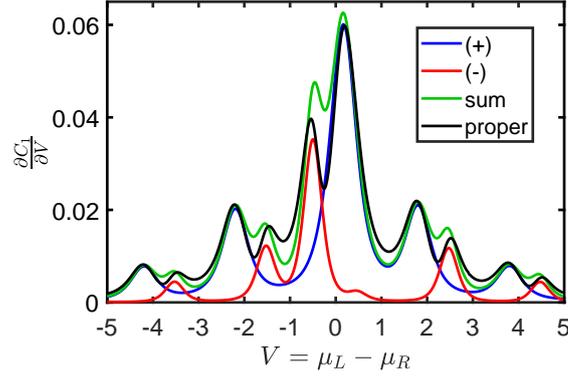
Figure 4.4: The differential conductance plotted against increasing voltage ($\mu_L = -\mu_R$). The leads are connected to the first level, which is further connected to the isolated second level. Here, the bonding and antibonding levels are plotted, disregarding the off-diagonal terms within the diagonalized linewidth function [Eq. 4.23], along with their sum and the full result, which does include the off-diagonal terms. The parameters are $\Gamma_L = \Gamma_R = 0.15$, $\varepsilon_0 = 0$, $\varepsilon_1 = 0.15$, $t = 0.15$, $T = 0.05$, $\Omega = 1$, and $\Delta_R = 0$.

ence patterns from the Fano resonance [see Fig. 4.3a], with the asymmetry being governed by the difference between the energies of the levels. Moreover, the asymmetric feature manifests in the central peak differently from within the photopeaks, with a change in the difference in the levels' energies pushing the feature in the opposite direction for the photopeaks compared to the central peak.

To understand the effects of the secondary level, one can diagonalize the central region Hamiltonian, allowing for the investigation of the current in terms of the bonding (-) and antibonding (+) molecular orbitals [139], which gives the energies

$$\epsilon_{\pm} = \frac{1}{2}\left(\epsilon_0 + \epsilon_1 \pm \sqrt{(\epsilon_0 - \epsilon_1)^2 + 4t^2}\right) \tag{4.22}$$

and a modified linewidth function:

$$\widetilde{\mathbf{\Gamma}}_{i,j}^{\alpha} = \Gamma^{\alpha}\begin{pmatrix} \cos^2(\beta) & \cos(\beta)\sin(\beta) \\ \cos(\beta)\sin(\beta) & \sin^2(\beta) \end{pmatrix}, \tag{4.23}$$

where

$$\beta = \frac{1}{2}\tan^{-1}\left(\frac{2t}{\epsilon_0 - \epsilon_1}\right). \tag{4.24}$$

The diagonalization of the central region allows us to identify the roles that the bonding and antibonding molecular levels play in the cumulants. Furthermore, the effects due to the interaction between these levels is relegated to the off-diagonal terms of the linewidth function [Eq. (4.23)], with their removal corresponding to a system without interaction between the bonding and antibonding levels.

The effects of the separation into the bonding and antibonding levels can be seen within Fig. 4.4. Here, the contributions by both levels are plotted for the case where the off-diagonals within the modified linewidth function [i.e. Eq. (4.23)] are disregarded. We see that the contributions from the diagonalized levels approximately explain the positions of the peaks within the differential conductance, with the off diagonal terms of the modified linewidth varying the final positions slightly. This analysis also helps to explain the features of the higher cumulants in terms of the bonding and antibonding molecular levels.

The effects of the asymmetrical feature due to the Fano resonance can be seen to effect the higher cumulants [see Fig. 4.3b and 4.3d]. While this complicates the features of the cumulants, it was found to not alter the junction's dynamics significantly. This is evident in $F_2 = C_2/C_1$ [see Fig. 4.3c], which suggests no significant changes in the efficiency of the device, with the introduction of a second level resulting in a splitting of the plateauing effect, seen in Fig. 4.1c, due to the shared influence of the bonding and antibonding levels.

4.4   Summary

The method investigated allows for the calculation of the time-averaged cumulants of the current for periodically driven molecular junctions. Expressing the Green's functions in terms of a Fourier series allows for the equation of motion to be cast as a matrix equation of infinite dimensions, which, following truncation, can be easily solved. The method was applied to investigate the time-averaged current cumulants for both a single-level system and a T-shaped double-level system. In investigating the higher cumulants the derivatives of the counting field were evaluated with the finite central difference method.

The method is applicable to many levels, and the wideband approximation is not essential. Furthermore, its application to systems considering extra correlations is conceivable.

It should be noted that the above method calculates the time averages of the cumulants of the current. These calculations should not be confused with the statistics one could calculate when considering the distribution of instantaneous values (for current, noise, etc.) that could be calculated within a period of the driving. While the latter would be more appropriate if one were interested in the instantaneous measurements, the former is more appropriate for devices which would cumulate large transmitted charges before measurement.

Within this chapter, it was found that the time-dependent driving of the leads not only induces photopeaks within the current but also generates features within the higher cumulants. The positioning of photopeaks relative to the voltage window was found to have a significant effect on the higher cumulants. Photopeaks that sit just outside resonance have the effect

of increasing both the second and third cumulants, while photopeaks that sit just within resonance see a relative decrease in both cumulants. Furthermore, it was found that the time-dependent driving broadened and skewed the current distribution. This was observable within C_2/C_1 and C_3/C_1 [see Figs. 4.1c and 4.2 respectively].

Even within the reduced picture of considering time averages, it is evident that the effects of time-dependent driving go beyond the current. This suggests that further investigations into the cumulants of important observables will be essential for understanding time-dependent driven systems.

On top of this, methods that can be extended to consider extra correlations (i.e., electron-phonon and electron-electron interactions) will allow for a fuller understanding of time-dependent driven molecular junctions as they are truly realized, which will hopefully lead to further interesting results.

Floquet Nonequilibrium Green's Functions for Phonon-Assisted Transport

This chapter contains material that has been previously published in the following journal article:

Quantum transport in driven systems with vibrations: Floquet nonequilibrium Green's functions and the self-consistent Born approximation,

T. D. Honeychurch and D. S. Kosov, Phys. Rev. B **107**, 035410 (2023)

5.1 Introduction

The transport properties of quantum dots, especially molecular junctions, can be significantly altered by vibrations coupled to the central region, causing an array of interesting phenomena [8]. Of particular importance is how vibrations, often in conjunction with other phenomena, inhibit device functionality and stability.

Investigations that cast vibrations as localized phonons have been extensively studied under various parameter ranges. When coupling between electronic and vibrational components is sufficiently small, differential conductance through a junction has been found to vary due to changes in bias voltage, with electrons inelastically interacting with central phonons [8, 32, 140], explaining the experimental phenomena observed in inelastic electron tunneling spectroscopy and point contact spectroscopy experiments [141–143]. For sufficiently large coupling between electrons and phonons, transport through the system is suppressed due to the Franck-Condon blockade [8, 69]. With semiclassical approaches to mechanical change within a junction, electron-friction and nonadiabatic effects with general potentials can be studied [114, 144–148].

In steady state, vibrations within a molecular junction have been investigated with a variety of methods [149]. Nonequilibrium Green's functions approaches have been used to model vibrations within self-consistent perturbation theory [32, 140, 150, 151], polaron and dressed tunneling approximations [152, 153], equation-of-motion methods [154], and many more. Vibrations can also be studied with master equation approaches, like the Redfield master equations [155], or more involved methods like hierarchical quantum master equations [156]. Vibrations often contribute significantly to junction failure. With the current lifetime of many molecular junctions being, at best, only seconds long [157], tackling the problem of junction instability stands as a significant hurdle for the field [144, 158].

The further addition of time dependence in the form of varying voltages and electric fields is frequent within the theory and experiment surrounding molecular electronics, allowing for the probing and control of dynamics within the junction. A prime example is recent work that has seen molecular junctions probed on picosecond time frames with a laser pulse-pair scheme [159]. Time-dependent potentials also allow for the realization of novel functionalities, including time-dependent molecular rectifiers [72, 126] and molecular pumps [124]. Beyond static driving, molecular junctions are often studied within time-dependent settings, like transience [63, 160], periodic driving of lead energies [161], couplings [162], or by laser pulses [79, 163], when the central junction is subject to monochromatic electric fields [164], or within the limit of slow driving [165, 166].

Given the importance of vibrations, understanding their dynamics under various time-dependent scenarios will be essentials for molecular junction designs that seek to capitalize on time-dependent effects. Recently, exploration into the effects of time-dependent driving upon vibrations has been growing: transient dynamics of vibrationally active molecular junctions have been investigated theoretically with the self-consistent perturbation theory [107] and dressed tunneling approximation [113]; harmonic driving of gate voltages was used to increase current within the Franck-Condon blockade region [167]; vibrations with perturbatively slow driving have been investigated with mean field in a nonequilibrium Green's functions setting [165] and with hierarchical master equations [166]; and nonequilibrium Green's functions and linear response theory have been utilized to investigate conductance profiles and properties of phonons under small drivings [108, 168, 169].

Of particular interest is whether time-dependent driving can be used to reduce vibrations while still allowing for current flow comparable to the equivalent static case. This has been predicted with a master equation approach[155] and for vibrations modeled semiclassically with a Langevin approach [170].

In This chapter, we use a Floquet nonequilibrium Green's function approach to investigate the effects of time-periodic driving on a single-level electronic molecule coupled to a single

phonon mode, making use of self-consistent perturbation theory in the form of the *GD* approximation [60, 63, 107].

It was found that changes in conductance, indicative of inelastic electron transport spectroscopy, gain photon-assisted side peaks. Following intuition from photon-assisted transport and inelastic electron transport spectroscopy, a simplistic form for the current and phonon occupation is hypothesized and found to be a good match in limiting cases. It was also observed that resonances between the vibrational and driving frequencies resulted in increases in phonon occupation, with two different contributing mechanisms.

5.2   Theory

To describe electrons moving through a junction while interacting with central phonons, we make use of a nonequilibrium Green's functions approach, considering the electron- vibration coupling within the *GD* approximation, also known as the self-consistent Born approximation [60, 61, 171].

The system is modeled with the following Hamiltonian,

$$H(t) = H_{el}(t) + H_{vib} + H_{e-v}. \tag{5.1}$$

The electronic component is given by:

$$H_{el}(t) = H_{central} + H_{leads}(t) + H_{coupling}, \tag{5.2}$$

$$H_{central}(t) = \sum_{ij} \epsilon_{ij} d_i^\dagger d_j, \tag{5.3}$$

$$H_{leads}(t) = \sum_{k,\alpha=L,R} \epsilon_{k\alpha}(t) c_{k\alpha}^\dagger c_{k\alpha}, \tag{5.4}$$

$$H_{coupling}(t) = \sum_{ik\alpha=L,R} t_{k\alpha i} \ c_{k\alpha}^\dagger d_i + \text{h.c.} \tag{5.5}$$

and the Hamiltonian for the vibrations is given as

$$H_{vibratons} = \sum_\alpha \omega_\alpha a_\alpha^\dagger a_\alpha, \tag{5.6}$$

and the coupling between the electronic and vibrational components is given by

$$H_{e-v} = \sum_{ij,\alpha} \lambda_{i,j}^\alpha Q_\alpha d_i^\dagger d_j. \tag{5.7}$$

(a)

(b)
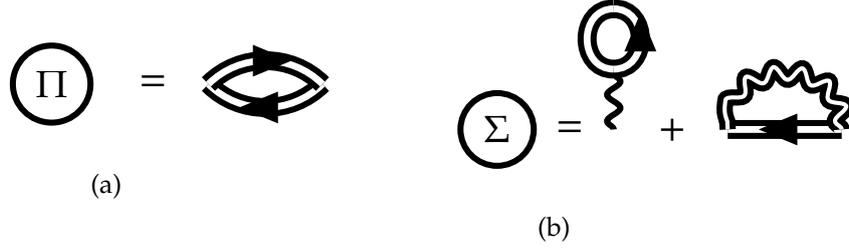
Figure 5.1: The phononic and electronic self-energies for the SCBA approximation.

Here, d_i ($d_i^\dagger$) and $c_{k\alpha}$ ($c_{k\alpha}^\dagger$) are annihilation (creation) operators for the site i in the central region and $k\alpha$ in the leads, respectively. For the phonons, the quantum operator for position is given by $Q_\alpha = \frac{1}{\sqrt{2}}\left(a_\alpha + a_\alpha^\dagger\right)$ and the momentum given by $P_\alpha = \frac{1}{\sqrt{2}i}\left(a_\alpha - a_\alpha^\dagger\right)$, where a_α ($a_\alpha^\dagger$) is the annihilation (creation) operator for the phonon α. Within this chapter, only the energies of the leads are considered to be time-dependent. It is a simple extension to consider time-dependence within the central energy levels, ϵ_{ij} and couplings, $t_{k\alpha,i}$.

The interaction between electrons and phonons can be approximated within the GD approximation [60, 61]:

$$\Sigma_{ij}^{int}(\tau,\tau') = \Sigma_{ij}^{har}(\tau,\tau') + \Sigma_{ij}^{XC}(\tau,\tau'), \tag{5.8}$$

where

$$\Sigma_{ij}^{har}(\tau,\tau') = -i\delta\left(\tau,\tau'\right)\sum_\beta \lambda_{ij}^\beta \int_c d\tau_1 d_\beta(\tau,\tau_1) \sum_{ml} \lambda_{ml}^\beta G_{lm}(\tau_1,\tau_1^+), \tag{5.9}$$

$$\Sigma_{ij}^{XC}(\tau,\tau') = i\sum_{\mu\nu,ml} D_{\mu\nu}\left(\tau,\tau'\right)\lambda_{im}^\mu G_{ml}\left(\tau,\tau'\right)\lambda_{lj}^\nu \tag{5.10}$$

and

$$\Pi_{\alpha\beta}^{int}(\tau,\tau') = -i\sum_{mlkp} \lambda_{ml}^\alpha G_{lk}\left(\tau,\tau'\right)\lambda_{kp}^\beta G_{pm}\left(\tau',\tau\right). \tag{5.11}$$

5.2.1 Floquet Theory

Moving the equations of motion from the contour to real time with the greater, lesser, retarded, and advanced projection, we can, using Floquet transformation of section 2.4.7, write the Kadanoff-Baym equations as follows:

$$(\omega + \Omega m)\,\bar{G}_{ij}^{R/A}\left(\omega,m,n\right) - \sum_k \epsilon_{ik}\bar{G}_{kj}^{R/A}\left(\omega,m,n\right) = \delta_{ij}\delta_{mn} + \sum_{k,r}\bar{\Sigma}_{ik}^{R/A}\left(\omega,m,r\right)\bar{G}_{kj}^{R/A}\left(\omega,r,n\right),$$

$$\tag{5.12}$$

$$\bar{G}_{ij}^{<}(\omega, m, n) = \sum_{kw,rs} \bar{G}_{ik}^{R}(\omega, m, r) \bar{\Sigma}_{kw}^{<}(\omega, r, s) \bar{G}_{wj}^{A}(\omega, s, n),$$ (5.13)

$$\frac{-1}{\omega_{\alpha}} \left(\omega_{\alpha}^2 - (\omega + \Omega m)^2 \right) \bar{D}_{\alpha\beta}^{R}(\omega, m, n) = \delta_{\alpha\beta}\delta_{mn} + \sum_{\gamma, r} \bar{\Pi}_{\alpha\gamma}(\omega, m, r) \bar{D}_{\gamma\beta}(\omega, r, n),$$ (5.14)

$$\bar{D}_{\alpha\beta}^{<}(\omega, m, n) = \sum_{\nu\gamma, rs} \bar{D}_{\alpha\nu}^{R}(\omega, m, r) \bar{\Pi}_{\nu\gamma}^{<}(\omega, r, s) \bar{D}_{\gamma\beta}^{A}(\omega, s, n).$$ (5.15)

In a similar manner, the current and occupation can be also cast in terms of Floquet matrices:

$$I_{\alpha}(n - m) = \bar{I}_{\alpha}(m, n)$$
$$= 2 \int_{-\infty}^{\infty} \frac{d\omega}{2\pi} \sum_{r,ij} \left[\bar{G}_{ij}^{R}(\omega, m, r) \bar{\Sigma}_{ji}^{<}(\omega, r, n) \right.$$
$$\left. + \bar{G}_{ij}^{<}(\omega, m, r) \bar{\Sigma}_{ji}^{R}(\omega, r, n) \right]$$ (5.16)

and

$$n_{j}^{el}(n - m) = \bar{n}_{j}^{el}(m, n) = -i \int_{-\infty}^{\infty} \frac{d\omega}{2\pi} \bar{G}_{jj}^{<}(\omega, m, n).$$ (5.17)

The time-resolved observables can then be found with equation (2.173), where $t' \rightarrow t$, and by taking only the real part, as per equations (2.225) and (2.229).

Unfortunately, the interaction self-energies cannot be brought to such an amenable form and must be calculated from the Fourier coefficients. The interaction self-energies follow the forms $C_{+}(t, t') = A(t, t')B(t, t')$, $C_{-}(t, t') = A(t, t')B(t', t)$ and $C_{H}(t, t') = \delta(t - t') \int_{-\infty}^{\infty} dt_1 A(t, t_1)B(t_1, t_1)$. These terms, when transformed into Fourier coefficients gives as convolution of the following forms:

$$C_{\pm}(\omega, n) = \sum_{m=-\infty}^{\infty} \int \frac{d\omega'}{2\pi} A(\omega', m) B(\pm\omega \mp \omega', n - m)$$
$$= [A \square_{\pm} B](\omega, n).$$ (5.18)

and

$$C_{H}(\omega, n) = \sum_{m=-\infty}^{\infty} A\left(-\frac{\Omega}{2}(n + m), n - m \right) B(n).$$ (5.19)

For this context, $C_{H}(\omega, n)$ simplifies when $A(t, t') = A(t - t')$, giving us

$$C_{H}(\omega, n) = \sum_{m=-\infty}^{\infty} \delta_{m,n} A(-\frac{\Omega}{2}(m + n), 0) B(n) = A(-\Omega n, 0)B(n).$$ (5.20)

The above allows us to cast the interaction self-energies in terms of their Fourier coefficients:

$$\Sigma^R_{har,ij}(\omega,r) = -i\sum_\beta \lambda^\beta_{ij} d^R_\beta(\omega=-\Omega r) \int \frac{d\omega}{2\pi} \sum_{kw} \lambda^\beta_{kw} G^<_{wk}(\omega,r), \tag{5.21}$$

$$\Sigma^R_{XC,ij}(\omega,r) = \int \frac{d\omega'}{2\pi} \sum_{n=-\infty}^{\infty} \sum_{\mu\nu,ml} iD^<_{\mu\nu}(\omega',n) \lambda^\mu_{im} G^R_{ml}(\omega-\omega',r-n) \lambda^\nu_{lj}$$
$$+iD^R_{\mu\nu}(\omega',n)\lambda^\mu_{im}G^<_{ml}(\omega-\omega',r-n)\lambda^\nu_{lj} + iD^R_{\mu\nu}(\omega',n)\lambda^\mu_{im}G^R_{ml}(\omega-\omega',r-n)\lambda^\nu_{lj}, \tag{5.22}$$

$$\Sigma^<_{XC,ij}(\omega,r) = \int \frac{d\omega'}{2\pi} \sum_{n=-\infty}^{\infty} \sum_{\mu\nu,ml} iD^<_{\mu\nu}(\omega',n) \lambda^\mu_{im} G^<_{ml}(\omega-\omega',r-n) \lambda^\nu_{lj}, \tag{5.23}$$

$$\Sigma^>_{XC,ij}(\omega,r) = \int \frac{d\omega'}{2\pi} \sum_{n=-\infty}^{\infty} \sum_{\mu\nu,ml} iD^>_{\mu\nu}(\omega',n) \lambda^\mu_{im} G^>_{ml}(\omega-\omega',r-n) \lambda^\nu_{lj}, \tag{5.24}$$

$$\Pi^R_{\alpha\beta}(\omega,r) = \int \frac{d\omega'}{2\pi} \sum_{n=-\infty}^{\infty} \sum_{mlkp} \tag{5.25}$$
$$-i\lambda^\alpha_{ml}G^<_{lk}(\omega',n)\lambda^\beta_{kp}G^A_{pm}(\omega'-\omega,r-n) - i\lambda^\alpha_{ml}G^R_{lk}(\omega',n)\lambda^\beta_{kp}G^<_{pm}(\omega'-\omega,r-n),$$

$$\Pi^<_{\alpha\beta}(\omega,r) = \int \frac{d\omega'}{2\pi} \sum_{n=-\infty}^{\infty} \sum_{mlkp} -i\lambda^\alpha_{ml}G^<_{lk}(\omega',n)\lambda^\beta_{kp}G^>_{pm}(\omega'-\omega,r-n) \tag{5.26}$$

and

$$\Pi^>_{\alpha\beta}(\omega,r) = \int \frac{d\omega'}{2\pi} \sum_{n=-\infty}^{\infty} \sum_{mlkp} -i\lambda^\alpha_{ml}G^>_{lk}(\omega',n)\lambda^\beta_{kp}G^<_{pm}(\omega'-\omega,r-n). \tag{5.27}$$

We can cast the average phonon positions, equation (2.223), and the subsequent average phonon momenta, equation (2.224), in terms of Fourier coefficients

$$\langle Q_\alpha \rangle(r) = -id^R_\alpha(\omega=-\Omega r) \int \frac{d\omega}{2\pi} \sum_{ml} \lambda^\alpha_{ml} G^<_{lm}(\omega,r), \tag{5.28}$$

$$\langle P_\alpha \rangle(r) = \frac{ir\Omega}{\omega_0} \langle Q_\alpha \rangle(r). \tag{5.29}$$

We can complete a similar process for the phonon momentum Green's functions, equation (2.245), allowing us to calculate the variance of the momentum operators:

$$\left\langle (\Delta P_\alpha)^2 \right\rangle(r) = iD^{PP,<}_{\alpha\alpha}(r) = \frac{i}{\omega_0^2} \int \frac{d\omega}{2\pi} \left(\omega^2 - \left(\frac{r\Omega}{2}\right)^2 \right) D^<_{\alpha\alpha}(\omega,r). \tag{5.30}$$

Solving for the Green's functions, the dimensions of the Floquet matrices, and the corresponding Fourier series, need to be truncated. The addition of more Fourier coefficients leads to more accurate results, converging on the exact result. Calculating the integrand of the Fourier coefficients was completed with an equidistant grid of points. After completing this procedure for the noninteracting case, the Floquet matrices were unraveled to Fourier coefficients using

(a)   (b)
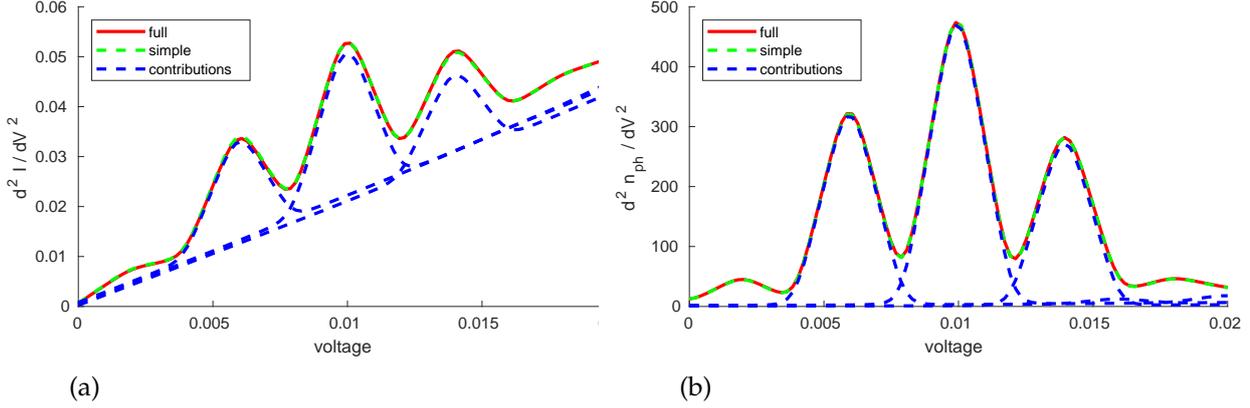
Figure 5.2: The changes in d^2I/dV^2 and d^2n_{ph}/dV^2 as voltage increases. Here the full method is plotted alongside the simplistic method and contributions from $n = -1, 0, 1$ of Eq. 5.33. The other parameters are $\Gamma_L = \Gamma_R = 0.015$, $\epsilon_c = 0.1$, $\eta_c = 3 \times 10^{-5}$, $\Omega = 0.004$, $\omega_c = 0.01$, $\lambda_c = 0.015$, $\Delta_L = 0.005$ and $T = 1.5 \times 10^{-4}$. The bounds of the integrands were taken at -0.3 and 0.3. Fourier coefficients ranging from -8 to 8 were used in the calculation. The uniform grid spacing was 2×10^{-5}. The convergence was below 10^{-6} for both the electronic and phonon occupations.

equation (2.176). The terms where $n + m = 0, -1$ of $\bar{A}(\omega, m, n)$, where taken for calculating the Fourier coefficients. These were then used to calculate the interaction self-energies before being reassembled into the Floquet matrices. The process was then completed iteratively, with convergence given by the Fourier coefficients of the phonon and electron occupations:

$$\frac{\sum_m \left| n_m^{k+1} - n_m^k \right|}{\sum_m \left| n_m^k \right|} \leq \delta, \tag{5.31}$$

where n_m^k is the kth iteration of the mth Fourier coeffecient of the occupation in question, with δ as the convergence.

5.3 Results

For simplicity, we focus on a single electronic level coupled to a single phonon mode, with driving within the left lead:

$$
\begin{aligned}
H(t) = \epsilon_c d^\dagger d + \sum_{ik\alpha=L,R} t_{k\alpha i}\, c_{k\alpha}^\dagger d + t_{k\alpha i}^*\, d^\dagger c_{k\alpha} \\
+ \sum_k \left(\epsilon_{kL} + \Delta_L \cos(\Omega t) \right) c_{kL}^\dagger c_{kL} + \epsilon_{kR} c_{kR}^\dagger c_{kR} \\
+ \omega_c a^\dagger a + \lambda_c Q d^\dagger d.
\end{aligned}
\tag{5.32}
$$

The parameters for the model are the following: ϵ_c, the energy of the central level; ω_c, the

(a)　　　　　　　　　　　　　　　　　　　　　　(b)
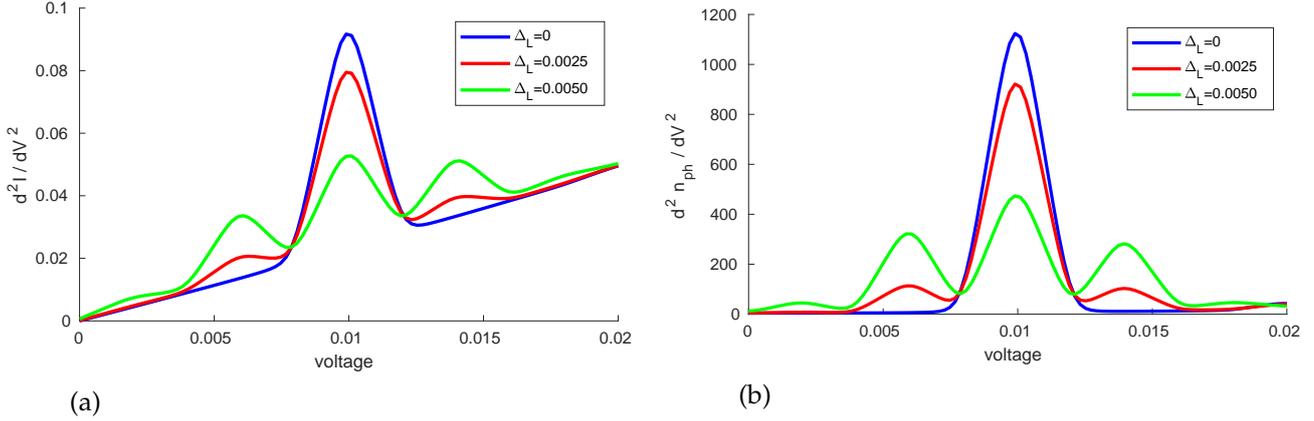
Figure 5.3: The changes in d^2I/dV^2 and d^2n_{ph}/dV^2 as voltage increases, given different driving energies Δ_L. The other parameters are $\Gamma_L = \Gamma_R = 0.015$, $\epsilon_c = 0.1$, $\eta_c = 3 \times 10^{-5}$, $\Omega = 0.004$, $\omega_c = 0.01$, $\lambda_c = 0.015$ and $T = 1.5 \times 10^{-4}$. The bounds of the integrand were taken at -0.3 and 0.3. Fourier coefficients ranging from -8 to 8 were used in the calculation. The uniform grid spacing was 2×10^{-5}. The convergence was below 10^{-6} for both the electronic and phonon occupation.

vibrational frequency of the phonon mode; Ω, the driving frequency of the left lead; Δ_L, the magnitude of the driving in the left lead; $\Gamma_{L/R}$, the couplings to the leads; λ_c, the coupling strength between the central level and phonon; η_c, the coupling of the phonon to its bath; and the temperature of both leads T. Within the calculations, the driving frequency of the left lead was assumed to be the frequency of the system's periodicity.

For the time-averaged picture of this model, we have two important limiting cases in the static, interacting case and the noninteracting case. The static case is well understood and extensively studied [8, 32, 140, 149]. In this context, the phonon mode causes elastic corrections and facilitates new, inelastic channels of transport through the junction by means of absorption or emission of phonons. The latter only occurs when the voltage window widens to accommodate electrons that enter the junction before absorbing (emitting) a phonon of energy. The addition of extra channels through the junction can be seen in subtle changes to the current, captured as peaks in the derivative of the differential conductance with respect to voltage.

The noninteracting case has also been extensively studied and can be explained with the notion of photon-assisted transport [36, 95, 172]. The periodic driving of the system (environment) results in contributions to the time-averaged observables from the equivalent static cases, with the driven energies shifted by integer multiples of the driving frequency of the time dependence. This can be interpreted as a proportion of the electrons emitting or absorbing quanta of the energy, hence the name photon-assisted transport. For the driving profile of section 2.4.8, limited to the left lead, we have

$$\frac{1}{P} \int_0^P I_\alpha(t)\,dt = \sum_{n=-\infty}^{n=\infty} \left[J_n \left(\frac{\Delta_\alpha}{\Omega_\alpha} \right) \right]^2 I_\alpha^{DC} \left(\mu_L + n\Omega_\alpha, \mu_R \right), \tag{5.33}$$

where $I_\alpha(t)$ is the AC-driven current through lead α and I_a^{DC} is the static case, where no driving is present.

Within certain parameter regimes, combining the reasoning from both limiting cases helps to explain the features observed in the full model. In Fig. (5.3a) we see the primary peak within dI^2/dV^2, indicative of inelastic collisions, gain additional satellite peaks due to absorption (emission) of quanta of energy by the electrons prior to entering the junction, per photon-assisted tunneling. A similar effect is observed within Fig. (5.3b), with $d^2 n_{ph}/dV^2$ gaining photon-assisted side peaks, suggesting that the photon-assisted side peaks of the left lead contribute to the occupation of the phonon independently of each other.

The above insights suggest a simplistic model where Eq. (5.33) is augmented, with the static components being calculated with the addition of electron-phonon interactions. This method was often found to successfully predict the inelastic features of the full model. See Fig. (5.2) for an example, where the contributions given by Eq. (5.33) are plotted alongside the full and simplistic methods. The convergence for the simplistic model was calculated by using the average occupation as if it were static.

The simplistic model can be motivated for situations where the timescales for interaction between the electronic and phononic components, $t_\lambda \sim 1/\lambda_c$, is far longer than the traversal time for the electrons within the junction[8]:

$$\frac{1}{\lambda_c} \gg \frac{1}{\sqrt{\Gamma^2 + \Delta E^2}}, \tag{5.34}$$

where $\Gamma = \Gamma_L + \Gamma_R$, and ΔE, the injection energy, is the distance of the energy level from resonance, usually taken as the difference between the energy level and closest chemical potential. In the regime specified by the above assumption, the phonon mode will see the time dependence of the electronic component averaged over the long interaction time, hence the ability of the simplistic model to capture the dynamics. This insight is similar to that used to investigate the effects of AC driving with master equations [77, 155], where weak coupling between the central region and leads results in the central region seeing an average picture of the leads' dynamics.

Within the model in question, it was found that resonance driving at $\Omega \approx \omega_c$ resulted in significant variations for several parameter ranges (see Figs. 5.4 and 5.5). This is mostly due to the sensitivity of the average position to resonant driving, which in turn influences the other observables. This can be seen in Fig. 5.4c. This sensitivity to resonance comes from Eq. 5.28, for which the single-level case simplifies to

$$\langle Q \rangle (m) = \lambda_c \, d^R (-\Omega m) \, n_{el}(m). \tag{5.35}$$

(a)

(b)

(c)

(d)

(e)

(f)

(g)

(h)
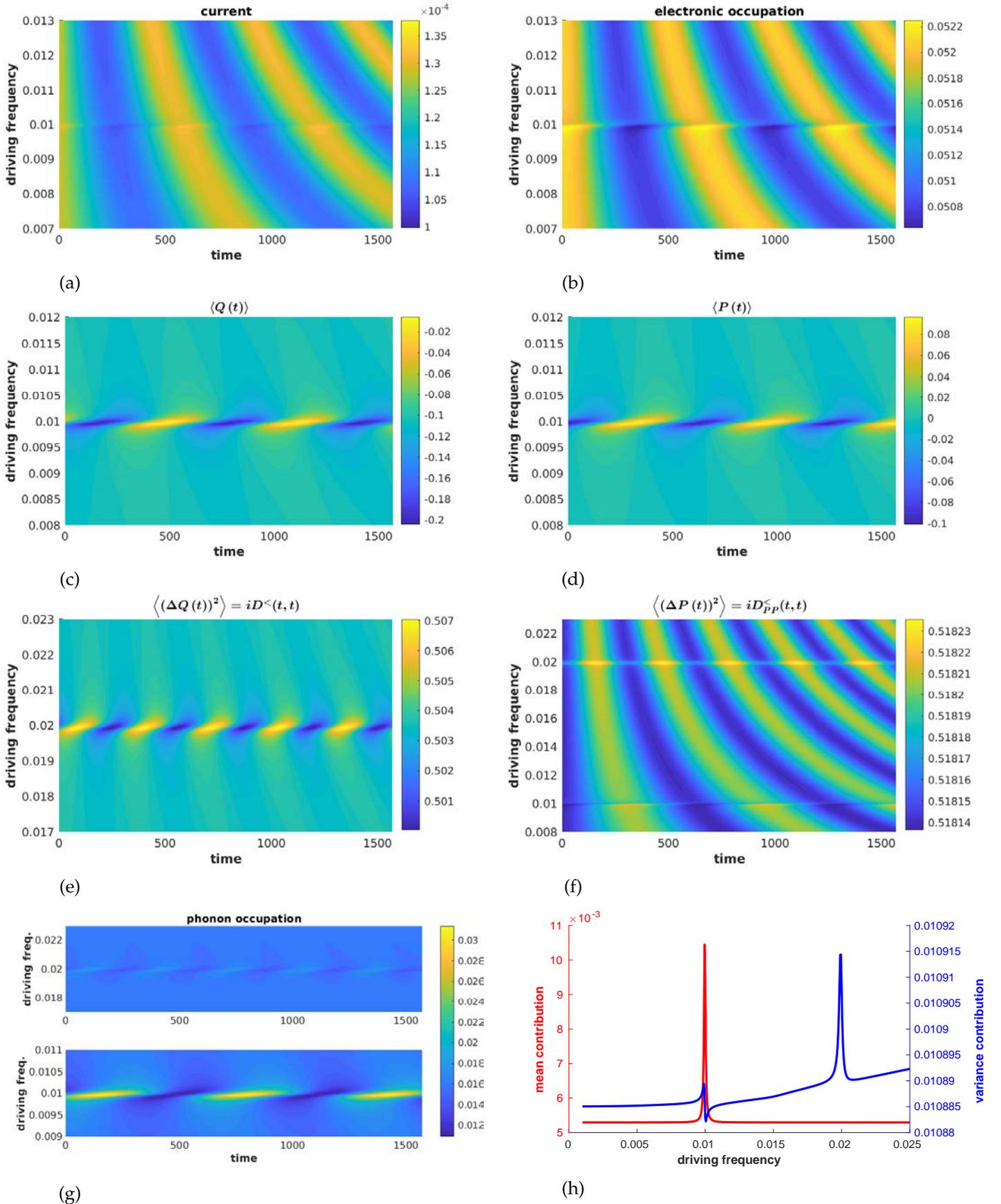
Figure 5.4: Figures (a)–(g) plot objects of interest over time, while figure (h) plots the time-averaged contributions to the phonon occupation, as given by Eq. 2.242. The physical parameters are $\Gamma_L = \Gamma_R = 0.015$, $T = 1.5 \times 10^{-4}$, $\omega_c = 0.01$, $\eta_c = 6 \times 10^{-5}$, $\Delta_L = 0.0015$ and $\lambda_c = 0.01$. Fourier coefficients ranging from -14 to 14 were used in the calculation, with an integrand discretization of 2.5×10^{-5} with bounds of -1 and 1. The convergence was below 10^{-4} for both the electronic and phonon occupation.
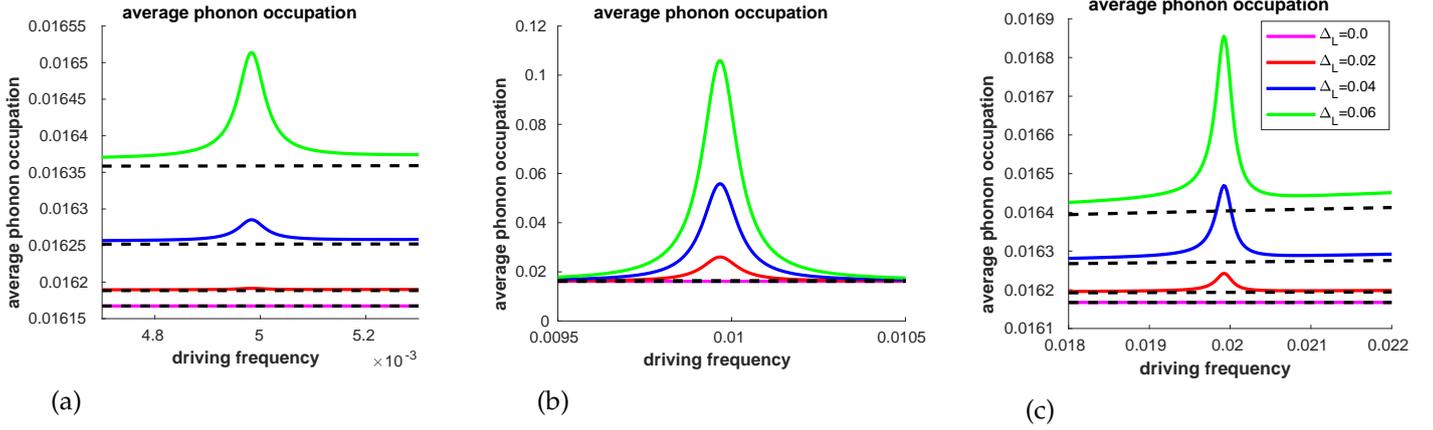
Figure 5.5: The time-averaged phonon occupation as driving frequency increases. Here, the driving energies of the left lead, Δ_L, have been varied. Furthermore, the simplistic method has been plotted in dashed black. The other parameters are $\Gamma_L = \Gamma_R = 0.015$, $\epsilon_c = 0.1$, $\eta_c = 6 \times 10^5$, $\omega_c = 0.01$, $\lambda_c = 0.01$ and $T = 1.5 \times 10^{-4}$. The bounds of the integrands were taken at -1 and 1. Fourier coefficients ranging from -8 to 8 were used in the calculation. The uniform grid spacing 5×10^{-6} for plots (a) and (b), while plot (c) was calculated with 1×10^{-5}. The convergence was below 10^{-4} for both the electronic and phonon occupation.

Focusing on the bare, retarded phonon Green's function, we can separate out the real and imaginary parts:

$$d^R(\omega) =$$

$$\frac{i}{2}\left(\frac{-\eta_c}{(\omega-\omega_c)^2+\eta_c^2}+\frac{\eta_c}{(\omega+\omega_c)^2+\eta_c^2}\right)+\frac{1}{2}\left(\frac{\omega-\omega_c}{(\omega-\omega_c)^2+\eta_c^2}+\frac{\omega_c+\omega}{(\omega_c+\omega)^2+\eta_c^2}\right). \quad (5.36)$$

The real and imaginary components of the above are maximized around $\pm\Omega n \approx \omega_c$, especially when $\eta_c \ll \omega_c$. This results in the average phonon position being sensitive to periodic variation in the electronic occupation, resulting in the primary resonance peak, seen in Figs. 5.4g, 5.4h, and 5.5b, around $\Omega \approx \omega_c$. Additionally, smaller subharmonic resonances can also be observed, see Figs. 5.4g and 5.5a, which indicates the existence of higher-order Fourier coefficients in the electronic site's occupation.

In addition to the resonance at $\Omega \approx \omega_c$, a higher, smaller resonance was observed at $\Omega \approx 2\omega_c$, see Figs. 5.4e, 5.4f, 5.4g, and 5.4h. In contrast to resonance at $\Omega \approx \omega_c$, the resonance at $\Omega \approx 2\omega_c$ is due to increases in the variance of the phonon's position and momentum, which is calculated with the phonon lesser GF. This can be seen in Fig. 5.4h, where the contributions from Eq. (2.242) are separated into the contributions from the mean position and momenta, $\langle Q_\alpha(t)\rangle^2 + \langle P_\alpha(t)\rangle^2$, and the variance terms, $iD_{\alpha\alpha}^<(t,t) + iD_{\alpha\alpha}^{<,PP}(t,t)$. This effect has also been observed in the linear-response regime [108, 168].

Within the parameter ranges investigated, the time-resolved observables were found to be explained primarily by the first- and second-order Fourier coefficients. For the resonances at

$\Omega \approx \omega_c$ and $\Omega \approx 2\omega_c$, the first-order Fourier coefficient was the prominent contributor to the time-resolved dynamics. For the subharmonic resonance at $2\Omega \approx \omega_c$, the second-order Fourier component was found to contribute significantly. This is expected, given that this resonance is sensitive to the second-order Fourier components within the electronic occupation, as seen in Eqs. (5.35) and (5.36).

Figure 5.5 also shows how the simplistic model fails to capture the resonance effects while still capturing the general trend of the phonon occupation. This is understandable, given the simplistic model disregards the driving's effects on the central system's dynamics.

5.4   Summary

In this work, we have investigated the periodic driving of a quantum dot with a Floquet nonequilibrium Green's function approach and SCBA approximation. Specifically, the case of sinusoidal driving of the left lead was investigated for a single-level and phonon system.

Particularly interesting for the stability of such driven systems, it was found that driving the lead energies in resonance with the vibrational frequency resulted in increased variations in average position, average momentum, and occupation of the phonon mode. Moreover, while the time-averaged phonon occupation shows an increase in occupation when resonance occurs [see Figs. 5.4h and 5.5)], the time-resolved result [Fig. 5.4g] reveals more pronounced increases in occupation over the period of driving, reflecting the need to analyze time-resolved results when dealing with periodically driven systems.

Also discussed was a simple phenomenological model that was found to replicate the time-averaged observables rather well in regimes away from resonance, particularly when the driving frequency was smaller than the vibrational frequency, see Fig. 5.2.

Floquet Nonequilibrium Green's Functions with Coulomb Interactions

6.1 Introduction

Capacitive coupling offers a unique tool for investigating and designing open quantum systems. Of particular interest are systems where energy transport occurs between regions without the addition of charge transport. Interesting phenomena that utilize capacitive coupling include coulomb drag[173, 174] and heat rectification[175]. Capacitively coupled quantum dots offer a simple testbed for such phenomena, with heat current across capacitively coupled quantum dots[176, 177] and their use in energy harvesting devices [178–182] having been investigated.

The addition of time-dependent drivings of lead and gate voltages offers a further avenue for exploring particle and energy transport within quantum devices, most usually in the case of periodic drivings[183]: energy transport and entropy production of a noninteracting single electronic level with a periodically modulated gate voltage has been discussed [184, 185]; the periodic modulation of parameters has also been utilized to investigate nanoscale thermal machines[186–188]; and the AC linear response of both particle and heat current has been investigated for a mesoscopic capacitor[189]. In the context of capacitively coupled devices, the electrothermal admittance has been calculated for a nanoscale parallel plate capacitor in the linear response regime[190], and, most recently, the energy transfer in a system of capacitively coupled dots was investigated when the gate voltage of one dot underwent periodic, adiabatic driving [191].

This chapter investigates the energy transfer between two capacitively coupled quantum dots, each connected to a respective lead [see Fig. 6.1]. We study the energy and particle transport within the system due to the periodic driving of one lead's energies. While particles cannot move between systems, the capacitive coupling between the dots allows energy trans-

fer through the system. We make use of a Floquet nonequilibrium Green's functions approach[98, 124, 161, 192, 193], allowing for the exploration of nonadiabatic drivings beyond the adiabatic limit previously investigated [191]. The Coulomb interaction is handled with self-consistent perturbation theory, using the fluctuation-exchange (FLEX) approximation[64]. A self-consistent approximation, FLEX includes both particle-particle and particle-hole T-matrix and GW terms [see Fig. 6.2]. FLEX subsumes the advantages of its constituent terms, making it applicable to a wide variety of interaction strengths and occupations[64].

It was found that the average energy current through the system is sensitive to the driving frequency, with a frequency corresponding to the maximum energy transference observed. This energy transfer was found to be described by a four-stage process. The effects of the other parameters were also investigated.
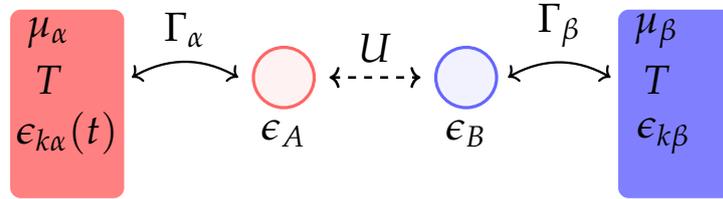
Figure 6.1: Schematic representation of the model investigated. The two quantum dots are coupled to noninteracting electron reservoirs and coupled to each other by Coulomb interaction. Within the investigation, energies of reservoir A are driven harmonically, resulting in a nonzero current between the dots and reservoirs and energy transfer between the reservoirs.

6.2 Theory

For simplicity, we focus on two spinless dots, A and B, coupled to an associated lead, labeled α and β, and coupled capacitively:

$$H(t) = H_A + H_B + H_{int} + H_{A\alpha} + H_{B\beta} + H_\alpha(t) + H_\beta, \tag{6.1}$$

$$H_S = \epsilon_S \hat{d}_S^\dagger \hat{d}_S, \qquad H_{int} = U \hat{d}_A^\dagger \hat{d}_A \hat{d}_B^\dagger \hat{d}_B, \tag{6.2}$$

$$H_{S\sigma} = \sum_k t_{k\sigma S} \, \hat{c}_{k\sigma}^\dagger \hat{d}_S + t_{k\sigma S}^* \, \hat{d}_S^\dagger \hat{c}_{k\sigma}, \tag{6.3}$$

and

$$H_\sigma = \sum_k \left(\epsilon_{k\sigma} + \psi_\sigma(t) \right) \hat{c}_{k\sigma}^\dagger \hat{c}_{k\sigma}. \tag{6.4}$$

Here, S refers to a dot, σ refers to its corresponding lead, and $\bar{S}$ and $\bar{\sigma}$ refer to the opposing dot and lead, respectively. The two interacting dots' energies are given by ϵ_S, and the electron-electron repulsion between the sites, given by H_{int}, has a strength U. The coupling of the quantum dots to their respective leads is governed by $H_{k\sigma S}$, with $t_{k\sigma S}$ denoting a hopping

between the lead site $k\sigma$ and the dot S. The leads are taken as noninteracting, with the explicit time-dependence entering the Hamiltonian via $\psi_\sigma(t)$, which varies the energies $\epsilon_{k\sigma}$, as set out in section 2.4.8.

$$\Sigma_S^{SB} = \qquad and \qquad \Sigma_S^H =$$

$$\Sigma_S^{GW} = \qquad + \qquad + \cdots$$

$$\Sigma_S^{TPP} = \qquad + \qquad + \cdots$$

$$\Sigma_S^{TPH} = \qquad + \qquad + \cdots$$

Figure 6.2: The Feynman diagrams considered within the investigation. Here, S refers to the red fermionic line and corresponds to $G_S(\tau, \tau')$. The blue fermionic line corresponds to the opposing dot's Green's function, $G_{\bar{S}}(\tau, \tau')$.

To model the system out of equilibrium, the self-energy term consists of contributions from the associated lead and the interaction between the quantum dots:

$$\Sigma_S(\tau, \tau') = \Sigma_\sigma(\tau, \tau') + \Sigma_S^{int}(\tau, \tau'). \tag{6.5}$$

To account for the capacitive coupling between the dots, we make use of self-consistent perturbation theory, as set out in chapter 2:

$$\Sigma_S^{int}(\tau, \tau') = -iU G_{\bar{S}}(\tau, \tau^+)\,\delta(\tau, \tau') + \Sigma_S^{corr}(\tau, \tau'), \tag{6.6}$$

where the correlations were investigated with the FLEX approximation[64]:

$$\Sigma_S^{FLEX}(\tau, \tau') = \Sigma_S^{TPP}(\tau, \tau') + \Sigma_S^{TPH}(\tau, \tau') + \Sigma_S^{GW}(\tau, \tau') - 2\Sigma_S^{SB}(\tau, \tau'). \tag{6.7}$$

The single-bubble, GW, particle-particle, and particle-hole T-matrix approximations follow standard definitions here [see Fig. 6.2]. The single-bubble approximation is given by

$$\Sigma_S^{SB}(\tau, \tau') = U G_{\bar{S}}(\tau, \tau')\, G_{\bar{S}}(\tau', \tau)\, U G_S(\tau, \tau'). \tag{6.8}$$

The *GW* self-energy, in the context of equation (6.2) where there is only electron-electron interaction between the dots and no tunnelling between them, is given by

$$\Sigma_S^{GW}(\tau, \tau') = i W_S^{ns}(\tau, \tau')\, G_S(\tau, \tau'), \tag{6.9}$$

$$W_S^{ns}\left(\tau,\tau'\right) = \Phi_S\left(\tau,\tau'\right) + \int_c \tau_1 \int_c \tau_2\, \Phi_S\left(\tau,\tau_1\right) P_S\left(\tau_1,\tau_2\right) W_S^{ns}\left(\tau_2,\tau'\right), \tag{6.10}$$

$$\Phi_S\left(\tau,\tau'\right) = U P_{\bar{S}}\left(\tau,\tau'\right) U \tag{6.11}$$

and

$$P_S\left(\tau,\tau'\right) = -i G_S\left(\tau,\tau'\right) G_S\left(\tau',\tau\right). \tag{6.12}$$

The particle-particle T-matrix self-energy is given by

$$\Sigma_S^{PP}\left(\tau,\tau'\right) = i\, T^{PP}(\tau,\tau') G_{\bar{S}}\left(\tau',\tau\right), \tag{6.13}$$

$$T^{PP}\left(\tau,\tau'\right) = -U G^H\left(\tau,\tau'\right) U + \int d\tau_1 U G^H\left(\tau,\tau_1\right) T^{PP}\left(\tau_1,\tau'\right) \tag{6.14}$$

and

$$G^H(\tau,\tau') = i G_A(\tau,\tau') G_B(\tau,\tau'). \tag{6.15}$$

The particle-hole T-matrix self-energy is given by

$$\Sigma_S^{PH}\left(\tau,\tau'\right) = i\, T_S^{PH}(\tau,\tau') G_{\bar{S}}\left(\tau,\tau'\right), \tag{6.16}$$

$$T_S^{PH}\left(\tau,\tau'\right) = U G_{S\bar{S}}^F\left(\tau,\tau'\right) U - \int d\tau_1 U G_{S\bar{S}}^F\left(\tau,\tau_1\right) T_S^{PH}\left(\tau_1,\tau'\right) \tag{6.17}$$

and

$$G_{S\bar{S}}^F(\tau,\tau') = -i G_S(\tau,\tau') G_{\bar{S}}(\tau',\tau). \tag{6.18}$$

The particle current is given by, from section 2.4.11.2,

$$I_\sigma^P(t) = 2\mathrm{Re}\left\{\int_{-\infty}^{\infty} dt_1\, \mathrm{Tr}\left[G_S^<(t,t_1)\Sigma_\sigma^A(t_1,t) + G_S^R(t,t_1)\Sigma_\sigma^<(t_1,t)\right]\right\}, \tag{6.19}$$

and the occupation of the dots is given by

$$n_S(t) = -i G_S^<\left(t,t\right), \tag{6.20}$$

where continuity dictates that $I_\sigma^P(t) = -\frac{dn_S(t)}{dt}$. To calculate the energy that passes from the leads into the system, we use, from section 2.4.11.3,

$$I_\sigma^E(t) = -i\langle [H(t), H_\sigma(t)]_-\rangle = -2\,\mathrm{Re}\left\{\int dt_1 \left[i\frac{d}{dt}\Sigma_\sigma^<(t,t_1)\right] G_S^A(t_1,t)\right.$$
$$\left. + \left[i\frac{d}{dt}\Sigma_\sigma^R(t,t_1)\right] G_S^<(t_1,t)\right\}. \tag{6.21}$$

Here, energy moves from the leads into the system and system-lead coupling, resulting in the continuity equation

$$I_A^E(t) + I_B^E(t) = \frac{d}{dt}\left(\langle H_{A\alpha}\rangle + \langle H_{B\beta}\rangle\right.$$
$$\left. + \langle H_A\rangle + \langle H_B\rangle + E_{int}(t)\right) \tag{6.22}$$

where

$$\langle H_S\rangle = \epsilon_S\, n_S(t), \tag{6.23}$$

$$\langle H_{S\sigma}\rangle = 2\,\mathrm{Im}\left\{\int dt_1 \Sigma_\sigma^<(t,t_1) G_S^A(t_1,t) + \Sigma_\sigma^R(t,t_1) G_S^<(t_1,t)\right\} \tag{6.24}$$

and

$$E_{int}(t) = \sum_{S=A,B} -\frac{i}{2}\left[\int dt_1\, \Sigma_S^{int,R}(t,t_1)\, G_S^<(t_1,t) + \Sigma_S^{int,<}(t,t_1)\, G_S^A(t_1,t)\right]. \tag{6.25}$$

The terms on the right-hand side of equation (6.22) are the reactance terms, which will disappear if we take the average:

$$\bar{I}_A^E = -\bar{I}_B^E, \tag{6.26}$$

where $\bar{O} = \lim_{\tau\to\infty}\left(\int_0^\tau O(t)\,dt\right)/\tau$.

Of the reactance terms, $E_{int}(t)$ is central to energy transfer process between the dots. Given this, it's beneficial to investigate the change in interaction energy due to energy transfer from the separate sections:

$$I_{S,int}^E(t) = I_S^E(t) - \frac{d}{dt}\left(\langle H_{S\sigma}\rangle + \langle H_S\rangle\right), \tag{6.27}$$

such that

$$I_{A,int}^E(t) + I_{B,int}^E(t) = \frac{dE_{int}(t)}{dt}. \tag{6.28}$$

6.2.1 Floquet approach

As in section 5.2.1, the equations of motion can, using Floquet transformation of section 2.4.7, be written as follows:

$$(\omega + \Omega m - \epsilon_S)\, G_S^{R/A}(\omega, m, n) = \delta_{mn} + \left[\Sigma_S^{R/A} \circ G_S^{R/A}\right](\omega, m, n) \tag{6.29}$$

and

$$G_S^<(\omega, m, n) = \left[G_S^R \circ \Sigma_S^< \circ G_S^A\right](\omega, m, n). \tag{6.30}$$

Using the Fourier and Floquet transformations of section 2.4.7, the interaction self-energies can also be written in terms of Fourier coefficient and Floquet matrices. To calculate the Fourier coefficients of the interaction self-energies, we utilise equation (2.180): for GW,

$$\Sigma_{GW,S}^{R/A}(\omega, n) = i \left[W_S^{ns,<} \square_+ G_S^{R/A} + W_S^{ns,R/A} \square_+ G_S^> \right](\omega, n), \tag{6.31}$$

$$\Sigma_{GW,S}^{</>}(\omega, n) = i \left[W_S^{ns,</>} \square_+ G_S^{</>} \right](\omega, n), \tag{6.32}$$

$$P_S^{R/A}(\omega, n) = -i \left[G_S^< \square_- G_S^{A/R} + G_S^{R/A} \square_- G_S^< \right](\omega, n), \tag{6.33}$$

$$P_S^{</>}(\omega, n) = -i \left[G_S^{</>} \square_- G_S^{>/<} \right](\omega, n), \tag{6.34}$$

$$W_S^{ns,R/A}(\omega, m, n) = \Phi_S^{R/A}(\omega, m, n) + \left[\Phi_S^{R/A} \circ P_S^{R/A} \circ W_S^{ns,R/A} \right](\omega, m, n) \tag{6.35}$$

and

$$\begin{aligned} W_S^{ns,</>}(\omega, m, n) &= \Phi_S^{</>}(\omega, m, n) + \left[\Phi_S^R \circ P_S^R \circ W_S^{ns,</>} \right](\omega, m, n) \\ &+ \left[\Phi_S^R \circ P_S^{</>} \circ W_S^{ns,A} \right](\omega, m, n) + \left[\Phi_S^{</>} \circ P_S^A \circ W_S^{ns,A} \right](\omega, m, n); \end{aligned} \tag{6.36}$$

for the particle-particle T-matrix,

$$\Sigma_S^{TPP,R/A}(\omega, n) = i \left[T^{TPP,<} \square_- G_{\bar{S}}^{A/R} + T^{TPP,R/A} \square_- G_{\bar{S}}^< \right](\omega, n), \tag{6.37}$$

$$\Sigma_S^{TPP,</>}(\omega, n) = i \left[T^{TPP,</>} \square_- G_{\bar{S}}^{>/<} \right](\omega, n), \tag{6.38}$$

$$T^{TPP,R/A}(\omega, m, n) = -U G^{H,R/A}(\omega, m, n) U + U \left[G^{H,R/A} \circ T^{TPP,R/A} \right](\omega, m, n), \tag{6.39}$$

$$\begin{aligned} T^{TPP,</>}(\omega, m, n) &= -U G^{H,</>}(\omega, m, n) U + U \left[G^{H,R} \circ T^{TPP,</>} \right](\omega, m, n) \\ &+ U \left[G^{H,</>} \circ T^{TPP,A} \right](\omega, m, n), \end{aligned} \tag{6.40}$$

$$G^{H,R/A}(\omega, n) = i \left[G_A^< \square_+ G_B^{R/A} + G_A^{R/A} \square_+ G_B^> \right], (\omega, n), \tag{6.41}$$

and

$$G^{H,</>}(\omega, n) = i \left[G_A^{</>} \square_+ G_B^{</>} \right](\omega, n); \tag{6.42}$$

and for the particle-hole T-matrix,

$$\Sigma_S^{TPH,R/A}(\omega, n) = i \left[T_S^{TPH,<} \square_+ G_{\bar{S}}^{R/A} + T_S^{TPH,R/A} \square_+ G_{\bar{S}}^> \right](\omega, n), \tag{6.43}$$

$$\Sigma_S^{TPH,</>}(\omega, n) = i \left[T_S^{TPH,</>} \square_+ G_{\bar{S}}^{</>} \right](\omega, n), \tag{6.44}$$

$$T_S^{TPH,R/A}(\omega, m, n) = U G_{S\bar{S}}^{F,R/A}(\omega, m, n) U - U \left[G_{S\bar{S}}^{F,R/A} \circ T_S^{TPH,R/A} \right](\omega, m, n), \tag{6.45}$$

$$T_S^{TPH,</>} (\omega, m, n) = UG_{S\bar{S}}^{F,</>} (\omega, m, n) U - U \left[G_{S\bar{S}}^{F,</>} \circ T_S^{TPH,A} \right] (\omega, m, n)$$
$$- U \left[G_{S\bar{S}}^{F,R} \circ T_S^{TPH,</>} \right] (\omega, m, n), \tag{6.46}$$

$$G_{S\bar{S}}^{F,R/A} (\omega, n) = -i \left[G_S^< \square_- G_{\bar{S}}^{A/R} + G_S^{R/A} \square_- G_{\bar{S}}^< \right] (\omega, n), \tag{6.47}$$

and

$$G_{S\bar{S}}^{F,</>} (\omega, n) = -i \left[G_S^{</>} \square_- G_{\bar{S}}^{>/<} \right] (\omega, n); \tag{6.48}$$

and for the Hartree self-energy, we have

$$\Sigma_S^H (n) = Un_{\bar{S}}(n) \tag{6.49}$$

or, in terms of Floquet matrices,

$$\Sigma_S^H (m, n) = Un_{\bar{S}}(m, n), \tag{6.50}$$

where

$$n_S (n - m) = n_S (m, n) = -i \int_{-\infty}^{\infty} \frac{d\omega}{2\pi} G_S^< (\omega, m, n). \tag{6.51}$$

In a similar manner to the equations of motion, the particle and energy currents can be cast in terms of Fourier coefficients:

$$I_\sigma^P (n - m) = I_\sigma^P (m, n) = 2 \int_{-\infty}^{\infty} \frac{d\omega}{2\pi} \left[G_S^R \circ \Sigma_\sigma^< + G_S^< \circ \Sigma_\sigma^A \right] (\omega, m, n) \tag{6.52}$$

and

$$I_\sigma^E (n - m) = I_\sigma^E (m, n) = -2 \int_{-\infty}^{\infty} \frac{d\omega}{2\pi} (\omega + m\Omega) \left[\Sigma_\sigma^< \circ G_S^A + \Sigma_\sigma^R \circ G_S^< \right] (\omega, m, n). \tag{6.53}$$

6.2.2 Implementation

To solve the equations of motion, we invert equations (6.29),(6.35),(6.36),(6.39),(6.40),(6.45) and (6.46) by first truncating the Floquet matrices, as defined in Eq. (2.176). Equations (6.31), (6.32), (6.33), (6.34),(6.37), (6.38), (6.41), (6.42), (6.43), (6.44), (6.47) and (6.48) are calculated by using the Fourier coefficient taken from the appropriate Floquet matrices. These Fourier coefficients were taken from the terms of the Floquet matrices given by $n + m = 0, -1$ of equation (2.176). The self-energy terms were then transformed back to Floquet matrix form, using equation (2.176), for use in the equations of motion. The self-consistent process begins
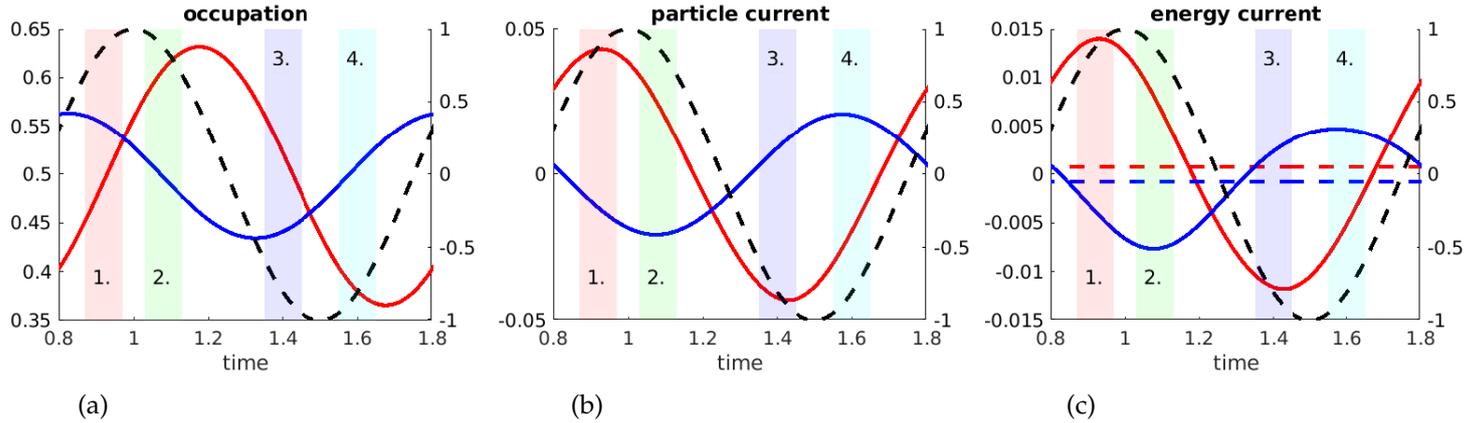
Figure 6.3: Observables measured over a period with driving of the left lead. Here, red lines correspond to the observables relating to the driven section, while blue lines refer to the undriven section of the model. Here, the energy current refers to the energy transfer from the lead and coupling region into the central region, as seen in equation (6.27). The black dashed line is given by $\cos(\Omega t)$, while the colored dashed lines of Fig. 6.3c correspond to the averages of similarly colored energy currents. The parameters are $\Gamma_\alpha = \Gamma_\beta = 0.5$, $U = 0.6$, $T = 0.001$, $\mu_\alpha = \mu_\beta = 0.3$, $\epsilon_A = \epsilon_B = 0$, $\Delta_\alpha = 0.2$ and $\Omega = 0.32$. The discretization was taken at 0.01, the bounds of integration between -40 and 40, and 49 Fourier coefficients were used. The convergence for both dots was taken as 10^{-4}.

with calculating the noninteracting case followed by the interaction self-energies, as specified above. The interaction self-energies are then used to calculate successive iterations of the Green's functions before the following convergence is satisfied:

$$\frac{\sum_m \left| n_m^k - n_m^{k-1} \right|}{\sum_m \left| n_m^k \right|} \leq \delta, \tag{6.54}$$

where n_m^k is the kth iteration of the mth Fourier coefficent of the occupation in question, with δ as the convergence. This convergence was satisfied for each dot's occupation.

6.3   Results and Discussion

Within the system, energy moves from the driven to the undriven section via the capacitive coupling of the two dots. In particular, energy transfer occurs when the driven dot is occupied at a higher energy and unoccupied at a lower energy, and the undriven dot is unoccupied at a higher energy and occupied at a lower energy. This process is complicated because the energies at which a dot is occupied are informed by the occupation of the opposing dot. This relationship is transparent in the Hartree approximation, where the average energy current into the central region due to current into the dot S is given by

$$\bar{I}_\sigma^E = U \int_0^P \frac{dt}{P} \, n_{\bar{S}}(t) I_\sigma^P(t). \tag{6.55}$$

These observations, coupled with the sinusoidal nature of the driving, suggest the following approximate cyclic stages in the energy transfer process:

1. Following stage 4, charge moves onto the driven dot while the undriven dot is largely occupied.

2. The driven dot is largely occupied as charge moves off the undriven dot.

3. Charge moves off the driven dot as the undriven dot is largely unoccupied.

4. The driven dot is largely unoccupied as charge moves onto the undriven dot.

These stages has been stages can be seen in figure 6.4.
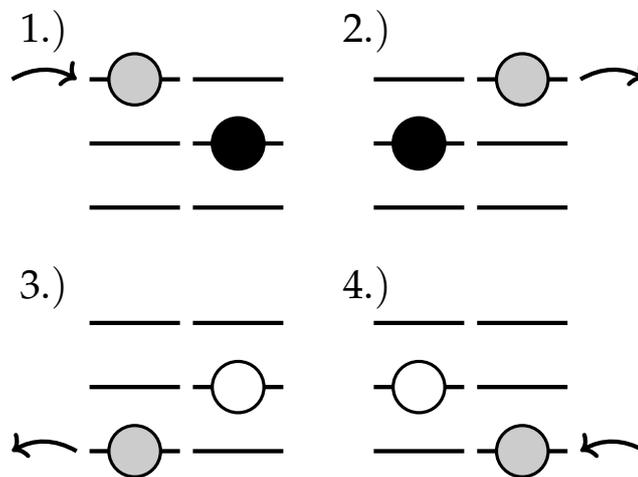
Figure 6.4: The four cyclic stages of the energy transfer process.

Stages one and two capture the movement of higher energy electrons moving onto the driven dot and off the undriven dot, resulting in the energy transfer from the driven to the undriven region. Stages three and four capture the lower energy electrons moving off the driven dot and onto the undriven dot, resulting in a lower energy transfer than the first two steps in the cycle in the opposite direction. An example of this can be seen in Fig. 6.3, where the regions in which the stages are most prominent have been highlighted.

The amount of energy transferred through the system is sensitive to the driving frequency, with the maximum transference a result of the balancing of the stages of energy transfer [see in Fig. 6.5]. As the driving frequency decreases from optimal driving frequency, electrons move between the dots and their respective leads quicker than the energy transfer stages can complete. In particular, the dots that remain largely occupied in stages one and two and largely unoccupied in stages three and four begin to change in occupation, resulting in less pronounced changes in the opposing dot's occupation energy and outgoing energy current. Conversely, as the driving frequency increases, the charge has less time to move between the

Figure 6.5: Time-averaged energy current through the system due to the periodic driving of the left lead. The parameters, unless specified, are $\Gamma_\alpha = \Gamma_\beta = 0.5$, $\epsilon_A = \epsilon_B = -0.2$, $U = 0.4$, $T = 0.001$, $\mu_\alpha = \mu_\beta = 0$ and $\Delta_\alpha = 0.2$. The discretization was taken at 0.01, th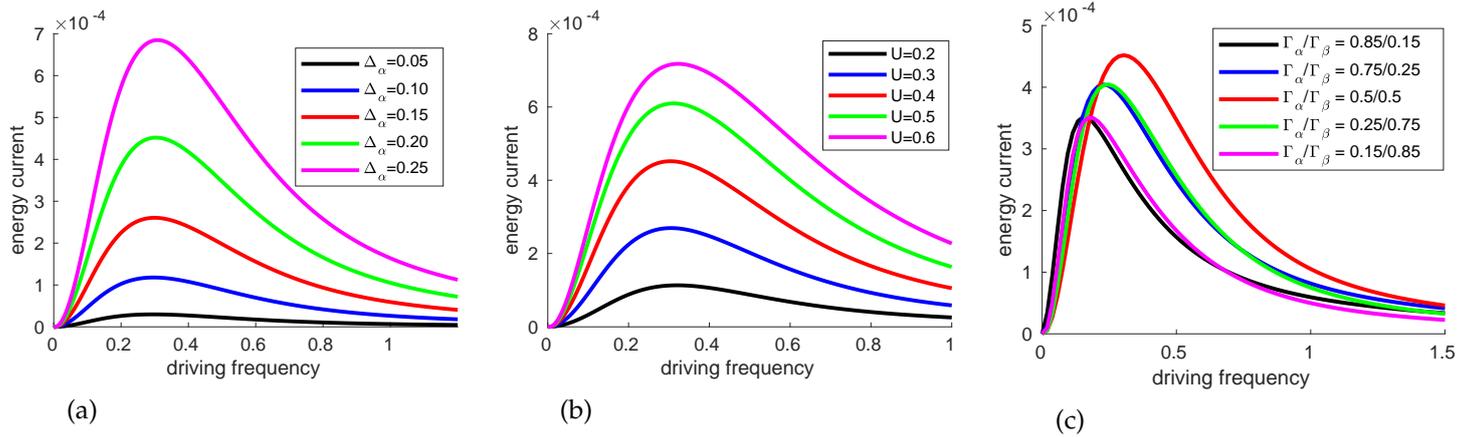e bounds of integration between -40 and 40, and 49 Fourier coefficients were used. The convergence for both dots was taken as 10^{-4}.

dots and their respective leads, resulting in smaller maxima and minima for the occupations over the period, which reduces the opposing dot's occupation energy and its outgoing energy current.

The driving profile and the system parameters beyond the driving frequency also inform the effectiveness of the energy transfer process. As expected, given Eq. (6.55), increases in the interaction strength U were found to increase the average energy current through the system [see Fig. 6.5b]. It was also found that significant asymmetry of the coupling strengths diminished energy flow through the system [see Fig. 6.5c]. This is due to uneven transfer rates, $\tau_\sigma \sim 1/\Gamma_\sigma$, for the movement of electrons between the dots and their respective leads, resulting in the inefficient completion of the stages of the energy transfer process. For the energies of the dots, the largest transference of energy through the system was achieved with dots with equal energies situated below the chemical potential of the two leads, such that, on average, the dots are both around half filled [see Fig. 6.6].

6.4   Conclusion

Within this chapter, the systems of two capacitively coupled quantum dots coupled to respective leads, where one lead's energies are driven sinusoidally were investigated. While particles cannot move between the dots, Coulomb repulsion between the dots allows for the transfer of energy. The stages of the energy transfer were identified, and the effects of system parameters' were investigated. In particular, it was found that energy transfer was maximized for a given driving, corresponding to the efficient completion of the identified energy transfer
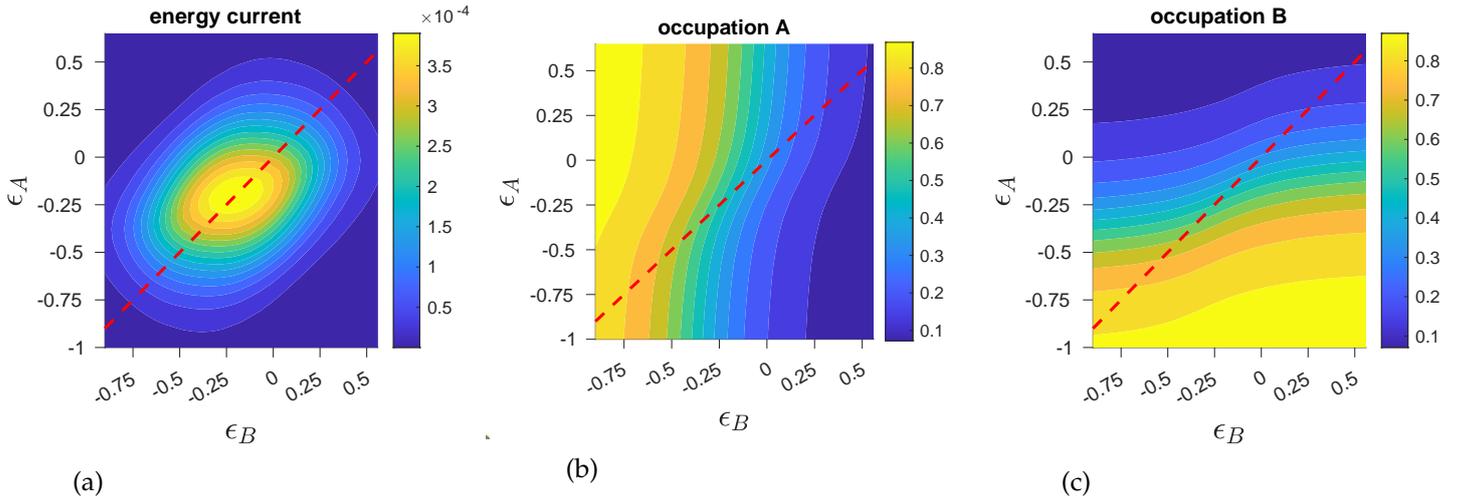
Figure 6.6: Time-averaged observables through the system, with driving of the left lead. The parameters are $\Gamma_\alpha = \Gamma_\beta = 0.5$, $U = 0.4$, $T = 0.001$, $\mu_\alpha = \mu_\beta = 0$, $\Delta_\alpha = 0.2$ and $\Omega = 0.4$. The discretization was taken at 0.01, the bounds of integration between -40 and 40 and 49 Fourier coefficients were used. The convergence for both dots was taken as 10^{-4}. The red dashed line follows $\epsilon_A = \epsilon_B$.

process.

This work has focused on a regime of relatively weak coupling with $\Gamma > U$. Further work in a regime of $\Gamma < U$ may result in different energy transfer stages, as outlined in Sec. 6.3, for various drivings, suggesting interesting possible avenues for further research. Moreover, more complicated driving profiles and statistics relating to energy transfer may prove valuable in understanding and manipulating energy transfer in systems like that investigated.

This result furthers the understanding of particle and energy transfer in capacitively coupled quantum dots, particularly within the context of nonadiabatic driving. This is particularly important as the miniaturization of nanoelectronics brings active elements closer together, resulting in the potential for unwarranted capacitive coupling.

Conclusion

In this thesis, the effects of alternating voltages on various nanoscale transport scenarios were explored, with a particular interest in the interplay between time-dependent driving and quantum correlations. The tool of choice was nonequilibrium Green's functions, emphasising on self-consistent perturbation theory, which was set out in chapter 2.

In Chapter 3, we developed a practical approach for time-dependent quantum transport with nonequilibrium Green's functions using the perturbative separation of fast electron tunnelling and slow driving timescales. The ratio of characteristic electron tunnelling time over the period of harmonic driving is used as a small parameter in the theory to obtain convergent time-derivative expansions of the Green's functions, which enabled the algebraic solution of the Kadanoff-Baym equations in Wigner space. The theory was applied to different transport scenarios: time-dependent transport through a driven single-resonant level was compared to exact results, and electron transport through a molecular junction described by the Holstein model with a time-oscillating voltage bias was also investigated.

The full-counting statistics of periodically driven junctions was investigated in Chapter 4. The combination of Floquet theory for time dynamics and nonequilibrium counting-field Green's functions enables the practical formulation of FCS for the system. The counting-field Green's functions were used to compute the moment-generating function, allowing for the calculation of the time-averaged cumulants of the electronic current. The theory was illustrated using both the single resonant level system and Fano resonance junction architecture.

In Chapter 5, the effects of alternating voltage on nonequilibrium quantum systems with localised phonon modes were investigated. Floquet nonequilibrium Green's functions were utilised, with electron-phonon coupling being considered with the self-consistent Born approximation. This approach allows us to investigate the influence of the driven electronic component on the nonequilibrium occupation of the vibrations. It was found that signatures of inelastic transport gained photon-assisted peaks. A simplistic model was proposed and found to be in good agreement with the full model in certain parameter ranges. Moreover,

it was found that driving the alternating current at resonance with vibrational frequencies caused an increase in phonon occupation.

Finally, in Chapter 6, the dynamics of two capacitively coupled quantum dots, each coupled to a lead, were studied under the presence of one lead's period driving. A Floquet Green's function approach was used to describe the system's dynamics, with the electron-electron interactions handled with the fluctuation-exchange approximation. While electrons cannot move between the separate sections of such a device, energy transfer occurs with the periodic driving of one of the leads. This process was found to be explained with four stages. The energy transfer was also found to be sensitive to the driving frequency of the leads, with an optimal frequency corresponding to the optimal completion of the four stages of the identified process.

The theory utilised in this thesis suffers several shortcomings. Firstly, the self-consistent perturbation theory has several drawbacks. The calculation of higher-order terms is intractable with the tools presented, which means that only a few self-energies are practically computable. This limits the theory's application to relatively low interaction strengths, missing potentially important regimes. Moreover, the models investigated are simplified, omitting complexity for tractability. Whilst capturing much of the physics contained in their experimental counterparts, important factors have yet to be addressed, including nontrivial leads, realistic coupling between vibrations and the surrounding environment and the effects of hot electrons. Including such considerations may improve understanding of various phenomena, particularly the heating seen in Chapter (5).

Furthermore, throughout the thesis, the periodicity of systems' dynamics has been invoked where external drivings have also been periodic. While a Floquet approach effectively captures dynamics in periodic driving, it may be unfeasible or undesirable in more realistic or experimental settings. This is likely in the context of non-periodic pulses, where involved driving profiles would make the Floquet approach computationally difficult.

The work of this thesis permits various possible extensions. The systems investigated in this work have been small, mostly single-level, systems connected to reservoirs. The tools of this thesis could be applied to far larger systems. Moreover, with respect to the findings of Chapter 5, the inclusion of Coulomb interactions, Feynman diagrams including both Coulomb and electron-phonon interactions, and various other molecular configurations could lead to interesting new conductance profiles. Finally, within this thesis, the ideas of optimal driving, which elicits specific functions, have not been investigated. This is an interesting possible further avenue of research.

Bibliography

[1] M. W. M. Graef, *More than moore white paper*, 2021 IEEE International Roadmap for Devices and Systems Outbriefs, 1–47 (2021).

[2] G. E. Moore, *Cramming more components onto integrated circuits, reprinted from electronics, volume 38, number 8, april 19, 1965, pp.114 ff.*, IEEE Solid-State Circuits Society Newsletter **11**, 33–35 (2006).

[3] M. Pourfath, *The non-equilibrium green's function method for nanoscale device simulation* (Springer, Vienna, 2014).

[4] K. Rupp and S. Selberherr, *The economic limit to moore's law [point of view]*, Proceedings of the IEEE **98**, 351–353 (2010).

[5] J. Ajayan, D. Nirmal, S. Tayal, S. Bhattacharya, L. Arivazhagan, A. A. Fletcher, P. Murugapandiyan, and D. Ajitha, *Nanosheet field effect transistors-a next generation device to keep moore's law alive: an intensive study*, Microelectronics Journal **114**, 105141 (2021).

[6] S. Zhang, *Review of modern field effect transistor technologies for scaling*, Journal of Physics: Conference Series **1617**, 012054 (2020).

[7] J. R. Powell, *The quantum limit to moore's law*, Proceedings of the IEEE **96**, 1247–1248 (2008).

[8] J. C. Cuevas and E. Scheer, *Molecular electronics*, 2nd (WORLD SCIENTIFIC, 2017).

[9] A. von Hippel, *Molecular engineering*, Science **123**, 315–317 (1956).

[10] R. P. Feynman, *There's plenty of room at the bottom*, Engineering and science **23** (1959).

[11] B. Mann and H. Kuhn, *Tunneling through Fatty Acid Salt Monolayers*, Journal of Applied Physics **42**, 4398–4405 (1971).

[12] A. Aviram and M. A. Ratner, *Molecular rectifiers*, Chemical Physics Letters **29**, 277–283 (1974).

[13] R. J. Nichols and S. J. Higgins, *Single-molecule electronics: chemical and analytical perspectives*, Annual Review of Analytical Chemistry **8**, PMID: 26048551, 389–417 (2015).

[14] T. Li, V. K. Bandari, and O. G. Schmidt, *Molecular electronics: creating and bridging molecular junctions and promoting its commercialization*, Advanced Materials **35**, 2209088 (2023).

[15] M. Fujihira, K. Nishiyama, and H. Yamada, *Photoelectrochemical responses of optically transparent electrodes modified with langmuir-blodgett films consisting of surfactant derivatives of electron donor, acceptor and sensitizer molecules*, Thin Solid Films **132**, 77–82 (1985).

[16] R. M. Metzger, *Unimolecular electrical rectification by hexadecylquinolinium tricyanoquinodimethanide*, Molecular Crystals and Liquid Crystals Science and Technology. Section A. Molecular Crystals and Liquid Crystals **337**, 37–42 (1999).

[17] Y. Zhao, W. Liu, J. Zhao, Y. Wang, J. Zheng, J. Liu, W. Hong, and Z.-Q. Tian, *The fabrication, characterization and functionalization in molecular electronics*, International Journal of Extreme Manufacturing **4**, 022003 (2022).

[18] F. Evers, R. Korytár, S. Tewari, and J. M. van Ruitenbeek, *Advances and challenges in single-molecule electron transport*, Rev. Mod. Phys. **92**, 035001 (2020).

[19] S.-L. Lv, C. Zeng, Z. Yu, J.-F. Zheng, Y.-H. Wang, Y. Shao, and X.-S. Zhou, *Recent advances in single-molecule sensors based on stm break junction measurements*, Biosensors **12**, 10.3390/bios12080565 (2022).

[20] M. L. Perrin, C. A. Martin, F. Prins, A. J. Shaikh, R. Eelkema, J. H. van Esch, J. M. van Ruitenbeek, H. S. J. van der Zant, and D. Dulić, *Charge transport in a zinc–porphyrin single-molecule junction*, Beilstein Journal of Nanotechnology **2**, 714–719 (2011).

[21] T. A. Su, M. Neupane, M. L. Steigerwald, L. Venkataraman, and C. Nuckolls, *Chemical principles of single-molecule electronics*, Nature Reviews Materials **1**, 16002 (2016).

[22] N. Xin, J. Guan, C. Zhou, X. Chen, C. Gu, Y. Li, M. A. Ratner, A. Nitzan, J. F. Stoddart, and X. Guo, *Concepts in the design and engineering of single-molecule electronic devices*, Nature Reviews Physics **1**, 211–230 (2019).

[23] M. Tsutsui and M. Taniguchi, *Single molecule electronics and devices*, Sensors **12**, 7259–7298 (2012).

[24] J. G. Sifan You Jing-Tao Lü and Y. Jiang, *Recent advances in inelastic electron tunneling spectroscopy*, Advances in Physics: X **2**, 907–936 (2017).

[25] H. Park, J. Park, A. K. L. Lim, E. H. Anderson, A. P. Alivisatos, and P. L. McEuen, *Nanomechanical oscillations in a single-c60 transistor*, Nature **407**, 57–60 (2000).

[26] B. C. Stipe, M. A. Rezaei, and W. Ho, *Single-molecule vibrational spectroscopy and microscopy*, Science **280**, 1732–1735 (1998).

[27] D. Djukic, K. S. Thygesen, C. Untiedt, R. H. M. Smit, K. W. Jacobsen, and J. M. van Ruitenbeek, *Stretching dependence of the vibration modes of a single-molecule* $Pt - H_2 - Pt$ *bridge*, Phys. Rev. B **71**, 161402 (2005).

[28] M. Kiguchi, R. Stadler, I. S. Kristensen, D. Djukic, and J. M. van Ruitenbeek, *Evidence for a single hydrogen molecule connected by an atomic chain*, Phys. Rev. Lett. **98**, 146802 (2007).

[29] M. Kiguchi, O. Tal, S. Wohlthat, F. Pauly, M. Krieger, D. Djukic, J. C. Cuevas, and J. M. van Ruitenbeek, *Highly conductive molecular junctions based on direct binding of benzene to platinum electrodes*, Phys. Rev. Lett. **101**, 046801 (2008).

[30] R. H. M. Smit, Y. Noat, C. Untiedt, N. D. Lang, M. C. van Hemert, and J. M. van Ruitenbeek, *Measurement of the conductance of a hydrogen molecule*, Nature **419**, 906–909 (2002).

[31] O. Tal, M. Krieger, B. Leerink, and J. M. van Ruitenbeek, *Electron-vibration interaction in single-molecule junctions: from contact to tunneling regimes*, Phys. Rev. Lett. **100**, 196804 (2008).

[32] M. Galperin, M. A. Ratner, and A. Nitzan, *Inelastic electron tunneling spectroscopy in molecular junctions: peaks and dips*, The Journal of Chemical Physics **121**, 11965–11979 (2004).

[33] C. Xu, C.-l. Chiang, Z. Han, and W. Ho, *Nature of asymmetry in the vibrational line shape of single-molecule inelastic electron tunneling spectroscopy with the stm*, Phys. Rev. Lett. **116**, 166101 (2016).

[34] P. K. Tien and J. P. Gordon, *Multiphoton process observed in the interaction of microwave fields with the tunneling between superconductor films*, Phys. Rev. **129**, 647–651 (1963).

[35] A. H. Dayem and R. J. Martin, *Quantum interaction of microwave radiation with tunneling between superconductors*, Phys. Rev. Lett. **8**, 246–248 (1962).

[36] G. Platero and R. Aguado, *Photon-assisted transport in semiconductor nanostructures*, Physics Reports **395**, 1–157 (2004).

[37] P. S. S. Guimarães, B. J. Keay, J. P. Kaminski, S. J. Allen, P. F. Hopkins, A. C. Gossard, L. T. Florez, and J. P. Harbison, *Photon-mediated sequential resonant tunneling in intense terahertz electric fields*, Phys. Rev. Lett. **70**, 3792–3795 (1993).

[38] L. P. Kouwenhoven, S. Jauhar, J. Orenstein, P. L. McEuen, Y. Nagamune, J. Motohisa, and H. Sakaki, *Observation of photon-assisted tunneling through a quantum dot*, Phys. Rev. Lett. **73**, 3443–3446 (1994).

[39] V. A. Chitta, C Kutter, R. E. M. de Bekker, J. C. Maan, S. J. Hawksworth, J. M. Chamberlain, M Henini, and G Hill, *Resonant tunnelling at far infra-red frequencies*, Journal of Physics: Condensed Matter **6**, 3945 (1994).

[40] C. Meyer, J. M. Elzerman, and L. P. Kouwenhoven, *Photon-assisted tunneling in a carbon nanotube quantum dot*, Nano Letters **7**, PMID: 17297993, 295–299 (2007).

[41] M. Wang, T. Wang, O. S. Ojambati, T. J. Duffin, K. Kang, T. Lee, E. Scheer, D. Xiang, and C. A. Nijhuis, *Plasmonic phenomena in molecular junctions: principles and applications*, Nature Reviews Chemistry **6**, 681–704 (2022).

[42] R. Arielly, A. Ofarim, G. Noy, and Y. Selzer, *Accurate determination of plasmonic fields in molecular junctions by current rectification at optical frequencies*, Nano Letters **11**, PMID: 21678941, 2968–2972 (2011).

[43] M. Vadai, N. Nachman, M. Ben-Zion, M. Bürkle, F. Pauly, J. C. Cuevas, and Y. Selzer, *Plasmon-induced conductance enhancement in single-molecule junctions*, The Journal of Physical Chemistry Letters **4**, 2811–2816 (2013).

[44] M. Kuperman, L. Nagar, and U. Peskin, *Mechanical stabilization of nanoscale conductors by plasmon oscillations*, Nano Letters **20**, PMID: 32538634, 5531–5537 (2020).

[45] E.-D. Fung, O. Adak, G. Lovat, D. Scarabelli, and L. Venkataraman, *Too hot for photon-assisted transport: hot-electrons dominate conductance enhancement in illuminated single-molecule junctions*, Nano Letters **17**, PMID: 28112947, 1255–1261 (2017).

[46] K. Yoshida, K. Shibata, and K. Hirakawa, *Terahertz field enhancement and photon-assisted tunneling in single-molecule transistors*, Phys. Rev. Lett. **115**, 138302 (2015).

[47] D. R. Ward, F. Hüser, F. Pauly, J. C. Cuevas, and D. Natelson, *Optical rectification and field enhancement in a plasmonic nanogap*, Nature Nanotechnology **5**, 732–736 (2010).

[48] A. Sakai, *Admittance of atomic and molecular junctions and their signal transmission*, Micromachines **9**, 10.3390/mi9070320 (2018).

[49] N. Ittah, G. Noy, I. Yutsis, and Y. Selzer, *Measurement of electronic transport through 1g0 gold contacts under laser irradiation*, Nano Letters **9**, PMID: 19317478, 1615–1620 (2009).

[50] N. Ittah and Y. Selzer, *Electrical detection of surface plasmon polaritons by 1g0 gold quantum point contacts*, Nano Letters **11**, PMID: 21204576, 529–534 (2011).

[51] K. Yamauchi, S. Kurokawa, and A. Sakai, *Admittance of Au/1,4-benzenedithiol/Au single-molecule junctions*, Applied Physics Letters **101**, 253510 (2012).

[52] C. AU Bureau-Oxton, J. AU Camirand Lemyre, and M. AU Pioro-Ladrière, *Nanofabrication of gate-defined gaas/algaas lateral quantum dots*, JoVE, e50581 (2013).

[53] T. Wagner, P. Talkner, J. C. Bayer, E. P. Rugeramigabo, P. Hänggi, and R. J. Haug, *Quantum stochastic resonance in an a.c.-driven single-electron quantum dot*, Nature Physics **15**, 330–334 (2019).

[54] F. Brange, A. Schmidt, J. C. Bayer, T. Wagner, C. Flindt, and R. J. Haug, *Controlled emission time statistics of a dynamic single-electron transistor*, Science Advances **7**, eabe0793 (2021).

[55] T. Fujisawa, T. Hayashi, and S. Sasaki, *Time-dependent single-electron transport through quantum dots*, Reports on Progress in Physics **69**, 759 (2006).

[56] J. P. Pekola, O.-P. Saira, V. F. Maisi, A. Kemppinen, M. Möttönen, Y. A. Pashkin, and D. V. Averin, *Single-electron current sources: toward a refined definition of the ampere*, Rev. Mod. Phys. **85**, 1421–1472 (2013).

[57] B. Kaestner and V. Kashcheyevs, *Non-adiabatic quantized charge pumping with tunable-barrier quantum dots: a review of current progress*, Reports on Progress in Physics **78**, 103901 (2015).

[58] J. R. Petta, A. C. Johnson, C. M. Marcus, M. P. Hanson, and A. C. Gossard, *Manipulation of a single charge in a double quantum dot*, Phys. Rev. Lett. **93**, 186802 (2004).

[59] G. Stefanucci and R. van Leeuwen, *Nonequilibrium many-body theory of quantum systems: a modern introduction* (Cambridge University Press, 2013).

[60] D. Karlsson and R. van Leeuwen, "Non-equilibrium green's functions for coupled fermion-boson systems", in *Handbook of materials modeling: methods: theory and modeling*, edited by W. Andreoni and S. Yip (Springer International Publishing, Cham, 2020), pp. 367–395.

[61] N. Säkkinen, Y. Peng, H. Appel, and R. van Leeuwen, *Many-body green's function theory for electron-phonon interactions: ground state properties of the holstein dimer*, The Journal of Chemical Physics **143**, 234101 (2015).

[62] N. Säkkinen, Y. Peng, H. Appel, and R. van Leeuwen, *Many-body Green's function theory for electron-phonon interactions: The Kadanoff-Baym approach to spectral properties of the Holstein dimer*, The Journal of Chemical Physics **143**, 234102 (2015).

[63] M Ridley, N. W. Talarico, D Karlsson, N. L. Gullo, and R Tuovinen, *A many-body approach to transport in quantum systems: from the transient regime to the stationary state*, Journal of Physics A: Mathematical and Theoretical **55**, 273001 (2022).

[64] N Schlünzen, S Hermanns, M Scharnke, and M Bonitz, *Ultrafast dynamics of strongly correlated fermions—nonequilibrium green functions and selfenergy approximations*, Journal of Physics: Condensed Matter **32**, 103001 (2019).

[65] G. Stefanucci, R. van Leeuwen, and E. Perfetto, *In and out-of-equilibrium ab initio theory of electrons and phonons*, Phys. Rev. X **13**, 031026 (2023).

[66] N. Säkkinen, *Application of time-dependent many-body perturbation theory to excitation spectra of selected finite model systems* (University of Jyväskylä, 2016).

[67] G. Baym, *Self-consistent approximations in many-body systems*, Phys. Rev. **127**, 1391–1401 (1962).

[68] J. Rammer, *Quantum field theory of non-equilibrium states* (Cambridge University Press, 2007).

[69] D. Ryndyk, *Theory of quantum transport at nanoscale: an introduction*, Springer Series in Solid-State Sciences (Springer International Publishing, 2015).

[70] A. O. Gogolin and A. Komnik, *Towards full counting statistics for the anderson impurity model*, Phys. Rev. B **73**, 195301 (2006).

[71] H. K. Yadalam and U. Harbola, *Statistics of an adiabatic charge pump*, Phys. Rev. B **93**, 035312 (2016).

[72] X. W. Tu, J. H. Lee, and W. Ho, *Atomic-scale rectification at microwave frequency*, J. Chem. Phys. **124**, 021105 (2006).

[73] C. Meyer, J. M. Elzerman, and L. P. Kouwenhoven, *Photon-assisted tunneling in a carbon nanotube quantum dot*, Nano Letters **7**, 295–299 (2007).

[74] M. Chauvin, P. vom Stein, H. Pothier, P. Joyez, M. E. Huber, D. Esteve, and C. Urbina, *Superconducting atomic contacts under microwave irradiation*, Phys. Rev. Lett. **97**, 067006 (2006).

[75] M. Galperin and A. Nitzan, *Molecular optoelectronics: the interaction of molecular conduction junctions with light*, Phys. Chem. Chem. Phys. **14**, 9421–9438 (2012).

[76] A. Purkayastha and Y. Dubi, *Quantum transport under ac drive from the leads: a redfield quantum master equation approach*, Phys. Rev. B **96**, 085425 (2017).

[77] U. Peskin, *Formulation of charge transport in molecular junctions with time-dependent molecule-leads coupling operators*, Fortschritte der Physik **65**, 1600048 (2017).

[78] M. Ridley, A. MacKinnon, and L. Kantorovich, *Partition-free theory of time-dependent current correlations in nanojunctions in response to an arbitrary time-dependent bias*, Phys. Rev. B **95**, 165440 (2017).

[79] M. A. Ochoa, Y. Selzer, U. Peskin, and M. Galperin, *Pump–probe noise spectroscopy of molecular junctions*, The Journal of Physical Chemistry Letters **6**, 470–476 (2015).

[80] M. H. Pedersen and M. Büttiker, *Scattering theory of photon-assisted electron transport*, Phys. Rev. B **58**, 12993–13006 (1998).

[81] M. Grifoni and P. Hänggi, *Driven quantum tunneling*, Physics Reports **304**, 229 –354 (1998).

[82] S. Camalet, J. Lehmann, S. Kohler, and P. Hänggi, *Current noise in ac-driven nanoscale conductors*, Phys. Rev. Lett. **90**, 210602 (2003).

[83] S. Kohler, J. Lehmann, and P. Hänggi, *Driven quantum transport on the nanoscale*, Physics Reports **406**, 379 –443 (2005).

[84] B. Trauzettel, Y. M. Blanter, and A. F. Morpurgo, *Photon-assisted electron transport in graphene: scattering theory analysis*, Phys. Rev. B **75**, 035305 (2007).

[85] M. Moskalets and M. Büttiker, *Floquet scattering theory of quantum pumps*, Phys. Rev. B **66**, 205320 (2002).

[86] M. Moskalets and M. Büttiker, *Adiabatic quantum pump in the presence of external ac voltages*, Phys. Rev. B **69**, 205316 (2004).

[87] M. V. Moskalets, *Scattering matrix approach to non-stationary quantum transport* (World Scientific, 2012).

[88] M. F. Ludovico, J. S. Lim, M. Moskalets, L. Arrachea, and D. Sánchez, *Dynamical energy transfer in ac-driven quantum systems*, Phys. Rev. B **89**, 161306 (2014).

[89] L. Arrachea, *Green-function approach to transport phenomena in quantum pumps*, Phys. Rev. B **72**, 125349 (2005).

[90] L. Arrachea and M. Moskalets, *Relation between scattering-matrix and keldysh formalisms for quantum transport driven by time-periodic fields*, Phys. Rev. B **74**, 245322 (2006).

[91] S.-H. Ke, R. Liu, W. Yang, and H. U. Baranger, *Time-dependent transport through molecular junctions*, J. Chem. Phys. **132**, 234105 (2010).

[92] R. Tuovinen, E. Perfetto, G. Stefanucci, and R. van Leeuwen, *Time-dependent landauer-büttiker formula: application to transient dynamics in graphene nanoribbons*, Phys. Rev. B **89**, 085131 (2014).

[93] B. Wang, J. Wang, and H. Guo, *Current partition: a nonequilibrium green's function approach*, Phys. Rev. Lett. **82**, 398–401 (1999).

[94] Q.-f. Sun, J. Wang, and T.-h. Lin, *Photon sidebands of the ground state and the excited state of a quantum dot: a nonequilibrium green-function approach*, Phys. Rev. B **58**, 13007–13014 (1998).

[95] A.-P. Jauho, N. S. Wingreen, and Y. Meir, *Time-dependent transport in interacting and noninteracting resonant-tunneling systems*, Phys. Rev. B **50**, 5528–5544 (1994).

[96] S. Datta and M. P. Anantram, *Steady-state transport in mesoscopic systems illuminated by alternating fields*, Phys. Rev. B **45**, 13761–13764 (1992).

[97] C. A. Stafford and N. S. Wingreen, *Resonant photon-assisted tunneling through a double quantum dot: an electron pump from spatial rabi oscillations*, Phys. Rev. Lett. **76**, 1916–1919 (1996).

[98] T. Brandes, *Truncation method for green's functions in time-dependent fields*, Phys. Rev. B **56**, 1213–1224 (1997).

[99] G. Stefanucci and C.-O. Almbladh, *Time-dependent partition-free approach in resonant tunneling systems*, Phys. Rev. B **69**, 195318 (2004).

[100] H. M. Pastawski, *Classical and quantum transport from generalized landauer-büttiker equations. ii. time-dependent resonant tunneling*, Phys. Rev. B **46**, 4053–4070 (1992).

[101] L. Y. Chen and C. S. Ting, *Dynamic properties of double-barrier resonant-tunneling structures*, Phys. Rev. B **43**, 2097–2105 (1991).

[102] J. Maciejko, J. Wang, and H. Guo, *Time-dependent quantum transport far from equilibrium: an exact nonlinear response theory*, Phys. Rev. B **74**, 085324 (2006).

[103] Y. Zhu, J. Maciejko, T. Ji, H. Guo, and J. Wang, *Time-dependent quantum transport: direct analysis in the time domain*, Phys. Rev. B **71**, 075317 (2005).

[104] M. Ridley, A. MacKinnon, and L. Kantorovich, *Current through a multilead nanojunction in response to an arbitrary time-dependent bias*, Phys. Rev. B **91**, 125433 (2015).

[105] M. Vanević, Y. V. Nazarov, and W. Belzig, *Elementary events of electron transfer in a voltage-driven quantum point contact*, Phys. Rev. Lett. **99**, 076601 (2007).

[106] M. F. Ludovico, F. Battista, F. von Oppen, and L. Arrachea, *Adiabatic response and quantum thermoelectrics for ac-driven quantum systems*, Phys. Rev. B **93**, 075136 (2016).

[107] R. S. Souto, R Avriller, A. L. Yeyati, and A Martín-Rodero, *Transient dynamics in interacting nanojunctions within self-consistent perturbation theory*, New Journal of Physics **20**, 083039 (2018).

[108] A. Ueda, Y. Utsumi, Y. Tokura, O. Entin-Wohlman, and A. Aharony, *Ac transport and full-counting statistics of molecular junctions in the weak electron-vibration coupling regime*, J. Chem. Phys. **146**, 092313 (2017).

[109] R. Avriller, R. S. Souto, A. Martín-Rodero, and A. L. Yeyati, *Buildup of vibron-mediated electron correlations in molecular junctions*, Phys. Rev. B **99**, 121403 (2019).

[110] G.-H. Ding and B. Dong, *Phonon effects on the current noise spectra and the ac conductance of a single molecular junction*, Journal of Physics: Condensed Matter **26**, 305301 (2014).

[111] Y. Zhang, C. Yam, and G. Chen, *Dissipative time-dependent quantum transport theory: quantum interference and phonon induced decoherence dynamics*, J. Chem. Phys. **142**, 164101 (2015).

[112] G.-H. Ding, B. Xiong, and B. Dong, *Transient currents of a single molecular junction with a vibrational mode*, Journal of Physics: Condensed Matter **28**, 065301 (2016).

[113] R. Seoane Souto, R. Avriller, R. C. Monreal, A. Martín-Rodero, and A. Levy Yeyati, *Transient dynamics and waiting time distribution of molecular junctions in the polaronic regime*, Phys. Rev. B **92**, 125435 (2015).

[114] N. Bode, S. V. Kusminskiy, R. Egger, and F. von Oppen, *Current-induced forces in mesoscopic systems: a scattering-matrix approach*, Beilstein J. Nanotechnol **3**, 144–162 (2012).

[115] A. A. Dzhioev, D. S. Kosov, and F. von Oppen, *Out-of-equilibrium catalysis of chemical reactions by electronic tunnel currents*, J. Chem. Phys. **138**, 134103 (2013).

[116] V. F. Kershaw and D. S. Kosov, *Non-adiabatic corrections to electric current in molecular junctions due to nuclear motion at the molecule-electrode interfaces*, J. Chem. Phys. **149**, 044121 (2018).

[117] V. F. Kershaw and D. S. Kosov, *Nonequilibrium green's function theory for nonadiabatic effects in quantum electron transport*, J. Chem. Phys. **147**, 224109 (2017).

[118] V. F. Kershaw and D. S. Kosov, *Non-equilibrium green's function theory for non-adiabatic effects in quantum transport: inclusion of electron-electron interactions*, J. Chem. Phys. **150**, 074101 (2019).

[119] W. Dou, G. Miao, and J. E. Subotnik, *Born-oppenheimer dynamics, electronic friction, and the inclusion of electron-electron interactions*, Phys. Rev. Lett. **119**, 046001 (2017).

[120] M. Hopjan, G. Stefanucci, E. Perfetto, and C. Verdozzi, *Molecular junctions and molecular motors: including coulomb repulsion in electronic friction using nonequilibrium green's functions*, Phys. Rev. B **98**, 041405 (2018).

[121] F. Chen, K. Miwa, and M. Galperin, *Current-induced forces for nonadiabatic molecular dynamics*, The Journal of Physical Chemistry A **123**, PMID: 30354167, 693–701 (2019).

[122] M. Galperin, M. A. Ratner, and A. Nitzan, *Hysteresis, switching, and negative differential resistance in molecular junctions: a polaron model*, Nano Letters **5**, PMID: 15792425, 125–130 (2005).

[123] A. Croy and U. Saalmann, *Full counting statistics of a nonadiabatic electron pump*, Phys. Rev. B **93**, 165428 (2016).

[124] P. Haughian, H. H. Yap, J. Gong, and T. L. Schmidt, *Charge pumping in strongly coupled molecular quantum dots*, Phys. Rev. B **96**, 195432 (2017).

[125] Y. Selzer and U. Peskin, *Transient dynamics in molecular junctions: picosecond resolution from dc measurements by a laser pulse pair sequence excitation*, The Journal of Physical Chemistry C **117**, 22369–22376 (2013).

[126] J Trasobares, D Vuillaume, D Théron, and N Clément, *A 17 GHz molecular rectifier*, Nature Communications **7**, 12850 (2016).

[127] L. Levitov and G. Lesovik, *Charge distribution in quantum shot noise*, JETP Lett. **58**, 230 (1993).

[128] L. S. Levitov, H. Lee, and G. B. Lesovik, *Electron counting statistics and coherent states of electric current*, Journal of Mathematical Physics **37**, 4845–4866 (1996).

[129] M. Esposito, U. Harbola, and S. Mukamel, *Nonequilibrium fluctuations, fluctuation theorems, and counting statistics in quantum systems*, Rev. Mod. Phys. **81**, 1665–1702 (2009).

[130] Y. V. Nazarov and Y. M. Blanter, *Quantum transport: introduction to nanoscience* (Cambridge University Press, 2009).

[131] D. A. Ivanov, H. W. Lee, and L. S. Levitov, *Coherent states of alternating current*, Phys. Rev. B **56**, 6839–6850 (1997).

[132] J. Zhang, Y. Sherkunov, N. d'Ambrumenil, and B. Muzykantskii, *Full counting statistics of quantum point contacts with time-dependent transparency*, Phys. Rev. B **80**, 245308 (2009).

[133] D. A. Ivanov and A. G. Abanov, *Phase transitions in full counting statistics for periodic pumping*, EPL (Europhysics Letters) **92**, 37008 (2010).

[134] M. Benito, M. Niklas, and S. Kohler, *Full-counting statistics of time-dependent conductors*, Phys. Rev. B **94**, 195433 (2016).

[135] Y. Zheng and F. L. H. Brown, *Single molecule counting statistics for systems with periodic driving*, The Journal of Chemical Physics **139**, 164120 (2013).

[136] J. Fransson and M. Galperin, *Inelastic scattering and heating in a molecular spin pump*, Phys. Rev. B **81**, 075311 (2010).

[137] D. Kambly and C. Flindt, *Time-dependent factorial cumulants in interacting nano-scale systems*, Journal of Computational Electronics **12**, 331–342 (2013).

[138] G.-M. Tang and J. Wang, *Full-counting statistics of charge and spin transport in the transient regime: a nonequilibrium green's function approach*, Phys. Rev. B **90**, 195422 (2014).

[139] H. Lu, R. Lü, and B.-f. Zhu, *Tunable fano effect in parallel-coupled double quantum dot system*, Phys. Rev. B **71**, 235320 (2005).

[140] M. Galperin, M. A. Ratner, and A. Nitzan, *On the line widths of vibrational features in inelastic electron tunneling spectroscopy*, Nano Letters **4**, 1605–1611 (2004).

[141] D. Djukic, K. S. Thygesen, C. Untiedt, R. H. M. Smit, K. W. Jacobsen, and J. M. van Ruitenbeek, *Stretching dependence of the vibration modes of a single-molecule* $Pt - H_2 - Pt$ *bridge*, Phys. Rev. B **71**, 161402(R) (2005).

[142] O. Tal, M. Krieger, B. Leerink, and J. M. van Ruitenbeek, *Electron-vibration interaction in single-molecule junctions: from contact to tunneling regimes*, Phys. Rev. Lett. **100**, 196804 (2008).

[143] S. You, J.-T. Lü, J. Guo, and Y. Jiang, *Recent advances in inelastic electron tunneling spectroscopy*, Advances in Physics: X **2**, 907–936 (2017).

[144] R. J. Preston, V. F. Kershaw, and D. S. Kosov, *Current-induced atomic motion, structural instabilities, and negative temperatures on molecule-electrode interfaces in electronic junctions*, Phys. Rev. B **101**, 155415 (2020).

[145] J.-T. Lü, M. Brandbyge, and P. Hedegård, *Blowing the fuse: berry's phase and runaway vibrations in molecular conductors*, Nano Letters **10**, 1657–1663 (2010).

[146] R. J. Preston, M. F. Gelin, and D. S. Kosov, *First-passage time theory of activated rate chemical processes in electronic molecular junctions*, The Journal of Chemical Physics **154**, 114108 (2021).

[147] J.-T. Lü, M. Brandbyge, P. Hedegård, T. N. Todorov, and D. Dundas, *Current-induced atomic dynamics, instabilities, and raman signals: quasiclassical langevin equation approach*, Phys. Rev. B **85**, 245444 (2012).

[148] V. F. Kershaw and D. S. Kosov, *Non-adiabatic effects of nuclear motion in quantum transport of electrons: a self-consistent keldysh–langevin study*, The Journal of Chemical Physics **153**, 154101 (2020).

[149] M. Galperin, M. A. Ratner, and A. Nitzan, *Molecular transport junctions: vibrational effects*, Journal of Physics: Condensed Matter **19**, 103201 (2007).

[150] T.-H. Park and M. Galperin, *Self-consistent full counting statistics of inelastic transport*, Phys. Rev. B **84**, 205450 (2011).

[151] L. K. Dash, H. Ness, and R. W. Godby, *Nonequilibrium electronic structure of interacting single-molecule nanojunctions: vertex corrections and polarization effects for the electron-vibron coupling*, The Journal of Chemical Physics **132**, 104113 (2010).

[152] S. Maier, T. L. Schmidt, and A. Komnik, *Charge transfer statistics of a molecular quantum dot with strong electron-phonon interaction*, Phys. Rev. B **83**, 085401 (2011).

[153] R. Seoane Souto, A. L. Yeyati, A. Martín-Rodero, and R. C. Monreal, *Dressed tunneling approximation for electronic transport through molecular transistors*, Phys. Rev. B **89**, 085412 (2014).

[154] M. Galperin, A. Nitzan, and M. A. Ratner, *Resonant inelastic tunneling in molecular junctions*, Phys. Rev. B **73**, 045314 (2006).

[155] M. Kuperman, L. Nagar, and U. Peskin, *Mechanical stabilization of nanoscale conductors by plasmon oscillations*, Nano Letters **20**, PMID: 32538634, 5531–5537 (2020).

[156] C. Schinabeck and M. Thoss, *Hierarchical quantum master equation approach to current fluctuations in nonequilibrium charge transport through nanosystems*, Phys. Rev. B **101**, 075422 (2020).

[157] C. R. Peiris, S. Ciampi, E. M. Dief, J. Zhang, P. J. Canfield, A. P. Le Brun, D. S. Kosov, J. R. Reimers, and N. Darwish, *Spontaneous s–si bonding of alkanethiols to si(111)–h: towards si–molecule–si circuits*, Chem. Sci. **11**, 5246–5256 (2020).

[158] Y. Ke, A. Erpenbeck, U. Peskin, and M. Thoss, *Unraveling current-induced dissociation mechanisms in single-molecule junctions*, The Journal of Chemical Physics **154**, 234702 (2021).

[159] R. Arielly, N. Nachman, Y. Zelinskyy, V. May, and Y. Selzer, *Picosecond time resolved conductance measurements of redox molecular junctions*, The Journal of Chemical Physics **146**, 092306 (2017).

[160] M. Ridley, V. N. Singh, E. Gull, and G. Cohen, *Numerically exact full counting statistics of the nonequilibrium anderson impurity model*, Phys. Rev. B **97**, 115109 (2018).

[161] T. D. Honeychurch and D. S. Kosov, *Full counting statistics for electron transport in periodically driven quantum dots*, Phys. Rev. B **102**, 195409 (2020).

[162] A. Erpenbeck, L. Götzendörfer, C. Schinabeck, and M. Thoss, *Hierarchical quantum master equation approach to charge transport in molecular junctions with time-dependent molecule-lead coupling strengths*, The European Physical Journal Special Topics **227**, 1981–1994 (2019).

[163] K. Beltako, N. Cavassilas, M. Lannoo, and F. Michelini, *Insights into the charge separation dynamics in photoexcited molecular junctions*, The Journal of Physical Chemistry C **123**, 30885–30892 (2019).

[164] G. Cabra, I. Franco, and M. Galperin, *Optical properties of periodically driven open nonequilibrium quantum systems*, The Journal of Chemical Physics **152**, 094101 (2020).

[165] T. D. Honeychurch and D. S. Kosov, *Timescale separation solution of the kadanoff-baym equations for quantum transport in time-dependent fields*, Phys. Rev. B **100**, 245423 (2019).

[166] J. Bätge, A. Levy, W. Dou, and M. Thoss, *Nonadiabatically driven open quantum systems under out-of-equilibrium conditions: effect of electron-phonon interaction*, Phys. Rev. B **106**, 075419 (2022).

[167] P. Haughian, S. Walter, A. Nunnenkamp, and T. L. Schmidt, *Lifting the franck-condon blockade in driven quantum dots*, Phys. Rev. B **94**, 205412 (2016).

[168] A. Ueda, Y. Utsumi, H. Imamura, and Y. Tokura, *Phonon-induced electron–hole excitation and ac conductance in molecular junction*, Journal of the Physical Society of Japan **85**, 043703 (2016).

[169] A. Ueda, O. Entin-Wohlman, and A. Aharony, *Effects of coupling to vibrational modes on the ac conductance of molecular junctions*, Phys. Rev. B **83**, 155438 (2011).

[170] R. J. Preston, T. D. Honeychurch, and D. S. Kosov, *Cooling molecular electronic junctions by ac current*, The Journal of Chemical Physics **153**, 121102 (2020).

[171] M. Schüler, J. Berakdar, and Y. Pavlyukh, *Time-dependent many-body treatment of electron-boson dynamics: application to plasmon-accompanied photoemission*, Phys. Rev. B **93**, 054303 (2016).

[172] H Haug and A. P. Jauho, *Quantum Kinetics in Transport and Optics of Semiconductors*, Vol. 123, Solid-State Sciences (Springer Berlin Heidelberg, Berlin, Heidelberg, 2008).

[173] A. J. Keller, J. S. Lim, D. Sánchez, R. López, S. Amasha, J. A. Katine, H. Shtrikman, and D. Goldhaber-Gordon, *Cotunneling drag effect in coulomb-coupled quantum dots*, Phys. Rev. Lett. **117**, 066602 (2016).

[174] M. A. Sierra, D. Sánchez, A.-P. Jauho, and K. Kaasbjerg, *Fluctuation-driven coulomb drag in interacting quantum dot systems*, Phys. Rev. B **100**, 081404(R) (2019).

[175] L. Tesser, B. Bhandari, P. A. Erdman, E. Paladino, R. Fazio, and F. Taddei, *Heat rectification through single and coupled quantum dots*, New Journal of Physics **24**, 035001 (2022).

[176] A. A. Aligia, D. P. Daroca, L. Arrachea, and P. Roura-Bas, *Heat current across a capacitively coupled double quantum dot*, Phys. Rev. B **101**, 075417 (2020).

[177] H. K. Yadalam and U. Harbola, *Statistics of heat transport across a capacitively coupled double quantum dot circuit*, Phys. Rev. B **99**, 195449 (2019).

[178] A.-M. Daré, *Comparative study of heat-driven and power-driven refrigerators with coulomb-coupled quantum dots*, Phys. Rev. B **100**, 195427 (2019).

[179] R. Sánchez and M. Büttiker, *Optimal energy quanta to current conversion*, Phys. Rev. B **83**, 085428 (2011).

[180] H. Thierschmann, R. Sánchez, B. Sothmann, F. Arnold, C. Heyn, W. Hansen, H. Buhmann, and L. W. Molenkamp, *Three-terminal energy harvester with coupled quantum dots*, Nature Nanotechnology **10**, 854–858 (2015).

[181] B. Sothmann, R. Sánchez, and A. N. Jordan, *Thermoelectric energy harvesting with quantum dots*, Nanotechnology **26**, 032001 (2014).

[182] N. Walldorf, A.-P. Jauho, and K. Kaasbjerg, *Thermoelectrics in coulomb-coupled quantum dots: cotunneling and energy-dependent lead couplings*, Phys. Rev. B **96**, 115415 (2017).

[183] M. F. Ludovico, L. Arrachea, M. Moskalets, and D. Sánchez, *Periodic energy transport and entropy production in quantum electronics*, Entropy **18**, 10.3390/e18110419 (2016).

[184] M. F. Ludovico, M. Moskalets, D. Sánchez, and L. Arrachea, *Dynamics of energy transport and entropy production in ac-driven quantum electron systems*, Phys. Rev. B **94**, 035436 (2016).

[185] M. F. Ludovico, J. S. Lim, M. Moskalets, L. Arrachea, and D. Sánchez, *Time resolved heat exchange in driven quantum systems*, Journal of Physics: Conference Series **568**, 052017 (2014).

[186] A.-M. Daré and P. Lombardo, *Time-dependent thermoelectric transport for nanoscale thermal machines*, Phys. Rev. B **93**, 035303 (2016).

[187] M. F. Ludovico and M. Capone, *Enhanced performance of a quantum-dot-based nanomotor due to coulomb interactions*, Phys. Rev. B **98**, 235409 (2018).

[188] S. Juergens, F. Haupt, M. Moskalets, and J. Splettstoesser, *Thermoelectric performance of a driven double quantum dot*, Phys. Rev. B **87**, 245423 (2013).

[189] J. S. Lim, R. López, and D. Sánchez, *Dynamic thermoelectric and heat transport in mesoscopic capacitors*, Phys. Rev. B **88**, 201304(R) (2013).

[190] J. Chen, M. ShangGuan, and J. Wang, *A gauge invariant theory for time dependent heat current*, New Journal of Physics **17**, 053034 (2015).

[191] M. F. Ludovico and M. Capone, *Charge and energy transfer in ac-driven coulomb-coupled double quantum dots*, The European Physical Journal B **95**, 99 (2022).

[192] T. D. Honeychurch and D. S. Kosov, *Quantum transport in driven systems with vibrations: floquet nonequilibrium green's functions and the self-consistent born approximation*, Phys. Rev. B **107**, 035410 (2023).

[193] H. Aoki, N. Tsuji, M. Eckstein, M. Kollar, T. Oka, and P. Werner, *Nonequilibrium dynamical mean-field theory and its applications*, Rev. Mod. Phys. **86**, 779–837 (2014).